PONTIFICIA UNIVERSIDAD CATOLICA DE CHILE

SCHOOL OF ENGINEERING

SEISMIC VULNERABILITY EVALUATION OF REINFORCED CONCRETE SHEAR WALL BUILDINGS IN CHILE

DAVID GUILLERMO UGALDE BEDOYA

Thesis submitted to the Office of Graduate Studies in partial fulfillment of the requirements for the Degree of Doctor in Engineering Sciences

Advisor:

DIEGO LÓPEZ-GARCÍA

Santiago de Chile, (dec, 2019)

PONTIFICIA UNIVERSIDAD CATOLICA DE CHILE

SCHOOL OF ENGINEERING

SEISMIC VULNERABILITY EVALUATION OF REINFORCED CONCRETE SHEAR WALL BUILDINGS IN CHILE

DAVID GUILLERMO UGALDE BEDOYA

Members of the Committee:

DIEGO LÓPEZ-GARCÍA

MATÍAS HUBE

JOSÉ LUIS ALAMAZÁN

RODRIGO JORDÁN

FINLEY CHARNEY

PABLO PARRA

JUAN DE DIOS ORTUZAR

Thesis submitted to the Office of Graduate Studies in partial fulfillment of the requirements for the Degree of Doctor in Engineering Sciences

Santiago de Chile, (dec, 2019)

To my beloved uncle
Marvin Ugalde (Bambi)

ACKNOWLEDGMENTS

First of all, I would like to thank Chile for giving me the opportunity to come and learn, while inspiring me with its great culture and nature.

Particularly, the financial support provided by the Comisión Nacional de Ciencia y Tecnología (CONICYT-PCHA/Doctorado Nacional/2015-21151184 scholarship) and the Vicerrectoría de Investigación from the Pontificia Universidad Católica de Chile (Ayudante Becario scholarship) is greatly acknowledged.

Then, I would like express my sincere gratitude to my advisor Dr. Diego López-García for his deep commitment with my research and my development. His valuable guidance and the confidence set on me, encouraged me to always challenge my abilities.

I also want to thank the members of the committee who made relevant observations during the development of this research. An additional thanks to Dr. Finley Charney who made possible my visit to the Virginia Polytechnic Institute and State University and to Dr. Pablo Parra who helped develop the nonlinear analyses and the related papers.

Finally, I want to thank my parents Marilia and Guillermo, who in spite of the distance, have supported and encouraged me during these years, and my loved Andrea who has been the closest support in this process. An additional acknowledgement is extended to my fellow Ph.D. students who provided advice and relevant comments that enriched this research.

RESUMEN

Un porcentaje muy bajo de edificios de concreto reforzado sufrieron daños en el terremoto del Maule en 2010 (M_w 8.8), pese a verse sometidos a aceleraciones significativamente mayores que las prescritas por el código de diseño sísmico de Chile. Esta observación sugiere que la capacidad de tales edificios es en realidad mucho mayor que la requerida por el código de diseño sísmico. Para profundizar en este tema, se analizan en esta disertación, tres edificios reales de 5, 17 y 26 pisos que resistieron el terremoto del Maule sin daños apreciables. Se realizaron tres análisis distintos, que corresponden con los tres artículos que componen esta disertación.

En una primera serie de análisis (artículo I) se adopta un modelo elástico lineal. Se parte con un análisis "nominal" que utiliza procedimientos de análisis convencionales para el cálculo de las demandas sísmicas y de las capacidades de los elementos. Posteriormente, se pasa a un análisis "efectivo" donde las demandas sísmicas se calculan realizando un análisis de respuesta en el tiempo, y las capacidades de los elementos se estiman mediante procedimientos más avanzados. Se evalúan varios supuestos de modelación y aspectos del código de diseño. También se considera el posible levantamiento de las fundaciones colocando en la base, resortes no lineales sin rigidez a tracción. Los resultados dados por el análisis nominal son consistentes con la falta de daño observada en el edificio de 5 pisos, pero no en los edificios de 17 y 26 pisos. Los resultados dados por el análisis efectivo (es decir de respuesta en el tiempo) sí son consistentes, pero solo cuando se considera el levantamiento de la fundación. Finalmente, se discute la idoneidad de los modelos linealmente elásticos de hormigón para evaluar la respuesta de estructuras de muros de corte sin daño aparente y sometidas a fuertes demandas sísmicas.

En la siguiente serie de análisis (artículo II), los dos edificios más altos (17 y 26 pisos) se analizaron utilizando modelos de elementos finitos totalmente no lineales, es decir, modelos que incluyen comportamiento no lineal de los materiales y no linealidades geométricas. La modelación de los muros se validó reproduciendo los resultados de ensayos estáticos cíclicos de muros aislados disponibles en la literatura. Se realizaron varios análisis de pushover para evaluar la influencia de varios aspectos de modelación en la respuesta global de los edificios. Se realizaron también, análisis de respuesta en el tiempo con un registro del Terremoto del Maule tomado en Santiago Centro. En general, los resultados del análisis dinámico (tanto para aspectos globales como locales) son consistentes con los resultados del análisis de

pushover y con la falta de daño observada empíricamente. una consistencia que no se encontró con los modelos linealmente elásticos. Se encontró que el drift de entrepiso *tangencial* se correlaciona mucho mejor con la falta de daño observable que el drift de entrepiso *total*, que el que típicamente se utiliza en la práctica. El análisis también reveló que el levantamiento de la fundación es posible pero no parece influir significativamente en la respuesta. Otros aspectos de modelación que mostraron ser relevantes son la rigidez a corte de los muros y la influencia de las losas. En general se observó que la degradación de rigidez que puede esperarse ante demandas sísmicas similares a las del Terremoto del Maule, conlleva un alargamiento del período que reduce las aceleraciones espectrales que enfrentan estos edificios, protegiendo la integridad estructural de los elementos.

Finalmente, en función de los resultados del análisis de pushover comentados anteriormente se estudió más a fondo la rigidez a corte de los muros y la rigidez a flexión de las losas. Se encontró que en la literatura existe una gran dispersión de valores recomendados de rigidez efectiva a corte de muros (GA_{eff}) y a flexión de las losas (EI_{eff}). Un análisis probabilístico basado en curvas de fragilidad es una metodología robusta para evaluar la influencia de estos parámetros en el desempeño esperado de este tipo de edificios, pero dichos estudios son escasos por requerir análisis muy demandantes computacionalmente con el Análisis Dinámico Incremental (IDA, por sus siglas en inglés). Es por esto que en la última serie de análisis (artículo III) se utiliza el recientemente introducido SPO2FRAG, un procedimiento simplificado que en lugar de IDA utiliza curvas de pushover para estimar curvas fragilidad, lo que resulta mucho más factible en términos computacionales. Las curvas obtenidas con SPO2FRAG se utilizaron para evaluar la influencia del GA_{eff} y el EI_{eff} en la respuesta sísmica de los 2 casos de estudio más altos. La fragilidad de los edificios demostró ser sensible a las variaciones de ambas rigideces. A pesar de tener muros bastante esbeltos, la influencia des GA_{eff} fue notable, particularmente en los estados límite bajos, donde los resultados obtenidos para valores altos de GA_{eff} fueron más consistentes con el desempeño empírico del edificio de 17 pisos. El análisis del edificio de 26 pisos muestra un desempeño sísmico que no es consistente con las observaciones empíricas, lo que sugiere que esta metodología tiene limitaciones en estructuras altas. Se identifica una contribución significativa de la rigidez a flexión de las losas, incluso cuando se asumen valores bajos del EI_{eff}.

ABSTRACT

A very low percentage of reinforced concrete building structures subjected to the M_w 8.8 2010 Chile earthquake suffered severe damage, even though they were affected by ground accelerations significantly larger than those prescribed by the Chilean seismic design code. This observation suggests that the seismic capacity of such buildings is actually much larger than that required by the seismic design code. In order to obtain insight into this issue, three actual building structures of 5, 17 and 26 stories that withstood the 2010 Chile earthquake with no observable damage are analyzed. Three different analyzes were performed, corresponding to the three papers presented in this dissertation.

In a first series of analyses (paper I), linearly elastic concrete material model is adopted. As an initial approach, nominal procedures are used to calculate seismic demands and member capacities. Then seismic demands are calculated by performing response history analysis, and member capacities are evaluated by state-of-the-art procedures. Several modeling assumptions and code issues are evaluated, and possible foundation uplift is accounted for through inclusion of nonlinear, compression-only vertical springs at the foundation level. Results given by nominal analyses are not consistent with the observed lack of damage in the 17- and 26-story buildings. Results given by response history analysis are indeed consistent but only when foundation uplift is accounted for. The suitability of linearly elastic concrete material models to assess the response of apparently undamaged reinforced concrete shear wall structures subjected to strong seismic demands is then discussed.

In a second series of analyses (paper II), the two taller buildings (17 and 26 stories) were analyzed using fully nonlinear finite element models, i.e., models that include nonlinear material behavior and geometric nonlinearities. The approach to model the RC shear walls was validated through comparisons with results experimentally obtained from cyclic static tests conducted on isolated wall specimens. Several pushover analyses were performed to assess the global response of the buildings under seismic actions and to evaluate the influence of several modeling issues. Response history analyses were performed considering a ground motion recorded in Santiago during the 2010 Chile earthquake. In general, results (in terms of both global and local response quantities) are consistent with results given by pushover analysis and with the empirically observed lack of damage, a consistency that was not found in the linearly elastic models. The tangential story drift deformation was found to correlate much better with the lack of observable damage than the total story drift

deformation typically considered in practice. The analysis also revealed that foundation uplift is possible but does not seem to significantly influence the response. Other modeling issues that were found to deserve further research are the shear stiffness of the walls and the influence of the slabs. The stiffness degradation expected for seismic demands similar to those of the 2010 Chile earthquake, lead to a period elongation that reduces the spectral accelerations faced by the structures without compromising the structural integrity of the members.

Finally, motivated by results of the previously commented pushover analysis, the influence of the walls shear stiffness and slabs bending stiffness was further studied. It was found that when modeling RC shear wall buildings for seismic analysis there is little consensus in the literature on the appropriate value of the wall effective shear stiffness (GA_{eff}) and the slab effective bending stiffness (EI_{eff}). A probabilistic analysis based on fragility curves is a robust technique to assess the influence of these parameters on the expected seismic performance, but such studies are scarce because they require computationally expensive analysis such as Incremental Dynamic Analysis (IDA). Then in the last series of analyses (paper III), fragility curves are developed following the recently introduced SPO2FRAG procedure, a simplified methodology that does not require IDA but the computationally more affordable incremental static (pushover) analysis. The fragility curves provided by SPO2FRAG are used to evaluate the influence of the values of GA_{eff} and EI_{eff} on the analytical seismic response of full 3D nonlinear models of two taller study cases. The accuracy of SPO2FRAG is also evaluated through comparisons with empirical fragilities. The building fragility showed to be sensitive to variations of both stiffness. Despite of having quite slender walls the influence of GA_{eff} was noticeable, particularly in low limit states, where results obtained for large GA_{eff} values were more consistent with the empirical performance of the 17-story building. The analysis of the 26-story building indicates a seismic performance that is not consistent with empirical observations, suggesting limitations of the methodology in tall structures. A significant contribution of bending stiffness in slab elements is identified, even when low values EI_{eff} are assumed.

Table of contents

1. INTRODUCTORY CHAPTER

1.1. Motivation

The continental territory of Chile is a seismic prone area with high tectonic activity. The continuous subduction of the Nazca plate beneath the South American plate along 3,200 km of the Chilean coast, frequently produce megathrust earthquakes that exceed the magnitude of M_w7.0 (Fig. 1.1a). Some of these earthquakes are indeed ranked among the most intense earthquakes recorded in the world (Fig. 1.1b). Besides, local faults produce shallow earthquakes that, despite having a smaller magnitude, can also be very destructive.

(a)

	Mag.	Location	Date (UTC)
1	9.5	Valdivia, Chile	22-May-1960
2	9.2	Alaska, USA	28-Mar-1964
3	9.1	Northern Sumatra, Indonesia	26-Dec-2004
4	9.1	Tohoku, Japan	11-Mar-2011
5	9.0	Kamchatka, Russia	04-Nov-1952
6	8.8	Maule, Chile	27-Feb-2010
7	8.8	Esmeraldas, Ecuador	31-Jan-1906
8	8.7	Aleutian Islands, USA	04-Feb-1965
9	8.6	Assam, India	15-Aug-1950
10	8.6	Northern Sumatra, Indonesia	11-Apr-2012
11	8.6	Northern Sumatra, Indonesia	28-Mar-2005
12	8.6	Aleutian Islands, USA	09-Mar-1957
13	8.6	Alaska, USA	01-Apr-1946
14	8.5	Banda Sea, Indonesia	01-Feb-1938
15	8.5	Atacama, Chile	11-Nov-1922
16	8.5	Kuril Islands, Russia	13-Oct-1963
17	8.4	Kamchatka, Russia	03-Feb-1923
18	8.4	Southern Sumatra, Indonesia	12-Sep-2007
19	8.4	Arequipa, Peru	23-Jun-2001
20	8.4	Honshu, Japan	02-Mar-1933

(b)

Fig. 1.1 – (a) Earthquakes with magnitude greater than 7.0 in South America since 1900. (b) Chilean earthquakes among the most intense earthquakes in the world since 1900 (USGS 2019)

This seismic context makes earthquakes the main hazard faced by most structures in Chile, what has encouraged the adoption of a particular lateral-force-resisting system for multistory residential buildings based virtually on Reinforced Concrete (RC) shear walls only. These

elements are widely implemented in other seismic prone regions, as they are very efficient in providing lateral strength and stiffness. However, in other countries, typical RC wall buildings have few walls, and these are combined with RC frames to carry gravity loads, while internal partitions are made with masonry or drywall. This conventional configuration is also used in Chile but only in office buildings, whose architectural layouts vary from floor to floor. On the other hand, residential RC wall buildings in Chile are virtually based on RC walls only to carry gravity and seismic loads, and frames are rarely observed. This configuration produces stiffer structures with a large number of RC walls, which are located along the corridors, around elevator shafts and as partitions between the apartment units (in-apartment partitions are typically drywall). In Chile, technically all the residential buildings higher than 5-stories are based on this "pure" RC wall system.

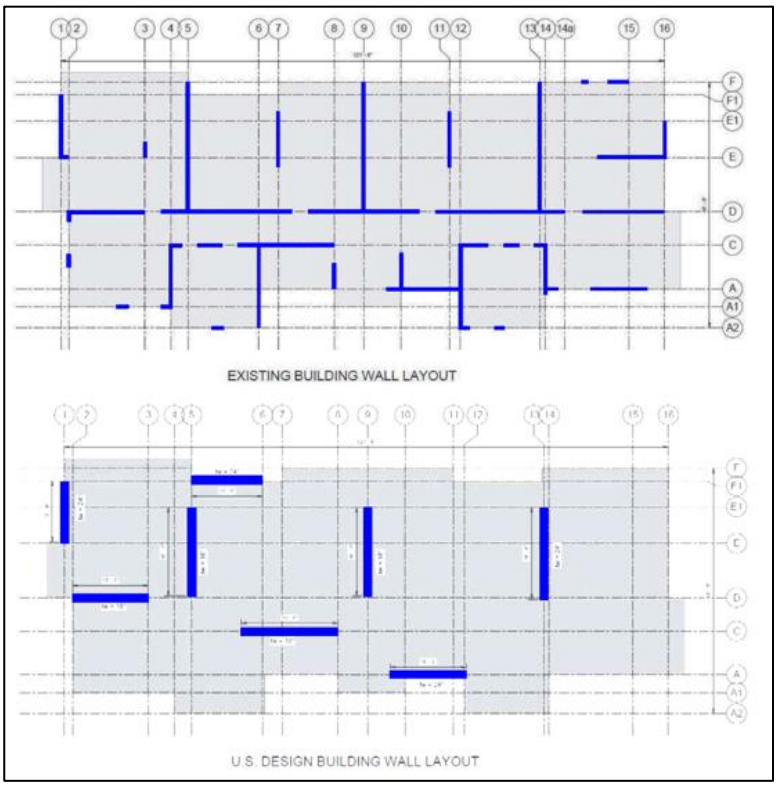

Fig. 1.2 – Comparison of an existing Chilean residential layout with an equivalent U.S. design (NIST 2012)

Fig. 1.2 shows the layout of an existing Chilean residential building and an equivalent U.S. design (NIST 2012). Notice in the Chilean layout that having many walls in both directions produces several non-planar walls, i.e., walls with non-rectangular cross-section shape, while the U.S. design has only planar walls. Having many walls also leads to a better distribution of stiffness along the story plan, and it makes it possible to have thinner walls than the U.S. design.

Unlike typical tall wall buildings elsewhere, the residential buildings in Chile usually do not have elements explicitly intended to provide coupling between walls, making the building to behave as a cantilever (although some unintended coupling is provided by slabs as commented later). Because of this particularity and the ones commented above, the behavior of Chilean residential wall buildings might show some differences from that of a conventional wall building, for instance, in terms of stiffness.

The Chilean experience with residential wall buildings has been in general satisfactory, as these structures have shown positive performance in past earthquakes, particularly in the 1985 Algarrobo earthquake (M_w 8.0), where the little damage observed was linked with the adecuate response of wall buildings (Wood 1991). This satisfactory performance validated the Chilean practice of that time regarding RC wall design that, as another relevant distinction did not require special boundary elements to provide confinement. In other aspects of wall design, the Chilean practice was quite similar to that prescribed by the American Concrete Institute. This is partly because in 1983 the Chilean engineering community informally adopted the provisions of ACI 318 (ACI 1983) over the outdated Chilean RC design codes NCh429 and NCh430 (INN 1957, 1961). This adoption became official when the Chilean seismic loading code NCh433 (INN 1993) referenced ACI 318 (ACI 1989) for RC design but excluding the wall boundary confinement requirement. This was confirmed in the next version of NCh433 (INN 1996a) that updated the referred version of ACI 318 (ACI 1995). In 2008 an updated version of NCh430 (INN 2008a) was released, becoming the official reference for RC design. This code again referenced ACI 318 (ACI 2005a) but this time, the omission of boundary confinement was removed.

On the early morning of February 27th, 2010 the 2010 Chile earthquake (8.8 M_w) struck the central-south regions of Chile where the largest cities are located (i.e. Santiago, Concepción and Viña del Mar). This megathrust earthquake, the sixth largest recorded in the world (Fig. 1.1b) and the subsequent tsunami caused more than 500 deaths (181 related to tsunamis according to the Chilean government) and some USD 30 billion in economic losses (Siembieda et al. 2012). Bearing in mind that by the time of this earthquake the updated NCh430 was recent, virtually all the existing residential buildings matched the description commented in the previous paragraphs. This is a large pool of typical Chilean residential buildings, given that the country experienced a construction boom of apartment towers since the 1990s. During this time however, some characteristics of the building inventory changed, as new constructions are taller and more slender (Junemann et al. 2015). These new configurations contributed to the fact that the damages observed in 2010 were certainly greater than those due to the 1985 earthquake, but this was also due to the fact that the magnitude of the 2010 earthquake was much greater.

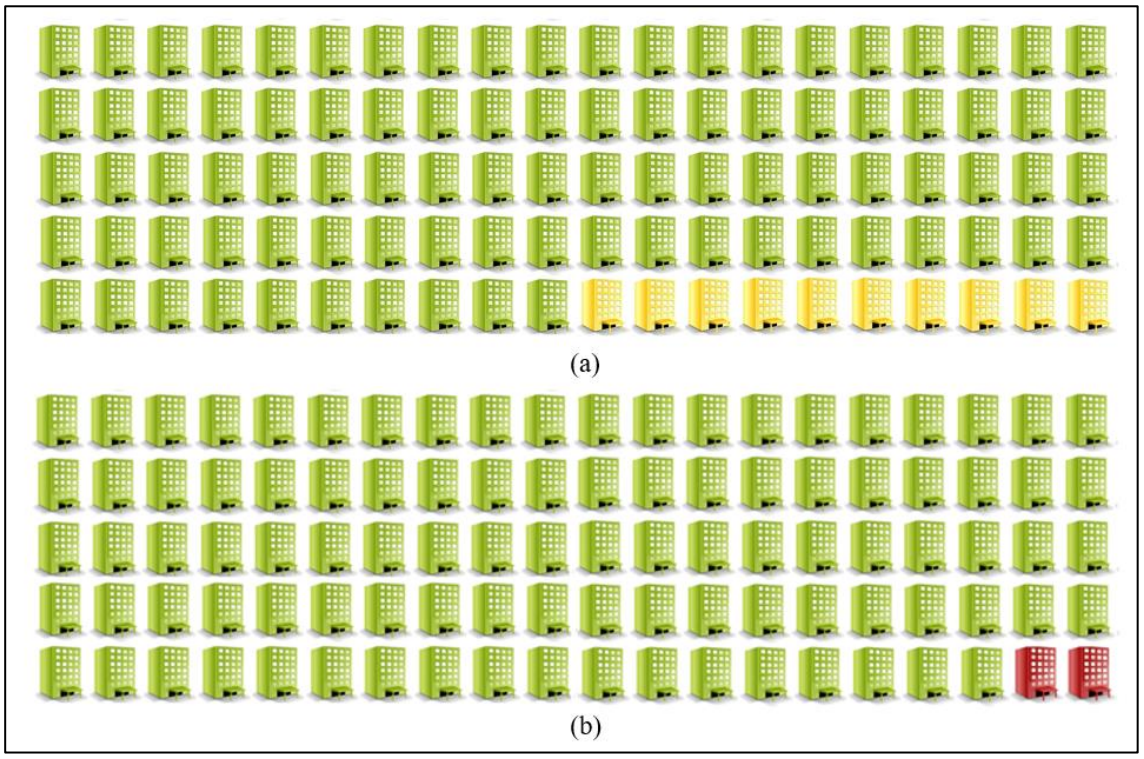

Fig. 1.3 – 2010 Chile earthquake: percentage of (a) buildings taller than three stories with some damage (Bonelli et al. 2011) and (b) buildings taller than nine stories with severe damage (Massone et al. 2012)

The reasons and implications of the damage due to the 2010 Chile earthquake have been extensively addressed in the literature (Carpenter et al. 2011; Rojas et al. 2011; Wallace et al. 2012; Westenenk et al. 2012 among others) and have motivated changes in the design codes (MINVU 2011a, b). However, considering the numerous buildings subjected to this strong earthquake, the percentage of damaged buildings was actually small. For instance, statistics shown in Fig. 1.3 say just 10% of buildings taller than three stories suffered some level of damage (Bonelli et al. 2011) and only 2% of the buildings taller than nine stories suffered severe damage (Massone et al. 2012).

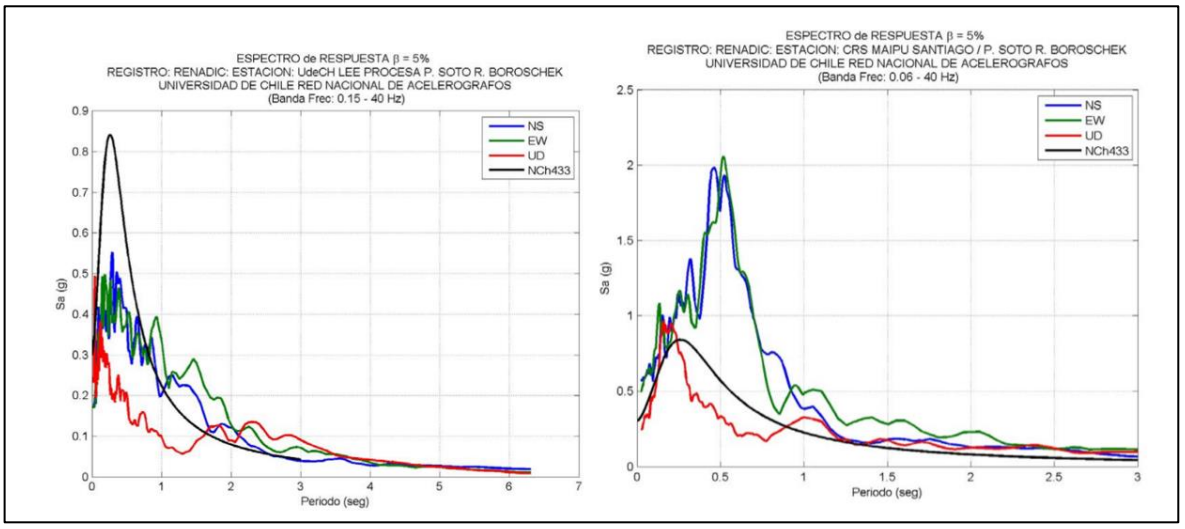

Fig. 1.4 – Elastic response spectrum of three components (NS, EW and UD) of 2010 Chile earthquake in stations Santiago Centro (left) and Maipu (right) compared with the elastic design spectrum of NCh433 (Boroschek et al. 2010)

It is acknowledged that even the little damage illustrated in Fig. 1.3 has an economic and social impact. However, it represents a satisfactory behavior of the building inventory, that again has been linked to the good performance of the Chilean wall system and design code (Saito et al. 2011). In Santiago for instance, where recorded ground accelerations exceeded the design prescribed accelerations in some stations (Fig. 1.4), most of the buildings did not show noticeable damage (Naeim et al. 2011). This performance is particularly good considering the design principles behind modern codes, that set the seismic demand based on an elastic response spectrum (intended to represent a severe rare event) reduced by a factor that accounts for nonlinear response of the structure. If the actual demand exceeds this reduced design demand, the structure is expected to have inelastic incursions that would produce structural damage. However, most of the buildings subjected to the 2010 Chile earthquake had no evidence of such incursions despite of the scenario shown in Fig. 1.4, where even the elastic design demand was exceeded.

The little extension of damage produced by ground accelerations larger than those prescribed for design suggests that Chilean buildings may have an important reserve of strength beyond

what is required by the code, i.e. they have a large overstrength. This is a recognized property of structures in general, studied mainly in the 1990's by several researchers who proposed some possible sources (Table 1.1), including the following:

- Higher strength and hardening of materials.
- Lower gravity loads than that considered in the design.
- The safety margin provided by load and resistance factors.
- Drift requirements that lead to members larger than necessary for strength design.
- The neglected strength and stiffness contribution of non-structural components such as interior partitions.
- Ductility requirements such as confinement, as it increases the strength of concrete and adds longitudinal bars.
- The design for ultimate conditions of gravity or wind loads that for certain elements could be larger than the earthquake loads.
- Non-structural criteria that require larger or more resistant elements than necessary for seismic design, for example aesthetics, safety, acoustics or fire protection.
- More steel than required due to the modulation of the bars.
- Moment redistribution that reduces the demands on highly stressed walls.

While some of these sources increase member capacities, other contribute to the fact that the actual demand on structural members is lower than that analytically computed. For instance, the use of gross stiffness in RC members, the overestimation of the modulus of elasticity, the overestimation of live loads or the considerations for accidental torsion, among others. Some of these factors may eventually generate "understrength" (i.e., increase demand or reduce strength). For example, an increase in f'_c would lead to higher stiffness and, consequently, to higher seismic demands.

Some of the sources of overstrength can be attributed to the design code or to engineering practice of the country, and they could be analytically identified to quantify its approximate

contribution to the total strength. Unfortunately, such analyses are scarce in literature, particularly for the specific case of the Chilean residential wall buildings that, as commented above, have certain distinctions. This limited information motivates the analyses presented in this thesis that explore if the overstrength of Chilean buildings can explain the lack of damage after the 2010 Chile earthquake and how this overstrength is affected by analysis considerations. Besides, additional studies are presented with the motivation of analytically support the good performance empirically evidenced by these kind of buildings.

Table 1.1 – Sources of overstrength according to several researchers

Mitchell and Paultre (1994)	Jain and Navin (1995)	Park (1996)	Humar and Rahgozar (1996)
Non-structural elements	Earthquake Load factor	Higher f'_c and f_y	Higher f'_c and f_y
Ductility requirements	Lower Gravity Loads	φ Factors	Larger sizes than required
Loading cases (gravity / wind)	φ Factors	Larger sizes than required	More steel than required
Larger sizes than required	Higher f'_c and f_y	Compression in beams	Moment redistribution
More steel than required	Larger sizes than required	More steel than required	Non-structural elements
Story drift Considerations	More steel than required	Loading cases	Architecture
Higher f'_c and f_y	Ductility requirements	Moment redistribution	Concrete confinement

Because most of the Chilean residential wall buildings showed no evidence of inelastic incursions following the 2010 Chile earthquake, it is expected that a large portion of its overstrength is contained in the linear range. Under this initial premise, chapter 2 introduces the concept of elastic overstrength as the ratio of the elastic limit to the design base shear. This variable is thoroughly analyzed using linearly elastic models of actual residential buildings. On the other hand, nonlinear analyses are presented in chapter 3 in order to study the complete extension of the overstrength, i.e., the one including the nonlinear portion.

In recent years, Performance-Based Design (PBD) has emerged as a more rational methodology to assess the response of buildings, receiving increasing attention that is evidenced in Chile with the recent publication of local PBD guidelines (ACHISINA 2017). However, implementations of this methodology in the country (either in an academic or professional context) are limited in part because the complexity of nonlinear wall modeling and the intricate layout of buildings make the models cumbersome to develop and computationally expensive. In order to fill this gap and provide more insight into the response of Chilean wall buildings, further analyses are presented in chapter 3 using PBD metrics obtained from dynamic analysis.

Another methodology to assess the performance of structures is the probabilistic seismic fragility analysis. This is a robust tool that provides a wider perspective of the response at several levels of performance and seismic intensity. It also takes into account the uncertainty related to the structural behavior and the excitation. A fragility study requires extensive nonlinear dynamic analyses that, similarly to PBD, makes it impractical for tall residential wall buildings. Thus, a simplified approach is required in order to perform fragility analysis of Chilean residential buildings. This approach is presented in chapter 4.

1.2. Hypothesis

The Chilean inventory of residential wall buildings exceeds the expected seismic performance due to unintended sources of strength that are related to code provisions or analysis considerations. This sources and can be identified and quantified in order to have a more rational design.

1.3. Objectives

The analyses presented in this thesis are intended to meet the following objectives:

1. To investigate if the performance of Chilean residential wall buildings that showed no evidence of damage following a severe earthquake is a result of linearly elastic response.

2. To explore the reason for the lack of damage after the 2010 Chile earthquake in most Chilean residential wall buildings, using recent advanced techniques to assess their inelastic strength.
3. To quantify how the seismic fragility of Chilean residential wall buildings is affected by nonlinear response of certain components.

1.4. Methodology

This dissertation is organized in a paper format, i.e., each of the following three chapters is a transcription of a scientific paper submitted to or published in a Web of Science (WoS) journal. Only the abstracts and the conclusions of the papers are compiled and presented together in page V and chapter 0 respectively. Besides, each of the following three chapters is intended to fulfill one of the objectives presented in section 1.3. Then, the thesis methodology is presented following the outline of these chapters.

In chapter 2 (paper I), the overstrength contained in the elastic range of Chilean residential buildings is explored. For this, three actual residential buildings of 5, 17 and 26 stories located in Santiago, and with no evidence of structural damage after the 2010 2010 Chile earthquake were selected as study cases. Linearly elastic models of the buildings were developed in the software ETABS (CSI 2011). The initial models and design procedures were quite similar to those developed in a structural design office, i.e., Response Spectrum Analysis was performed to compute the code-prescribed demand and code formulae were used to compute shear and axial-bending capacities. Then, Capacity-Demand ratios of each wall were computed and the smallest value was taken as the elastic overstrength, i.e., the relative reserve of elastic strength beyond what is required by the code. For a demand larger than this reserve, the first element would have its nominal capacity exceeded. The elastic overstrength is used to scale the nominal capacity, represented by the design spectrum which then was compared to the 2010 Chile earthquake spectra.

After finding the first approach of the elastic overstrength, the models were modified taking considerations that are deemed more realistic than those taken in practice or required by the

code. Variations included the use of expected material capacities and the omission of load combinations among others. For each of the variations the influence on the elastic overstrength was quantified separately as well as all combined, to obtain (within the capabilities of linear models) a more realistic value of the elastic overstrength.

Finally, Demand-Capacity ratios were reevaluated using demands obtained from response history analysis (RHA) and capacities computed with state-of-the-art methodologies. Models with both, linear and nonlinear support springs were considered to evaluate the tentative foundation uplift.

In chapter 3 (paper II), the overstrength and the performance of residential wall buildings is analyzed using nonlinear techniques. For this, the two tallest buildings analyzed the previous chapter were fully modeled with nonlinear elements in the software PERFORM-3D (CSI 2016a). The wall model was validated reproducing experimental tests available in literature (Thomsen and Wallace 1995). The models were subjected to static nonlinear analysis (pushover) to find the overstrength. Then, several variations were performed in order to quantify how modeling issues could affect the computed value of overstrength. Besides, pushover curves were converted into an equivalent single degree of freedom in order to plot them in Acceleration vs. Displacement Response Spectrum (ADRS) format and compare the capacity with the demands recorded in the 2010 Chile earthquake.

The nonlinear models were also subjected to RHA using the 2010 Chile earthquake record of the station closest to the buildings. These analyses were intended to evaluate if analytical metrics are consistent with empirical performance. This metrics included story drift, capacity-demand ratios and material strains. Again models with and without foundation uplift were analyzed as this issue seemed to be relevant in linear analysis.

In chapter 4 (paper III) a fragility analysis of the buildings analyzed in the previous chapter is presented. Given the impractical time and computational resources required for running an Incremental Dynamic Analysis, the fragility curves were obtained using the approximate procedure SPO2FRAG (Baltzopoulos et al. 2017). This tool estimates fragility curves based

on results of a pushover analysis and some building properties. Three limit states were considered, namely immediate occupancy (IO), life safety (LS) and collapse prevention (CP), whose threshold values were taken from ASCE 41-13 guidelines (ASCE 2014). The procedure was validated reproducing the fragility analysis of a wall building available in literature (Araya-Letelier et al. 2019).

The nonlinear models used to obtain the input pushover curves for SPO2FRAG were the same developed in chapter 3. These models were used to perform sensitivity analyses of two variables that showed to be relevant in the pushover analyses of that chapter: the wall effective shear stiffness and the slab effective bending stiffness. Then, for each of the two buildings 4 models were developed with different values of wall shear stiffness and 5 with different values of slab bending stiffness. For each model, a pushover analysis was performed and then used to compute fragility curves, what allowed quantifying the influence of both effective stiffness in the fragility of the buildings. In order to properly compare the fragility curves these were converted from period-dependent intensity measure (spectral acceleration at fundamental period) into period-independent one (mean return period). The conversion was performed using seismic hazard curves for west Santiago.

In addition to the three journal papers composing this document, six conference papers were published, three of them in English (Ugalde and Lopez-Garcia 2017a, b; Ugalde et al. 2018) and three of them in Spanish (Ugalde and Lopez-Garcia 2017c; Ugalde et al. 2019a, b). These conference papers address the same topics that are developed with more detail in this dissertation and for the sake of brevity are not included in this document.

1.5. Results and contributions

Main results and contributions of this dissertation are briefly presented in this section. A deeper discussion is presented in the Conclusions (chapter 5).

The analysis presented in paper I (chapter 2) revealed that the three study cases comply with the code prescribed requirements in terms of story drift, wall shear capacity and wall axial-

bending capacity (Fig. 2.7). The three buildings met the drift requirements by a wide margin, showing that code limits would hardly influence the design of these kind of structures. The 5-story building also met force demands by a wide margin suggesting that the conventional layout for residential buildings in Chile (based on a large wall density) could be over conservative in low-rise buildings even when walls are detailed with minimum steel ratios. Because of this wide margin of code compliance, the 5-story building shows a large elastic overstrength that, when used to scale the nominal capacity (represented by the effective reduced spectrum) makes possible to reach the demands given by the 2010 Chile earthquake spectra (Fig. 2.5). On the other hand, the two taller buildings showed modest values of elastic overstrength, insufficient to justify the empirical good performance. The models were modified to better approximate (within the scope of linear analysis) the expected conditions of existing structures, avoiding the conservative approaches of the design process. Due to the particularities of each building, when variations were performed separately the elastic overstrength was either increased, reduced or remain essentially unaffected, but when all variations were applied together the elastic overstrength reported substantial increases ranging from 35 to 61% (Table 2.4).

RHA with 2010 Chile earthquake records in these linear models produced shear and axial-bending demands much larger than the capacities given by conventional design procedures, what is inconsistent with the evidence. Much larger wall shear capacities were obtained with an alternative procedure (Krolicki et al. 2011), which reduced shear demand/capacity (D/C) ratios to values smaller or slightly greater than the maximum acceptable value of 1.0 (Fig. 2.10). On the other hand, computing the axial-bending capacity of walls with a more sophisticated procedure that accounted for the non-planar sections of walls (Fig. 2.12) showed D/C ratios quite similar to those obtained with the simplified planar assumption commonly adopted in design offices (Fig. 2.13). In the two taller buildings, most of these D/C ratios were larger than 1.0. Upon examination, it was found that the reported failures of these walls were produced by tension or low compression forces (Fig. 2.12). Further examination at the base of the walls showed that during the RHA with the 2010 Chile earthquake many walls reported unrealistic tension forces (Fig. 2.14). This motivated to

perform nonlinear RHA where the only nonlinear elements were the support springs which had no tension stiffness. In these nonlinear analyses the shear and axial demands reported a significant reduction leading to D/C ratios still large but reasonably acceptable and more consistent with the lack of noticeable damage (Fig. 2.10 and Fig. 2.13). The foundation uplift reported in the nonlinear models are smaller than 15mm (Fig. 2.17) and the story drift ratios are still within acceptable values (Fig. 2.9) suggesting the foundation uplift was at least feasible. It is momentarily concluded that either (a) foundation uplift did occur and played a crucial role in the protection of residential RC wall buildings or (b) despite not showing evidence of structural damage, these buildings had non-linear incursions that make it unlikely to estimate their response with linear models. This conclusions will be re-evaluated with the results of nonlinear analysis of the following chapter.

In paper II (chapter 3) the results of assessing the performance of Chilean residential buildings using nonlinear analyses are presented. First, the nonlinear wall models were tested reproducing experimental results of single walls available in the literature. This validation (Fig. 3.4) showed that the selected model reproduces very well the local and global response of the planar specimen. On the other hand, larger differences are observed for the non-planar specimen but not significantly different from that obtained by more sophisticated models that have also been implemented in the literature to reproduce these test specimens. Then, the model was deemed acceptable.

The static pushover analysis performed in the 17-story building indicate overstrength values of 3.11 in the short direction and 6.34 in the long direction. Notice that this building has a long direction much stiffer than the short direction. For the 26-story building whose short and long direction are quite similar the overstrength was 2.03 and 2.12 respectively. From the modeling issues whose influence on the pushover analysis was assessed (Fig. 3.7), the soil-structure interaction (i.e. foundation uplift and soil flexibility) showed to be relevant only for the short direction of the 17-story building which is significantly slender and whose ultimate strength could be overestimated if soil-structure interaction is omitted. Other issue that affected the computed ultimate strength was the omission of slab elements, which

reduced the strength in all the analyses to approximately half of the model with slabs. The omission of slabs not only reduced the strength but also the stiffness of the models. Then, if the contribution of slabs was actually negligible, and the models without slabs were more realistic, these buildings should have shown extensive degradation during the 2010 Chile earthquake, what is not consistent with their empirical performance. It is then expected that the coupling effect provided by the stiffness of the slab elements played a relevant role in the good performance of these buildings and other similar structures. Other modeling issues analyzed with static pushover analysis, showed to have a negligible effect on the capacity or stiffness before the peak strength, as the influence of these issues was noticeable only after the onset of strength loss.

The RHA of nonlinear models of paper II showed that foundation uplift could have occurred, as the models with linear support springs develop tension forces unrealistically large at the base of the walls (Fig. 3.9). These forces dropped to almost zero when nonlinear compression-only supports are used and the foundation nodes are unrestrained to move upwards during the dynamic analysis. This finding is similar to that obtained with the linearly elastic models of paper I, however, unlike those models, the nonlinear models of paper II showed that foundation uplift produces negligible variations in the story drift ratios (Fig. 3.8) and the wall force demands (Fig. 3.13b).

When maximum total story drift ratio during RHA was analyzed it was found that several walls exceeded the limits linked with the onset of damage. However, a significant reduction is observed when analyzing the corresponding values of tangential story drift ratio, which accounts only for wall deformations and no rigid-body rotations (Fig. 3.11). Unlike total story drift ratio, the tangential story drift values were consistent with the lack of noticeable damage. As rigid-body rotations are not expected to produce structural damage in RC walls, the tangential story drift ratio was found to be a better indicator of wall performance.

The maximum compression and tension strains obtained during nonlinear RHA (Fig. 3.12) show that the limits linked with the onset of damage (i.e., concrete softening and steel

yielding) were exceeded at very few locations, even after adjusting the strains based on the results of the validation exercise. Similarly, the D/C ratios during nonlinear RHA (Fig. 3.13b) were larger than 1.0 only for the axial-bending response of 2 out of the 12 monitored walls. These results (i.e., strains and D/C ratios) indicate that the nominal capacity of some walls could have been exceeded even when no damage was noticed.

When the pushover curves were plotted in ADRS format along with the 2010 Chile earthquake spectra (Fig. 3.14), it was found that the demand curves intersect the capacity curve before the maximum strength is reached. At this intersection point the curves show a moderate stiffness degradation that leads to a significant period elongation. Then, the spectral accelerations of the 2010 Chile earthquake at the nominal design period, are quite larger than those at the elongated secant period and this was crucial for preventing the widespread of damage in these structures.

The results obtained with the nonlinear models of paper II allow reevaluating the preliminary global conclusions drawn with the linear models of paper I and commented a few paragraphs above. From those two possible conclusions, the conclusion (b): linear models are not capable of reproducing the response the undamaged study cases, seems to be the more accurate. In fact, the nonlinear response of the buildings during the 2010 Chile earthquake was necessary to analytically support their good performance. The other possible conclusion (a): foundation uplift did occur and played a crucial role in the protection of residential RC wall buildings, is just partially right, as the nonlinear models confirmed that foundation uplift is in principle feasible, but its influence in the performance was minimal.

Finally, paper III (chapter 4) presents the results of the fragility analyses approximated with the SPO2FRAG procedure. The validation of this tool using a wall building whose IDA data was available, showed good agreement between the actual and the approximated fractile curves for low to moderate story drift ratios, but not for collapse intensities (Fig. 4.8). Consequently, the matching of the actual and the approximated fragility curves was good

for IO and LS limit states, and moderate for CP limit state. Then, the procedure was deemed reasonably acceptable for the analyses intended here.

A large dispersion of values was found in literature for the wall effective shear stiffness (GA_{eff}) and the slab effective bending stiffness (EI_{eff}) and then, some of those values were selected for a sensitivity analysis. Both building models showed to be sensitive to the assumed value of these variables as noticed in the pushover curves (Fig. 4.9), in the period variations (Table 4.2) and in the fragility curves (Fig. 4.10 and Fig. 4.13).

Even though the validation exercise initially suggested that the procedure provides a good approach, the fragility curves obtained for the taller building (26 stories) indicate a large fragility that, for intensity levels similar to those of the 2010 Chile earthquake would implicate extensive damage. Given the good performance that this specific building showed in that earthquake, it is concluded that SPO2FRAG procedure has limitations to properly capture the response of tall buildings, as warned by the methodology developers.

On the other hand, the analysis on the 17 story building showed levels of fragility that are consistent with its empirical performance. It was found that once the fragility curves are presented with a period independent intensity measure (IM) that allow a direct comparison among the models (Fig. 4.13), there is less dispersion between the curves, meaning that the influence of wall GA_{eff} and slab EI_{eff} is moderate. Even so, the assumed value of wall GA_{eff} could still change the probability of exceeding the IO or the LS limit states in about 30%, while the influence in the CP limit state is marginal. The curves with different slab EI_{eff} virtually overlap with the clear exception of the model with no slab, whose probability of exceeding the LS and CP limit states is much larger than the rest of models. This confirms the observation of paper II about the relevance of the slabs for the seismic response of residential wall buildings. Surprisingly, once the bending stiffness of the slabs is accounted for (even with a low value of EI_{eff}) the reduction in the fragility is abrupt and virtually independent of the stiffness value.

2. PAPER I: AN ANALYSIS OF THE SEISMIC CAPACITY OF CHILEAN RESIDENTIAL BUILDINGS

2.1. Introduction

On February 27th, 2010 the south-central region of Chile was struck by a M_W 8.8 earthquake, one of the strongest in recorded history. Most (around 75%) of the Chilean population lives in the affected regions, which include the largest Chilean metropolitan areas (Santiago, Concepcion, and Valparaiso-Vina del Mar). The subduction-type earthquake (and the associated tsunamis) caused more than 500 deaths (181 related to the tsunami according to the Chilean government) and some USD 30 billion in economic losses due to damage and downtime (Siembieda et al. 2012).

In Chile, as in many other countries in the world, building structures are designed to withstand a *reduced* level of seismic forces, i.e., the elastic seismic demand is divided by a response modification factor (usually denoted R), the value of which depends mainly on the inelastic deformation capacity of the structure. Therefore, if the demand imposed by an actual earthquake is greater than the (reduced) design level, inelastic incursions are then expected. However, during the 2010 Chile earthquake only 2% of the buildings having 9 or more stories suffered significant damage (Massone et al. 2012) even though the elastic response spectra of many recorded ground motions are larger than the (reduced) design spectrum specified in the Chilean seismic design code. This observation is illustrated in Fig. 2.1, which shows the elastic response spectra of several ground motions recorded during the 2010 Chile earthquake in Seismic Zones 2 (medium level of seismic activity) and 3 (high level of seismic activity) along with the (reduced) design spectra for soil types II (intermediate) and III (soft) specified in the 1996 version of the Chilean seismic design code NCh433 (1996b). Much of the building inventory in 2010 was designed according to this code, which was still in effect at that year. The (reduced) design spectra shown in Fig. 2.1 are valid for Reinforced Concrete (RC) shear wall structures and for fundamental periods T_0 equal to 0.5 s and 2.5 s (the value of factor R is period-dependent in NCh433). The design spectrum for structures with periods between 0.5 s and 2.5 s lies between the spectra for

these two periods. The great majority of the 2010 building inventory was located in the area affected by the 2010 Chile earthquake, and the seismic zone, soil type and fundamental period of a very large percentage of such buildings are those considered in Fig. 2.1. It can be seen that most recorded spectral ordinates are much greater than the (reduced) design values. Nevertheless, unlike what can be expected in such situation, the number of damaged buildings was quite modest. These observations clearly indicate that the actual seismic capacity of Chilean RC multistory buildings is considerably larger than the capacity required by the Chilean seismic design code.

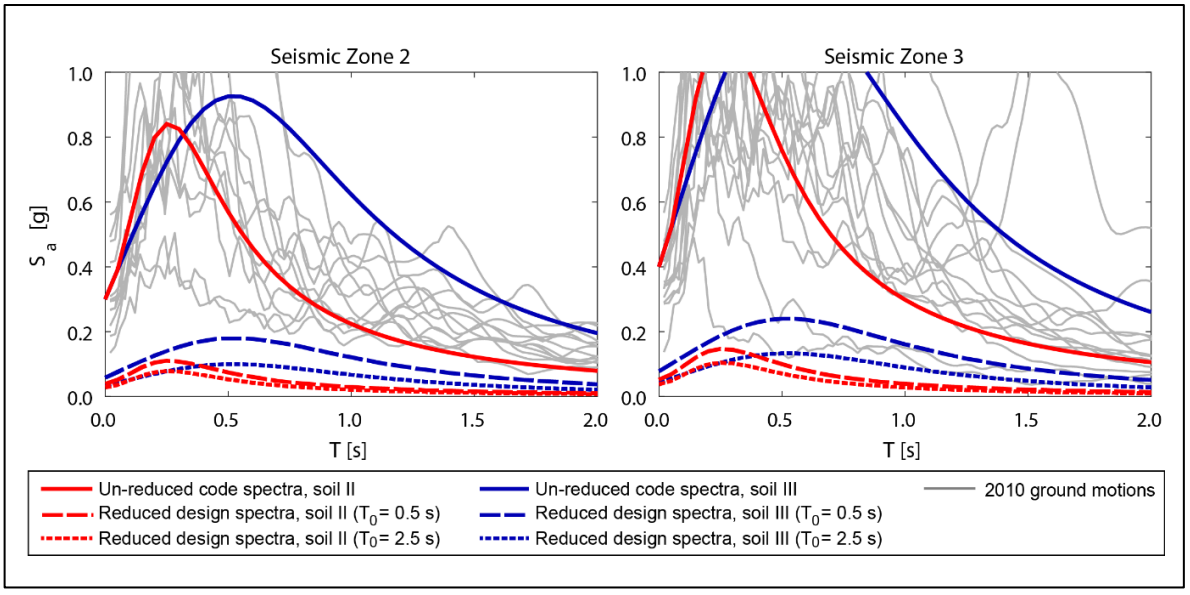

Fig. 2.1 – 2010 Chile earthquake: 5% damped recorded and design response spectra (fundamental period equal to 0.5 s and 2.5 s).

Following the 2010 Chile earthquake comprehensive research was carried out to analyze the observed damage (Carpenter et al. 2011; Rojas et al. 2011; Wallace et al. 2012). Linear analysis was performed to validate whether damaged buildings met code requirements (Westenenk et al. 2013; Alarcon et al. 2015) and sophisticated nonlinear models were developed to reproduce the observed failure modes (Telleen et al. 2012b; Parra and Moehle 2014; Junemann et al. 2016) and validate seismic retrofits (Sherstobitoff et al. 2012).

Statistical surveys of structural properties were carried out to analyze patterns related to the observed damage (Alarcon et al. 2015; Junemann et al. 2015), collapsed buildings were studied in detail (Hube et al. 2012; Song et al. 2012), and code-oriented analyses revealed the possible implications of the observed damage on future editions of seismic design codes in Chile and the United States (Wallace 2011; Bonelli et al. 2012). However, in spite of the good building performance mentioned before, little research on undamaged buildings was carried out.

Junemann et al. (2015) conducted a statistical analysis of the global properties of buildings subjected to the 2010 Chile earthquake, both damaged (36 buildings) and undamaged (7 buildings). The study found that while undamaged buildings turned out to be somewhat more flexible than damaged buildings, "most of the analyzed properties of undamaged buildings are very similar to those of damaged buildings". Junemann et al. (2015) is apparently the only study, to date, that includes some analysis of undamaged buildings. In order to fill this gap, the objective of this paper is to analyze the reasons for the good performance of RC buildings that undergone the 2010 Chile earthquake with no damage even though they were subjected to demands that were larger (much larger in many cases) than the capacity required by design provisions. The main motivation of this study is to get more insight into why the actual seismic capacity of typical Chilean RC shear wall multistory buildings seems to be larger than the capacity required by the Chilean seismic design code. Particular attention is paid not only to code requirements but also to assumptions and simplifications typical of Chilean professional practice.

An important question related to the analysis of RC buildings with no observable damage (i.e., presumed *undamaged*) is whether a linear concrete material model is appropriate or not. In favor of linearly elastic models it can be argued that the amount of inelastic deformations is likely to be very low (if any at all) in undamaged structures, and linearly elastic models are also attractive because they do not require neither sophisticated modeling techniques nor large computational efforts. In favor of nonlinear concrete material models, on the other hand, it can be argued that the stress-strain relationship of concrete is nonlinear

both in tension (i.e., cracking) and in compression (i.e., nonlinear behavior at low deformation levels), and such nonlinearity might significantly affect the overall structural response even in the absence of observable damage. Since, apparently, this issue has not been definitely settled in the literature (as mentioned before the literature focuses on damaged buildings rather than on undamaged structures), the authors of this paper are convinced that there is a need for a comprehensive study using linearly elastic models. For these reasons, a linearly elastic concrete material model is adopted in the study reported in this paper. This study, however, is part of a broader research project on undamaged buildings in which concrete behavior is modeled by both types of models (i.e., linearly elastic and nonlinear). Results obtained considering linearly elastic concrete behavior are the only ones reported in this paper. Results given by nonlinear concrete models will be reported elsewhere.

This study focuses on RC shear wall residential multistory buildings, which are representative of the Chilean building inventory. The sample set is made up of three actual buildings of 5, 17 and 26 stories located in Santiago, Chile. Code compliance was first validated according to the aforementioned Chilean seismic design code NCh433. Seismic demands were assessed by modal Response Spectrum Analysis (RSA) and by Response History Analysis (RHA). Axial-flexural and shear capacity of structural members were evaluated with different levels of sophistication. The relative relevance of several code requirements and modeling assumptions was evaluated. Results are presented mainly in terms of demand-to-capacity (D/C) ratios. Possible nonlinear soil-structure interaction was also considered.

2.2. Typical characteristics of pre-2010 Chilean RC buildings

While reinforced concrete shear walls are used all around the world, they are particularly relevant in Chile (a country where the level of seismic activity is high), where they have been the preferred structural system for residential buildings higher than five stories. Unlike what is typical in other countries, RC shear walls are usually not combined with frames,

braces, masonry infills or coupling beams in Chilean *residential* buildings. Consequently, RC shear walls perform as gravity system and as lateral force-resisting system as well, and no other structural members are intended to dissipate energy through inelastic deformations.

In Chilean *office* buildings, RC shear walls are indeed combined with RC frames and coupling beams, which results in structures having a seismic behavior different from that typical of residential buildings. This paper, however, focuses only on *residential* RC shear wall buildings, which comprise a very significant portion of the Chilean multistory building inventory (Instituto de la Construccion 2015). Typical Chilean residential buildings have a floor plan pattern referred to in the literature as "fish-bone" pattern (Wallace 2011; Westenenk et al. 2013). This pattern consists of long walls along the corridors and perpendicular walls at the boundaries between the apartment units (e.g., Fig. 2.4a and Fig. 2.4b). If the floor plan is square-shaped then the long corridor is situated around the wall core (e.g., Fig. 2.4c). In either case, it is important to notice that the "fish-bone" pattern is characterized by a significant number of L-, T- and C-shaped walls.

Chilean residential buildings are usually quite stiff due to their large wall density, being the wall density the ratio of the cross section area of the walls A_w to the floor plan area A_f. In Chilean residential buildings the wall density typically varies from 2.5% to 3.5% along each direction (a range that has remained fairly constant in the last decades) and was found typical of buildings both damaged and undamaged by the 2010 Chile earthquake (Massone et al. 2012; Junemann et al. 2015). Although other structural properties have also been found relevant (Lagos et al. 2012), large wall densities were particularly highlighted as the main reason of the good performance of buildings during the M_w 7.8, 1985 Valparaiso (Chile) earthquake (Wood 1991). Since structures affected by this earthquake were not provided with special confinement at wall ends, special boundary elements were subsequently deemed not necessary and were explicitly excluded when Chile adopted the ACI-318 provisions in 1996. Such exclusion was not reverted until 2008, which means that almost all pre-2010 Chilean RC buildings do not have special boundary elements at the ends of structural walls.

2.3. Elastic Overstrength

The lack of damage in most buildings during the 2010 Chile earthquake despite the large seismic demands (Fig. 2.1) suggests that the strength of Chilean buildings is much larger than that required by the design code. The existence of significant levels of strength beyond that nominally required is a well-known phenomenon called overstrength (usually denoted by Ω) and has been observed in structures built according to modern seismic design codes worldwide. Overstrength is a recognized property of engineered structures, and is sometimes explicitly accounted for in seismic design codes. For instance, ASCE 7-16 (ASCE 2017) requires that those elements not capable of safely resisting ground-shaking demands through inelastic behavior (e.g. diaphragm collectors) be designed for the reduced seismic forces multiplied by the overstrength factor.

Overstrength is most commonly defined as the ratio of the maximum strength (typically in terms of base shear) of the structure V_{max} to the design strength V_d, Eq.(1), and is typically illustrated in base shear vs. roof displacement curves (i.e., "pushover" curves) such as the ones shown in Fig. 2.2. It is important to note that in ductile structures the maximum strength V_{max} is usually developed well into the inelastic range.

$$\Omega = \frac{V_{max}}{V_d} \tag{1}$$

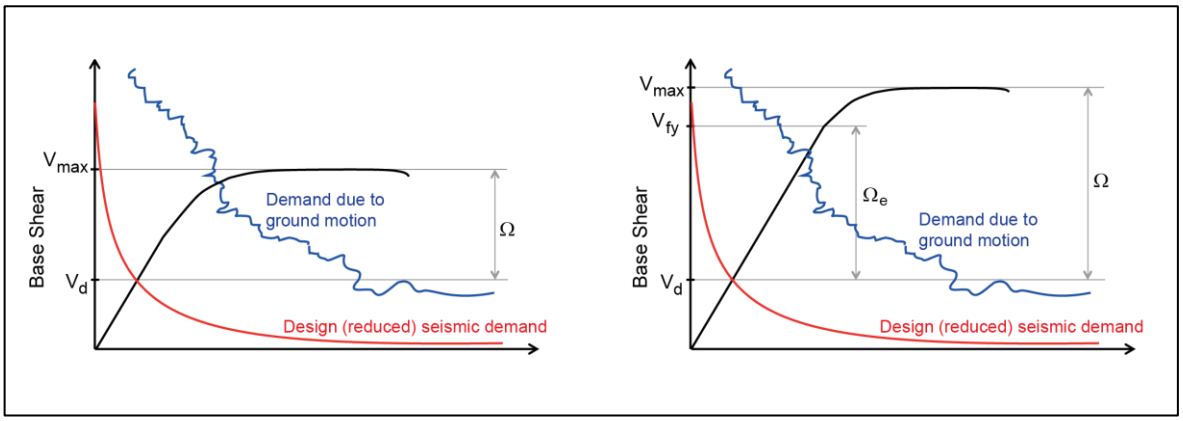

(a) (b)

Fig. 2.2 – Graphical representation through pushover plots of: (a) "standard" overstrength Ω; and (b) elastic overstrength Ω_e

Overstrength has been widely analyzed in the literature (Mitchell and Paultre 1994; Jain and Navin 1995; Humar and Rahgozar 1996; Elnashai and Mwafy 2002). The most commonly identified sources of overstrength are higher material strength, element sizes larger than required, conservative load combinations, contribution of non-structural elements, ductility requirements, strength reduction factors, moment redistributions, and others previously commented in section 1.1. The actual contribution of each of these factors, however, remains unclear. Consequently, the assessment of overstrength is affected by a large degree of uncertainty. For instance, Mitchell & Paultre (1994) (Mitchell and Paultre 1994) found values of overstrength varying from 2.1 to 4.6 in concrete frames, and values varying from 2.8 to 5.3 in concrete frame-walls. Humar & Rahgozar (1996) (Humar and Rahgozar 1996) found values ranging from 2.0 to 2.4 in steel frames. Elnashai & Mwafy (2002) (Elnashai and Mwafy 2002) found values varying from 2.1 to 2.5 in concrete frames and values ranging from 2.2 to 2.8 in concrete frame-walls. Jain & Navin (1995) (Jain and Navin 1995) found larger values (up to 15) in concrete frames. As it can be seen, the variability of Ω is large.

Although the values of overstrength found in literature seem to be large, the typical formulation given by Eq. (1) cannot fully explain the behavior of buildings undamaged by large earthquakes. Structures designed according to modern seismic codes are intended to

reduce the probability of collapse in the occurrence of a rare earthquakes, although it is accepted that they might undergo major structural damage. This is conceptually shown in Fig. 2.2a, where the demand curve of a severe earthquake intersects the pushover curve in the inelastic range (which means that the structure is damaged) at a "point" where the strength is less than V_{max}. Therefore, the traditional definition of overstrength is not useful to explain the lack of structural damage because a structure (particularly a ductile structure) might still suffer significant damage even if the demand does not force the structure to develop its maximum strength V_{max}.

What the authors of this paper believe is representative of buildings undamaged by the 2010 Chile earthquake is conceptually illustrated in Fig. 2.2b, where the demand curve intersects the pushover curve at a point that is beyond the code-required capacity (consistent with Fig. 2.1) but still within the elastic range (i.e., no damage, consistent with post-earthquake observations). In this perspective, it becomes clear that the relevant quantity is actually the *elastic* strength of the structure (denoted V_{fy} in this paper), i.e., the strength level at the onset of non-linear response. Consistent with this observation, a more useful (for the purposes of this paper) quantity is the ratio of the elastic strength V_{fy} to the design strength V_d, Eq. (2). Such quantity will be referred to in this study as *elastic* overstrength Ω_e, Eq. (2).

$$\Omega_e = \frac{V_{fy}}{V_d} \tag{2}$$

Conceptually, the elastic overstrength Ω_e is useful in that it indicates that damage occurs only when the seismic demand is greater than Ω_e times the nominal capacity V_d (i.e., the one required by the design code). Hence, the reasons why most Chilean buildings were not damaged by the 2010 Chile earthquake could in principle be found by identifying the sources of elastic overstrength Ω_e.

In this study, it is assumed that the structure develops its linear strength V_{fy} when the first structural member develops its nominal capacity (i.e,. strength reduction factor $\phi = 1.0$). Let C be the capacity of a given structural member, let D be the demand on the same structural

member when the structure is subjected to the design (i.e., reduced) seismic demand, and let D/C be the demand/capacity ratio of the same member. The first structural member that will eventually develop its full capacity should the seismic demand be greater than the nominal is then the structural member having the maximum value of the D/C ratio, and the inverse of such value is then directly equal to Ω_e, i.e.:

$$\Omega_e = \left[\max\left(\frac{D}{C} \right) \right]^{-1} \tag{3}$$

The elastic overstrength Ω_e is then computed using demands D given by linearly elastic analysis rather than by examining base shear vs. roof displacement curves given by nonlinear pushover analysis (as mentioned before a linearly elastic concrete material model is adopted in this study). It is important to note that in Eq. (3) D is the demand due to seismic loading only, whereas C is the remaining member capacity after the application of the gravity loads.

2.4. Case Studies

In this study, three actual buildings of 5, 17 and 26 stories were analyzed. They are representative of typical low-, medium- and high-rise Chilean RC shear wall buildings. All of them are apartment complex located in Santiago city (Fig. 2.3). Following the 2010 Chile Earthquake (8.8Mw), the buildings had immediate occupancy. A few days after the earthquake they were visually inspected by the structural engineering office in charge of the design and no visible damage was reported. It is acknowledged that small cracks (if any) may have opened and closed during the earthquake, and though such cracks would indicate some non-linear response, they can hardly be considered as damage.

All the vertical elements of the 5-story building (Fig. 2.4a) are RC walls of 150 mm thickness. These walls have only the minimum code-required longitudinal reinforcement for flexure. The 17-story building (Fig. 2.4b) has two columns at the basement levels but the rest of the vertical elements are walls of 150 mm and 170 mm thickness. Some retention walls of 200 mm thickness are located at the perimeter of the basement levels. The 26-story

building (Fig. 2.4c) is mostly made up of 170 mm thickness walls, but thicker walls (up to 250 mm) are located at the basement levels, either for shear or for soil retention. The thickness of the slabs in these buildings varies between 120 mm and 160 mm and typically have two layers of reinforcement. These and other building properties are summarized in Table 2.1. Typical of Chilean RC shear wall buildings all nonstructural partitions are light partitions of negligible stiffness.

The beams were not detailed as coupling beams in any of the buildings. Further, the structural models used in the actual design process (i.e., carried out at the structural engineering firm that designed the buildings) include moment releases at the ends of the beams. However, none of the beams in any of the buildings was damaged by the 2010 Chile earthquake. Values of wall density A_w/A_f are shown in Table 2.2. According to values of this parameter presented in the literature (Massone et al. 2012; Junemann et al. 2015), the buildings can be considered representative of the typical Chilean practice. None of the walls in any of the buildings has confinement detailing at the boundaries. Some relevant construction drawings of the buildings are presented in Appendix 1.

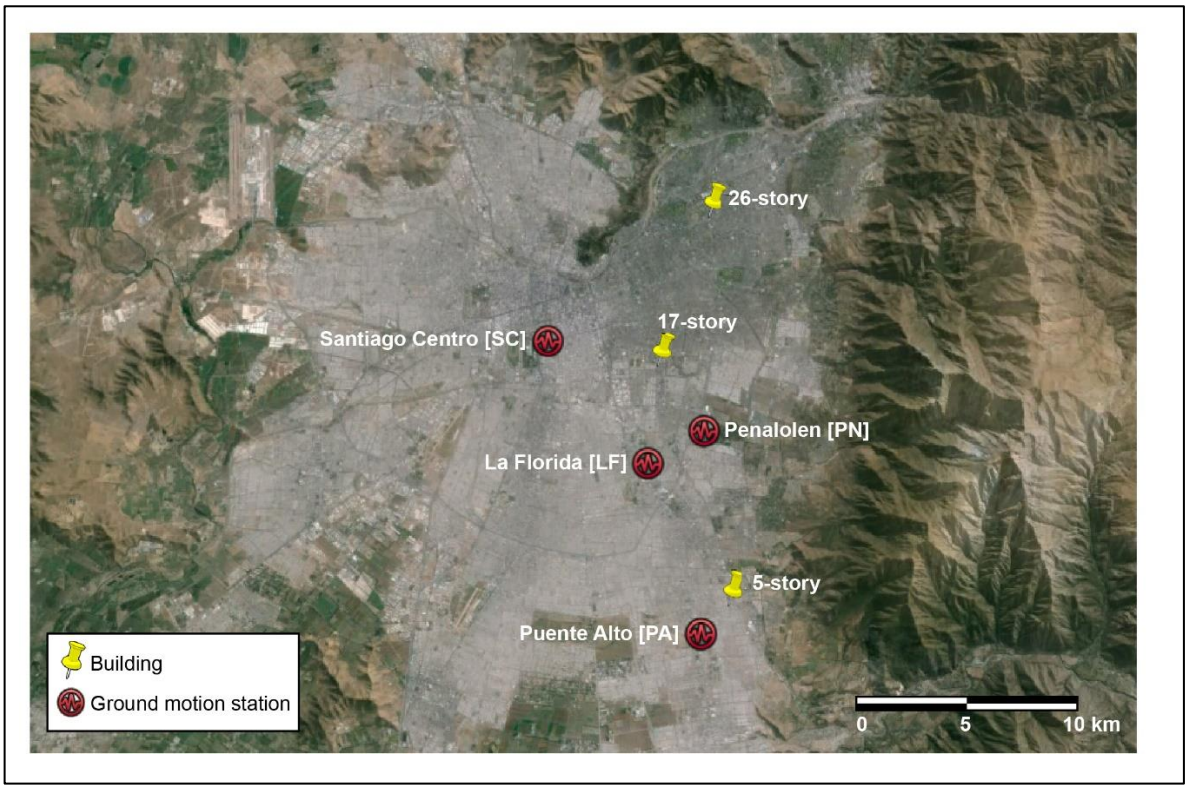

Fig. 2.3 – Location of the 3 buildings and the 4 stations in Santiago city.

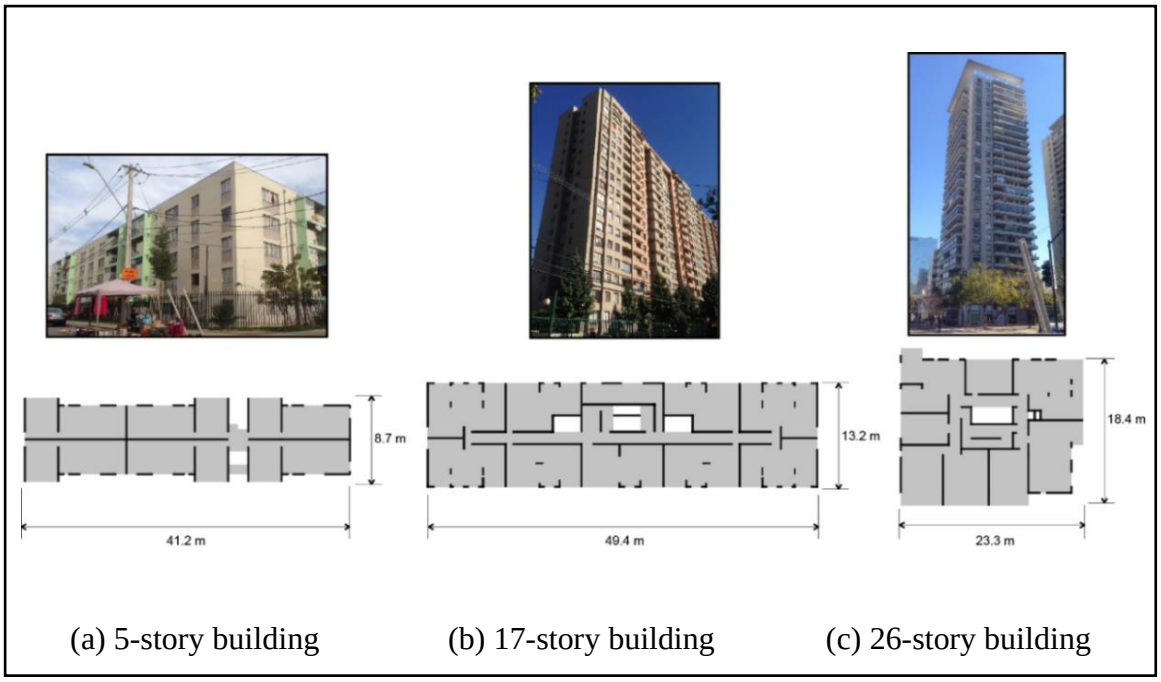

(a) 5-story building (b) 17-story building (c) 26-story building

Fig. 2.4 – Picture and typical floor plan of the three selected buildings.

Table 2.1 Geometric properties, seismic classification and nominal material properties

		Geometric Properties			Seismic Classification			Design Material Properties	
Building	Year	Basement Levels	Height [m]	Typical floor dimension [m]	Seismic Zone	Soil type*	Importance Factor	Concrete compressive strength [MPa]	Steel yielding strength [MPa]
5-story	2009	0	12.1	41.2 x 8.7	2	III	1	20	420
17-story	2006	2	42.2	49.4 x 13.2	2	II	1	20	420
26-story	2005	4	72.2	23.3 x 18.4	2	II	1	25	420

*: after the geotechnical report considered by the structural engineering office that designed the buildings

The buildings were designed in accordance with the 1996 edition of the Chilean seismic design code NCh433 (1996b). The design response spectrum in NCh433 is given by an

elastic spectrum divided by a period-dependent response modification factor R* (this and the following terms used in the estimation of seismic demand are shown in Table 2.2). The resulting spectrum is the so-called "reduced" spectrum. The corresponding reduced base shear demand on the structure (V_{base}) is then calculated by modal RSA. The value of this reduced base shear demand must lay within specified limits. For instance, the maximum base shear of the 5-story building is 12.6% of the seismic weight and the minimum for the other two buildings is 5.0%. These limits are based on engineering judgement as it is believed that the seismic demands predicted by the code NCh433 can be extremely high in stiff buildings and extremely low in the flexible ones. If the base shear does not lay within the minimum and maximum limits R* must be scaled until the base shear (again, calculated by modal RSA) comply with the required limits. The corresponding scale factor is presented as "Base Shear Adjustment Factor, K_{base}" in Table 2.2. The final value of the response modification factor due to such adjustment is then the effective response modification factor R_{eff}. In other words $R_{eff}= R^*/K_{base}$. As shown in Table 2.2, values of R_{eff} can be very different from those of R*. The design spectrum (reduced by R_{eff}) is used to assess story drift demands. Both the elastic spectra of NCh433 and the effective reduced spectra of the three buildings are shown in Fig. 2.5, where the nominal fundamental period of the structure (calculated as described at the beginning of Section 2.5) is indicated by a short-dashed vertical line. It must be noted that the maximum value of the horizontal axis is equal to roughly twice the value of the nominal fundamental period in all the plots of Fig. 2.5 (the other curves presented in Fig. 2.5 are to be explained throughout the paper).

Table 2.2 - Summary of seismic design properties

Building	5-story		17-story		26-story	
Number of modes in modal analysis	5		12		12	
Direction	Long	Short	Long	Short	Long	Short
Modal participating mass ratio recovered	0.97	0.97	0.99	0.99	0.91	0.93
Nominal fundamental period T_o[(a)] [s]	0.11	0.25	0.47	1.1	1.39	1.62
Wall density A_w/A_f [%]	2.9	2.6	2.6	2.4	2.5	2.4
Code modification factor R*	2.30	3.52	7.45	9.46	9.89	10.13
Seismic base shear before adjustment V_{base} [% of seismic weight]	17.12	15.74	6.06	2.06	1.73	1.43
Base shear adjustment factor K_{base}	0.74	0.80	1.00	2.42	2.90	3.50
Seismic base shear after adjustment V_d [% of seismic weight]	12.6	12.6	6.1	5.0	5.0	5.0
Effective modification factor R_{eff}	3.13	4.41	7.45	3.90	3.41	2.89

[(a)] The basis for computing these nominal fundamental period is presented in the first paragraph of section 2.5.

Earthquake loads are multiplied by a 1.4 factor in all the LRFD seismic load combinations specified in NCh433 (note that such factor is usually equal to unity in other seismic design codes, e.g. (ASCE 2017)), and such load combinations are then used to calculate member internal forces. Thus, the actual seismic *force* demand is then given by the effective reduced spectrum multiplied by 1.4. Such demand is also shown in Fig. 2.5.

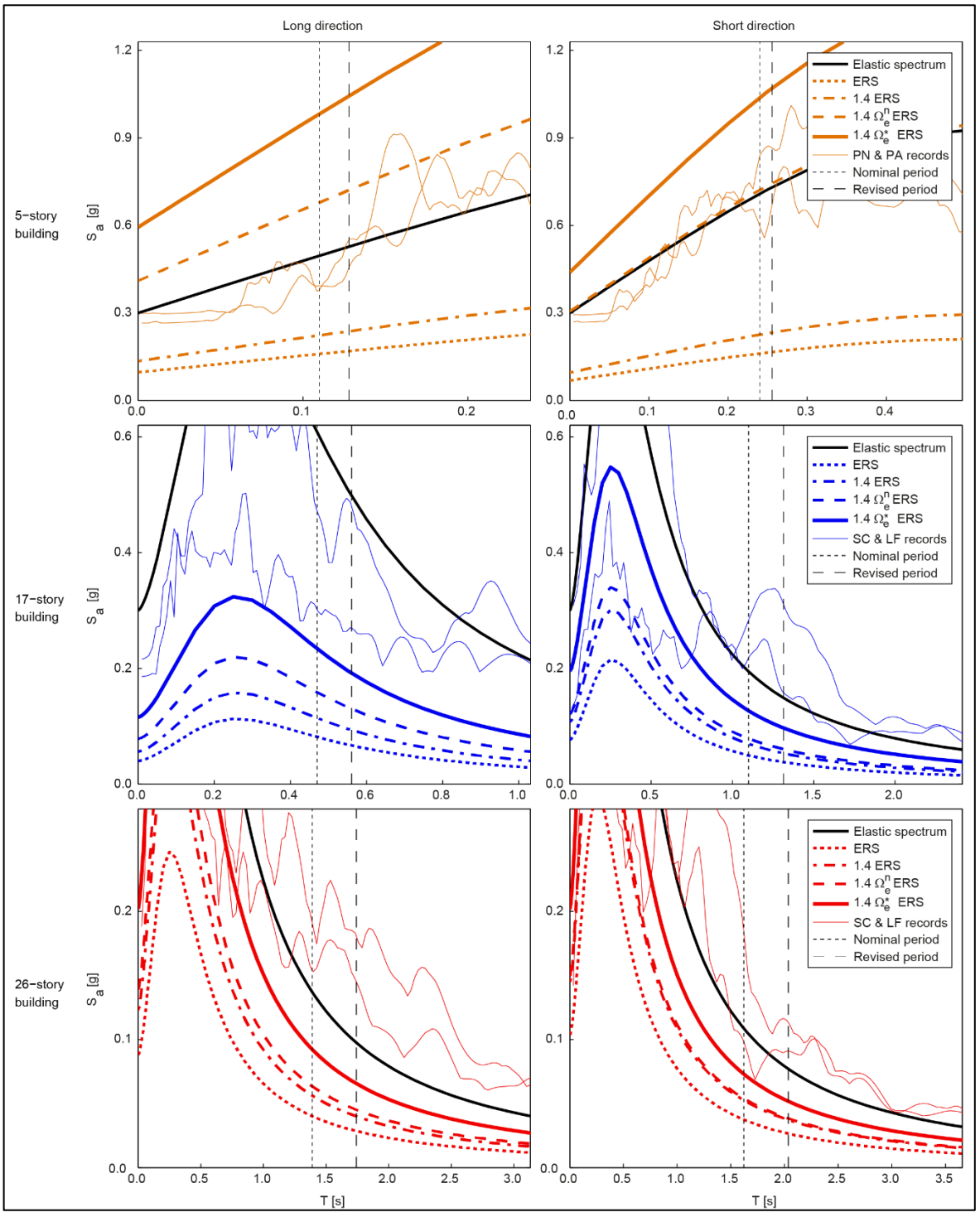

Fig. 2.5 – Response spectra 2010 Chile earthquake of ground motions, elastic design spectra and Effective Reduced Spectra (ERS) with and without scaling due to elastic overstrength.

Finally, Fig. 2.5 also shows the elastic response spectra of the ground motions recorded during the 2010 Chile earthquake that are assumed most similar to the ground motions the buildings were actually subjected to. Out of the ground motions recorded in Santiago on soil (not on rock) at locations close to the location of the buildings, two ground motions were selected for each building based on distance and soil type. The name and location of the stations are also shown in Fig. 2.3, and further information about the records is presented in Table 2.3. The records selected for each building are shown in the legends of Fig. 2.5. The epicenter of the city is 350 km from Santiago city, but the closest distance to the rupture is much smaller, about 150km. The records are corrected by baseline and a filter for high and low frequencies. It can be seen that whereas the elastic design spectrum is fairly similar to the spectra of the recorded ground motions, the ordinates of the effective reduced spectra (representative of the actual code-required capacity) are smaller (much smaller in most cases), particularly at the nominal fundamental period. This observation still applies when the effective reduced spectrum is multiplied by 1.4, which is representative of the seismic forces accounted for in the LRFD load combinations of NCh433. These remarks are consistent with what is illustrated in Fig. 2.1 (i.e., actual seismic demands larger than the code-required capacity in undamaged buildings), and is the main motivation of this study.

Table 2.3 – Properties of selected ground motions recorded during the 2010 Chile earthquake

Station	Code	Soil type*	PGA Nort-South [g]	PGA East-West [g]	Record duration [s]	Distance to 5-story building [km]	Distance to 17-story building [km]	Distance to 26-story building [km]
Santiago Centro	SC	II	0.21	0.31	205	13.3	4.8	9.1
Puente Alto	PA	II	0.27	0.27	147	2.0	11.9	18.3
Penalolen	PN	II to III	0.30	0.29	171	7.1	3.7	9.7
La Florida	LF	II	0.19	0.13	208	6.5	4.6	11.4

*: after the data reported in Kayen et al. (2014)

2.5. Validation of code compliance

The first part of this study consists of validating the design of the sample buildings. Structural models were then developed following the standard practice in Chile, i.e., models are tridimensional and include (when applicable) the basement levels, member shear and bending stiffness were based on gross cross-section properties (rather than on effective properties), walls and slabs were modeled with shell elements and therefore, they have in-plane and out-of-plane stiffness. Diaphragm constraints were incorporated at each floor level, and nonstructural partitions were not considered (they are light partitions of negligible stiffness). Following NCh433 mass properties were set equal to those consistent with 100% of the dead load plus 25% of the live load. Soil flexibility was accounted for by incorporating undamped linear vertical springs at the nodes located at the foundations (this feature is not always part of standard Chilean practice, it was incorporated into the models because so was done in the models used in the actual design process of the buildings). Some architectural features of the actual floor layouts of the buildings were slightly modified in order to simplify the structural models (for instance, walls having slightly separated parallel axes were assumed coaxial). Accidental torsion was included by applying a moment that is equal to the eccentricity defined in NCh433 (section 6.2.8) times the total lateral force applied to the diaphragm. This moment is applied at the diaphragm center of mass. The fundamental periods of these models are denoted "nominal fundamental periods" and are summarized in Table 2.2.

2.5.1. Story drift

Story drift compliance was checked according to NCh433, which establishes a limit for story drift ratio (structure subjected to the effective reduced seismic demand) at the center of mass (Δ_{CM}) equal to 0.002. Besides, to prevent excessive plan rotations NCh433 also establishes that the maximum story drift ratio at any location of a given story (Δ_{max}) cannot exceed Δ_{CM} at the same story by more than 0.001. Story drift ratios Δ_{CM} and Δ_{max} are shown in the left-

side plots of Fig. 2.7, being all of them much smaller than the acceptable limit. Hence, the design of the three buildings was not controlled by story drift requirements.

2.5.2. Shear forces on walls

In Chile the design of RC members is ruled by the Chilean code NCh430 (INN 2008a), which refers to ACI 318-05 (ACI 2005b) with some minor modifications. Thus, the shear capacity of the walls V_n was computed using equations from both Chapter 11 and Chapter 21 of ACI 318-05 considering the material strength indicated in Table 2.1 as well as a strength reduction factor $\phi = 0.6$.

Shear strength compliance is presented through D/C ratios so that Ω_e may be computed later using Eq. (3). As mentioned in Section 2, demands and capacities do not include the gravity loads. This is illustrated in Fig. 2.6a, where T indicates the total design demand on a given wall due to a given design load combination (e.g., 0.9 Dead + 1.4 Earthquake) and G indicates the demand on the same wall due only to the gravity portion of the same load combination (e.g., 0.9 Dead). Thus, $D = T - G$ and $C = \phi V_n - G$. For each wall, values of D and C were calculated considering each load combination. Results are summarized in the second column of plots in Fig. 2.7, which shows the largest D/C ratio (over all the load combinations) of each wall. It can be seen that the three buildings comply with shear requirements as all the D/C ratios are smaller than (at most equal to) unity. Unlike the two taller buildings, the walls of the 5-story building have small shear D/C ratios, i.e., no wall design in this building is controlled by shear demands.

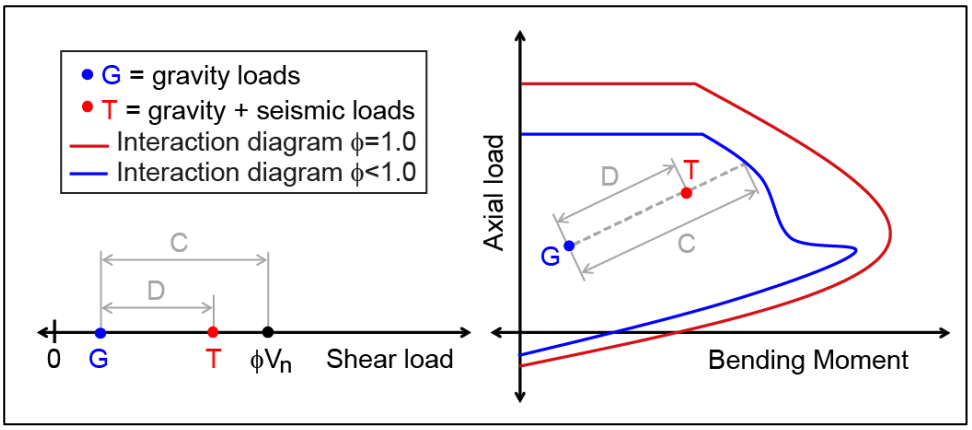

(a) (b)

Fig. 2.6 – Approach to calculate D/C ratios for (a) shear forces and (b) axial-flexural forces.

2.5.3. Axial-flexural forces on walls: the planar approach

Non-planar RC shear walls (i.e. walls made up of several non-parallel planar walls) may have many possible cross-sections (e.g., T, L, U or C shapes), some of them intricate. The plan views in Fig. 2.4 illustrate the variety of these possible shapes in Chilean residential buildings. Although the complex interaction between the legs of a non-planar wall is a well-recognized issue, such interaction is cumbersome to model when computing the axial-flexural capacity of non-planar walls in multi-story buildings. Because of this, structural design offices in Chile typically adopt a simplified approach, which consists of computing the capacity of each leg separately as a planar wall and then adding the corresponding steel areas at the leg intersections. This “planar approach” is believed to be conservative because the steel areas required by each leg are separately provided and then summed, though it is unlikely that they are required for the same load combination. Besides, the contribution of the steel bars in the wall flanges is not accounted for. More refined assessments are seldom performed, only when the planar approach leads to highly excessive amounts of steel. Thus, in accordance with standard Chilean practice, in this study the planar approach was initially

adopted to calculate the flexural-compressive strength of non-planar walls. The relevance of such simplification will be examined later.

Consistent with standard practice bending moments along the weak axis of a planar wall were then not accounted for. In the resulting axial-flexural 2D space, the demand due to a given load combination is a "point", and the capacity is given by a continuous curve. Thus, the values of D and C are not self-evident. In this study, values of D and C were calculated following the approach illustrated in Fig. 2.6b, where again point T indicates the forces on a given wall due to a given load combination, and G indicates the forces on the same wall due only to the gravity loads of the same load combination. The demand D is then the norm of the line between points G and T. This line is then extended until it intersects the interaction (capacity) curve, and the new norm (i.e., between G and the intersection point) indicates the capacity C. As for shear, with this approach D and C refer only to seismic loads.

The interaction curve used to validate the design was obtained using the nominal procedures of ACI 318-05 with specified (Table 2.3) material properties and strength reduction factors. For a given wall at a given story, D/C ratios were calculated for each load combination, and the largest values of each wall (over all the load combinations) is plotted in the right-side column of plots in Fig. 2.7. All the walls satisfy axial-flexural strength requirements as the D/C ratios are smaller than (at most equal to) unity. Again, the walls of the 5-story building have small D/C ratios, i.e., no wall design in this building is controlled by axial-flexural shear demands.

2.5.4. Summary

As expected, the three buildings considered in this study comply with the Chilean seismic design code NCh433, but some results obtained in the validation process are worthy of further comments.

The 5-story building comply with the seismic code requirements by a considerable margin. Upon further research it was found that such feature is a consequence of both architectural

requirements (e.g., the exterior walls of each apartment unit are structural walls) and constructability issues (e.g., it is difficult to build walls thinner than 150 mm). In other words, the larger than required seismic capacity of this building is not a consequence of issues related to either the seismic design code or the structural engineering practice.

Both the 17- and 26-story buildings, on the other hand, comply with the *strength* code requirements by a very small margin but comply with the *story drift* code requirements by a large margin. This result is somewhat surprising because it is widely believed in the Chilean earthquake engineering community that the story drift requirements of the Chilean seismic design code strongly influence (and in a positive way) the seismic design of Chilean tall buildings (Lagos et al. 2012).

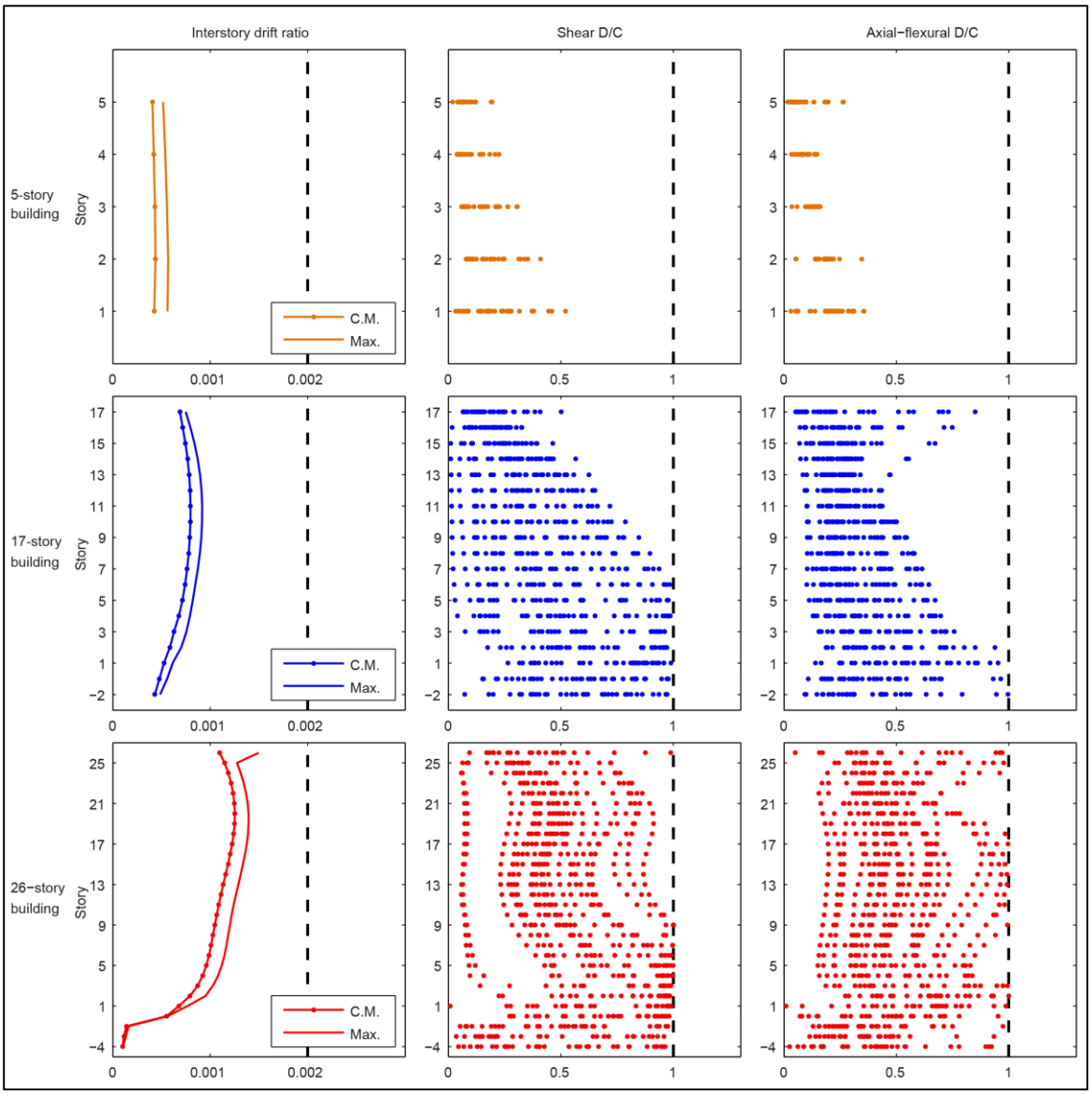

Fig. 2.7 – Validation of code compliance.

2.6. Elastic overstrength based on nominal assessments

A first evaluation of the elastic overstrength was calculated using Eq. 3. Initially demand D was set equal to the nominal demand described in Section 5, and capacities C were set equal to the capacities described in Section 5 but with strength factors ϕ equal to unity. In doing so, the resulting capacity is still based on nominal properties but is, nevertheless, closer to

the actual strength. Obviously, this modification leads to different values of shear and axial-flexural D/C ratios but story drift demands remain unchanged.

The elastic overstrength calculated as described in the former paragraph is denoted Ω_e^n, and values are shown in the first row of Table 2.4. It can be observed that the values corresponding to the 5-story building are significant, but those corresponding to the taller buildings are barely greater than unity. In terms of response spectra, the structural capacity associated with Ω_e^n is given by the effective reduced spectrum multiplied by 1.4 and by Ω_e^n. The resulting spectra are also shown in Fig. 2.5.

In the case of the 5-story building, it can be observed that the ordinates of the spectra associated with Ω_e^n are greater than those of the recorded ground motions in the long direction, and very similar in the short direction. This observation is consistent with the observed behavior of the building during the earthquake, and the reason for significant values of Ω_e^n are most likely the reasons mentioned in Section 5.4, i.e., wall thickness is larger than that required to comply with force demands because of architectural requirements and constructability issues.

In the case of the 17- and 26-story structures, on the other hand, it can be observed in Fig. 2.5 that the ordinates of the spectra associated with Ω_e^n are still (much) smaller than those of the recorded ground motions. In other words, building capacity associated with Ω_e^n is not enough to cope with the demands imposed by the 2010 Chile earthquake, which is *not* consistent with the observed response of these buildings. The most immediate explanation for such inconsistency is that either the demand or the capacity (perhaps both) is calculated in a very conservative way. In an attempt to identify the source of such conservatism the elastic overstrength was recalculated considering more realistic conditions of several issues that were identified (based on what is reported in the literature) as most likely to significantly influence the elastic overstrength. Other possible sources of overstrength, such as nonstructural components or concrete confinement, were not considered because they were deemed not relevant to the class of buildings analyzed in this study. The selected issues are

presented in the following sections and its influence is evaluated in terms of percentage variations of the elastic overstrength with respect to Ω_e^n. The corresponding values are reported in Table 2.4.

2.6.1. Accidental torsion

Like other typical modern seismic design codes, the Chilean code NCh433 includes accidental torsion provisions intended to account for possible eccentricities due to random variations in mass and/or stiffness properties. Such provisions lead to additional demands on members, especially on vertical members located at floor edges.

Although accidental torsion requirements provide a necessary degree of safety, actual accidental torsion of significant level is unlikely, especially in buildings having regular floor plans with lateral stiffness well distributed among several walls. The possible influence of accidental torsion is then assessed by reevaluating the D/C ratios without taking into account the accidental torsion when assessing the seismic demand (omission of accidental torsion changes demands D only, it does not change capacities C). The intention of this evaluation is not to question whether accidental torsion should be included in the analysis or not, but rather to evaluate its possible contribution to the elastic overstrength. All results reported in Table 2.4 are positive but nevertheless relatively small (less than 6%).

2.6.2. Concrete compressive strength

The average concrete compressive strength is actually greater than the specified (nominal) strength by a secure margin. In recognition of this reality, performance-based design methodologies allow the use of a concrete compressive strength higher than the nominal when realistically assessing the performance of buildings. The Los Angeles Tall Buildings Structural Design Council(LATBSDC 2015), for instance, recommends that f_c'(expected) = 1.3 f_c'(nominal) be used. Obviously such approach leads to different values of capacities C, and if it is further assumed that a higher value of concrete strength leads to a higher value of the modulus of elasticity, demands D change as well. This approach was adopted in this

study to reevaluate the elastic overstrength, and results are shown in Table 2.4. Surprisingly, higher concrete compressive strength has a negative effect in most cases. It was found that such decrease of the elastic overstrength Ω_e is due to the fact that a higher value of the modulus of elasticity leads to an increase in demands that is actually greater than the increase in capacities.

2.6.3. Steel yielding strength

Similar to what was mentioned in the former paragraph, the actual yielding strength f_y of steel rebars tend to be larger than the nominal. For instance, between 2006 and 2008 Chilean steel manufacturers reported mean test values of yielding stress that are 20% to 30% larger than the nominal values, and (LATBSDC 2015) recommends that f_y (expected) = 1.17 f_y (nominal) be used. This latter recommendation was adopted to recalculate values of the elastic overstrength. Results are summarized in Table 2.4, where it can be observed that a higher value of steel yielding strength always has a positive effect but not significantly large. It must be noted that a higher value of steel yielding strength leads to higher capacities C but does affect demands D. Certainly, higher values of f_y could increase shear demands on members where demands are calculated by capacity design principles, such as special moment frames or coupling beams, but there are no such kind of members in the buildings considered in this study.

2.6.4. Gravity load and seismic weight

The LRFD seismic load combinations specified in NCh433 are given by:

$$1.4 \cdot D + 1.4 \cdot L_r + 1.4 \cdot E \tag{4}$$

$$0.9 \cdot D + 1.4 \cdot E \tag{5}$$

where D, L_r and E are the dead, reducible live, and earthquake loads, respectively. As these combinations are intended to represent extreme load conditions, the elastic overstrength was

reevaluated using a load combination in which the gravity loads are more consistent with the expected loads during normal operation. In the selected load combination (Eq. (6)) the gravity loads are set equal to those recommended by the (LATBSDC 2015), i.e.:

$$1.0 \cdot D + 0.25 \cdot L + 1.4 \cdot E \tag{6}$$

where L represents the unreduced live load. Besides, the source of mass was also re-evaluated. According to NCh433 100% of the dead load plus 25% of the live load shall be used to compute the seismic mass of building structures. On the other hand, LATBSDC (2015) and (ASCE 2017) recommend not to include live loads in mass computation, and such recommendation was adopted in this study.

Loads and mass accounted for as described in the former paragraph led to the results shown in Table 2.4. As expected, more realistic gravity loads lead to higher values of the elastic overstrength. It is interesting to point out, however, that such an increase is not necessarily caused by a reduction of gravity loads (loads given by Eq. (6) are actually higher than those given by Eq. (5)). In fact, the elastic overstrength increases on one hand because lesser seismic mass lead to lesser seismic forces, and on the other hand because higher gravity loads leads to higher axial-flexural strength in walls (true only when the level of axial load is not too large, as on the walls of the buildings considered in this study).

2.6.5. Rigid diaphragm constraint

It is widely common in Chilean practice to incorporate floor diaphragm constraints at all floor levels when modeling multistory structures. In the case of concrete buildings this practice is justified on the basis that concrete floor systems have a large in-plane stiffness and essentially behave as rigid diaphragms. The main motivation of this practice is to reduce the number of degrees of freedom of the model, which in turn reduces the computational effort. However, as computer capabilities increase, reduction of computational cost is becoming increasingly irrelevant, and it is nowadays possible to explicitly model the floor systems.

Floor diaphragm constraints were included in the computer models used in the actual design of the buildings even though the slabs were explicitly modeled with shell elements. This is a common practice in Chile and its intention is to correctly calculate member forces due to gravity loads. Hence, in order to assess the possible influence of floor modeling, the floor diaphragm constraints were removed from the structural models and the elastic overstrength was reevaluated. Results (presented again in Table 2.4) show large dispersion, as they go from 17% for the 5-story building to -41% for the 26-story building, and are very small for the 17-story building. Removing the floor diaphragm constraints slightly changes modal shapes and periods, which could lead to changes in the internal demands on specific walls, particularly on those where internal forces are highly influenced by one of the modes. It must be kept in mind that, as presented in Eq. 3, the elastic overstrength value is derived from a single wall, i.e. the one with the largest D/C ratio, and then, this parameter can change drastically if that wall has a significant change of demand or capacity. These results indicate that the precise assessment of the influence of floor modeling might require more detailed research.

2.6.6. Modulus of elasticity

It is currently mandatory in Chile to use ACI 318 to estimate the modulus of elasticity of concrete, i.e. $E_c=4700\sqrt{f_c'}$ [MPa]. However, previous versions of the Chilean seismic design code had a different equation, namely $E_c=5900\sqrt{R28}$ [MPa], being R28 the cubic concrete strength at 28 days (but often confused with the cylinder strength f_c'). In particular, the buildings considered in this study were designed using the value of E_c given by the latter equation. Then, E_c was updated according to ACI 318 and values of Ω_e were reevaluated. Naturally, a smaller value of E_c increases the modal periods, which leads to larger nominal demands on the 5-story building but to smaller nominal demands on the taller buildings, as it can be deduced by observing the spectra shown in Fig. 2.5. Because of this, results shown in Table 2.4 are negative for the shortest building but positive for the taller structures.

2.6.7. Effective inertia of slabs

It is expected that small cracks develop in RC components even under service loads. Such cracks modify the effective flexural stiffness, which in turn change the overall stiffness of the building and hence the seismic demands as well. Besides, when the flexural stiffness of some components change so does the internal distribution of forces, which leads to different internal demands. Slab cracking effects are not accounted for in the Chilean seismic design code, although, they have been sometimes included in structural models after the 2010 earthquake. In particularly, the study cases of this study were designed using gross inertia (i.e., without reduction). Other seismic design codes do account for an effective slab inertia. For instance, ACI 318 suggests an inertia reduction factor for slabs of 0.25, i.e. I_g (expected) = 0.25 I_g. This approach was adopted in this study to reevaluate the elastic overstrength. As mentioned before, the slabs of the three buildings were modeled using shell elements, i.e. elements with both in-plane and out-of-plane stiffness. Naturally, the reduction of inertia was applied only to the latter.

Consideration of effective inertia of slabs reduces the overall building stiffness. For the same reasons mentioned in the former issue, a reduction in seismic forces on the taller buildings is then expected. However, results shown in Table 2.4 indicate that the elastic overstrength always decreases. Such effect might be due to the fact that the possible coupling effect provided by the slabs reduces when their flexural stiffness decreases, which leads to higher internal forces on the walls (i.e., increase in demands D).

- Effective inertia of walls

Effective inertia of walls is not accounted for neither in Chilean seismic design codes nor in Chilean practice. But again, ACI 318 suggests gross inertia reduction factors of 0.70 and 0.35 for uncracked and cracked walls, respectively. Proper consideration of such recommendation requires that a first analysis be performed with I (effective) = 0.70 Ig for all walls to identify uncracked and cracked walls, the latter being the ones in which tensile stresses are larger than the modulus of rupture f_r (also given by ACI 318). I (effective) = 0.35 I_g is then adopted for the latter, and the analysis is then repeated.

The elastic overstrength was reevaluated considering the effective inertia of walls described in the former paragraph. Results shown in Table 2.4 indicate that the elastic overstrength increases in all cases. Logically, flexural stiffness of walls as small as 35% of the gross cross section inertia leads to lesser internal forces on the walls, and so does the increase in modal periods due to reduced overall stiffness.

The values of the effective flexural inertia defined in the last two items for slabs and walls actually came from analysis recommendations made by MacGregor and Hage (1977) that were adopted by ACI 318-14 (Table 6.6.3.1(a)) and therefore, they are currently intended for factored load analysis. This values were deemed adequate in this study because (a) the seismic demands used in this and the following sections are similar or greater than that used for factored load design; and (b) this effective inertia values are not significantly different from others presented in the literature for the assessment of existing structures (ASCE 2014; LATBSDC 2015), as it will be shown later in this dissertation (Fig. 4.3).

2.6.8. Revised elastic overstrength Ω_e*

While the influence of each of the aforementioned issues was separately assessed, a more appropriate analysis is that in which all these issues are simultaneously accounted for, which is more realistic (i.e., the most likely scenario). The corresponding results are also shown in Table 2.4, and the resulting revised elastic overstrength is denoted Ω_e^*. Surprisingly, while most analysis/modeling issues have, by themselves, a marginal (and sometimes negative) influence on the elastic overstrength, all of them together lead to an average 46% increase with respect to Ω_e^n. Besides, it can be easily observed that the change with respect to Ω_e^n due to all issues together differs sharply from the simple sum of the changes due to each issue separately. The most drastic example of this difference appears in the short direction of the 26-story building: some issues, separately, lead to negative changes as large as -41% but the change due to all issues together is equal to +35%.

Table 2.4 – Values of Ω_e^n and Ω_e^* and individual percentage variations due to several analysis/modeling issues

		5-story		17-story		26-story	
		Long dir.	**Short dir.**	**Long dir.**	**Short dir.**	**Long dir.**	**Short dir.**
Nominal Ω_e^n		3.04	3.20	1.39	1.13	1.13	1.03
Percentage variation with respect to Ω_e^n	No accidental torsion	6%	5%	3%	1%	2%	2%
	Expected f_c'	-1%	8%	-7%	-11%	-4%	-7%
	Expected f_y	13%	8%	7%	8%	8%	7%
	Expected grav. load/mass	13%	8%	5%	9%	16%	13%
	No diaphragm constraint	5%	17%	0%	0%	-4%	-41%
	E_c according ACI 318	-1%	-3%	6%	4%	9%	8%
	Reduced slab inertia	-3%	-3%	-27%	-9%	-3%	-31%
	Reduced wall inertia	9%	4%	10%	22%	17%	17%
	All criteria combined	45%	44%	47%	61%	45%	35%
Revised Ω_e^*		**4.40**	**4.60**	**2.05**	**1.82**	**1.64**	**1.39**

Values of Ω_e^* shown in Table 2.4 tend to decrease with increasing building height and fundamental period. This trend is consistent with trends identified in values of "standard" overstrength Ω reported by Jain & Navin (1995) and Humar & Rahgozar (1996).

Table 2.5 – Values of nominal and revised fundamental period, and its percentage variations due to several analysis/modeling issues

		5-story		17-story		26-story	
		Long dir.	**Short dir.**	**Long dir.**	**Short dir.**	**Long dir.**	**Short dir.**
Nominal T_0	[s]	0.11	0.25	0.47	1.10	1.39	1.62
Percentual T_0 variation	No accidental torsion	0%	0%	0%	0%	0%	0%
	Expected f_c'	-4%	-2%	-6%	-4%	-6%	-6%
	Expected f_y	0%	0%	0%	0%	0%	0%
	Expected grav. load/mass	-3%	-3%	-3%	-3%	-3%	-3%
	No diaphragm constraint	3%	2%	2%	1%	3%	4%
	E_c according ACI 318	6%	3%	10%	8%	11%	11%
	Reduced slab inertia	2%	1%	6%	9%	9%	8%
	Reduced wall inertia	9%	2%	11%	9%	11%	12%
	All criteria combined	14%	4%	20%	19%	25%	26%
Revised T_0	[s]	**0.13**	**0.26**	**0.56**	**1.31**	**1.74**	**2.04**

The fundamental period of the models in which all of the aforementioned analysis/modeling issues were considered is denoted "revised" period (i.e., consistent with revised elastic overstrength Ω_e^*). Values are summarized in Table 2.5 and are also indicated by long-dashed vertical lines in Fig. 2.5. It can be observed that revised periods might be as large as 26% longer than the nominal periods.

Finally, the building capacity associated with Ω_e^* is that given by the effective reduced spectra multiplied by 1.4 and by Ω_e^*. Such spectrum represents the maximum seismic demand under which member forces are less than (at most equal to) member capacities. The resulting spectra are deemed the most accurate assessment of the building capacity that is possible to achieve with nominal procedures, and are also shown in Fig. 2.5. It is recalled that in all these nominal analyses seismic loads are obtained by modal RSA, and are combined with the gravity loads as indicated by the load combinations. In the case of the 5-story building it can be observed that the ordinates of the spectra associated with Ω_e^* are well above those of the recorded ground motions, which again is consistent with the observed

behavior. In the case of the 17- and 26-story buildings, however, it can be observed that the ordinates of the spectra associated with Ω_e^* are still smaller than those of the recorded ground motions, which, again, is *not* consistent with the observed response of these buildings. This observation indicates that assessments of the elastic overstrength (and, consequently, of the building capacity) based on nominal procedures properties (even when considering realistic values of relevant quantities) is not accurate enough for structures similar to the 17- and 26-story buildings.

2.7. Response of the buildings during the 2010 Chile earthquake

In an attempt to overcome the inconsistencies described in the former paragraph, a different analysis approach is adopted in this section. Firstly, demands are obtained by modal RHA considering the recorded ground motions deemed most similar to the ones the buildings were actually subjected to during the 2010 Chile earthquake. In doing so, demands are then representative of the actual demands imposed by the 2010 Chile earthquake, as opposed to the nominal (i.e., associated with code-type response spectra and obtained by modal RSA) demands considered in the former section. Secondly, shear and axial-flexural capacities are evaluated considering procedures associated with the state of the art rather than the nominal, more related to the state-of-the-practice procedures considered in the former section.

After an extensive literature survey it was decided to evaluate the shear capacity of the walls based on the model proposed by Krolicki et al. (2011). This model is based on the model formerly presented by Kowalsky and Priestley (2000) and was calibrated with experimental data of walls with shear failure modes. The Krolicki et al. (2011) model is more sophisticated than the design-oriented ACI 318 shear strength equations because it considers the contribution of longitudinal steel, introduces a variable cracking angle proportional to shear span, and includes the effect of displacement ductility demand. For instance, several shear wall tests have shown that the ACI 318 equations underestimates the shear capacity of walls with low displacement ductility (Moehle 2014). This effect is accounted for in the Krolicki et al. (2011) model and therefore this model is deemed suitable for the buildings analyzed in

this study as their unconfined walls are expected to have low displacement ductility. According to Krolicki et al. (2011) the shear capacity of walls V_n is given by the sum of three contributions: the one due to concrete (V_C), the one due to horizontal steel (V_S), and the one due to the axial force (V_P). Given that the walls have no confinement detailing, the displacement ductility factor was set equal to 0.29 (value for low ductility walls, in MPa units). The experimental data used to calibrate the Krolicki et al. (2011) model did not include walls in tension (which are difficult to test and scarcely analyzed in the literature), for which V_P becomes negative. Therefore, the minimum value of V_P was set equal to zero, a limit that controls for walls in tension. As bending moments and axial and shear forces take different values at each instant, shear capacities were evaluated at each time step of the RHAs.

Moment-curvature analyses were performed to assess the axial-flexural capacity of the walls. The analyses were performed with OpenSEES (McKenna et al. 2000) using fiber models. Nonlinear material models available in OpenSEES were used to account for strength and stiffness degradation. Material properties are equal to those considered when the revised elastic overstrength Ω_e^* was evaluated in Section 2.6. Concrete was modeled using the Concrete02 material model (Yassin 1994), Fig. 2.8a, and was assumed unconfined because no confinement is provided in any wall. Steel was modeled using the Steel02 material model (Filippou et al. 1983), and the backbone curve was adjusted to match that of typical Chilean steels (Alarcon 2013), Fig. 2.8b. For each wall crosbs-section several moment-curvature analyses were performed considering different values of axial loads. Bidimensional axial-flexural interaction diagrams were then obtained by plotting the flexural capacity versus the corresponding axial load.

The structural models are the same models used to evaluate the revised elastic overstrength Ω_e^* in Section 2.6, including the gravity loads and the seismic weight. Both horizontal components of each ground motion were applied simultaneously. The number of modes used in the modal RHA and the recovered mass are shown in Table 2.2. Modal damping was set to 5.0% for all the modes.

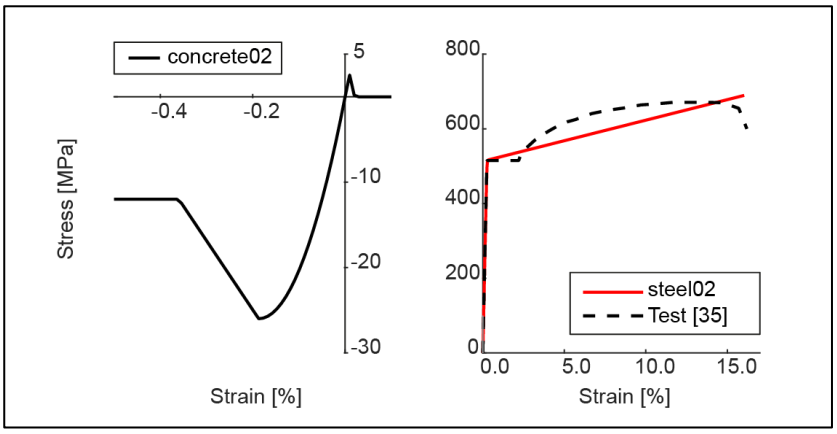

(a) (b)

Fig. 2.8 – Concrete (left) and steel (right) material models considered in the moment-curvature analyses performed with OpenSEES.

2.7.1. Linear response history analysis

Results given by Linear Response History Analysis (LRHA) are analyzed first. The story drift response is illustrated in Fig. 2.9, where it can be seen that the response of the 26-story building to the Santiago Centro record is the only one in which the peak response value at some stories is slightly greater than the value commonly associated with the onset of damage (namely 0.005, (LATBSDC 2015)). In all other cases, the response is well within the range where no damage is expected.

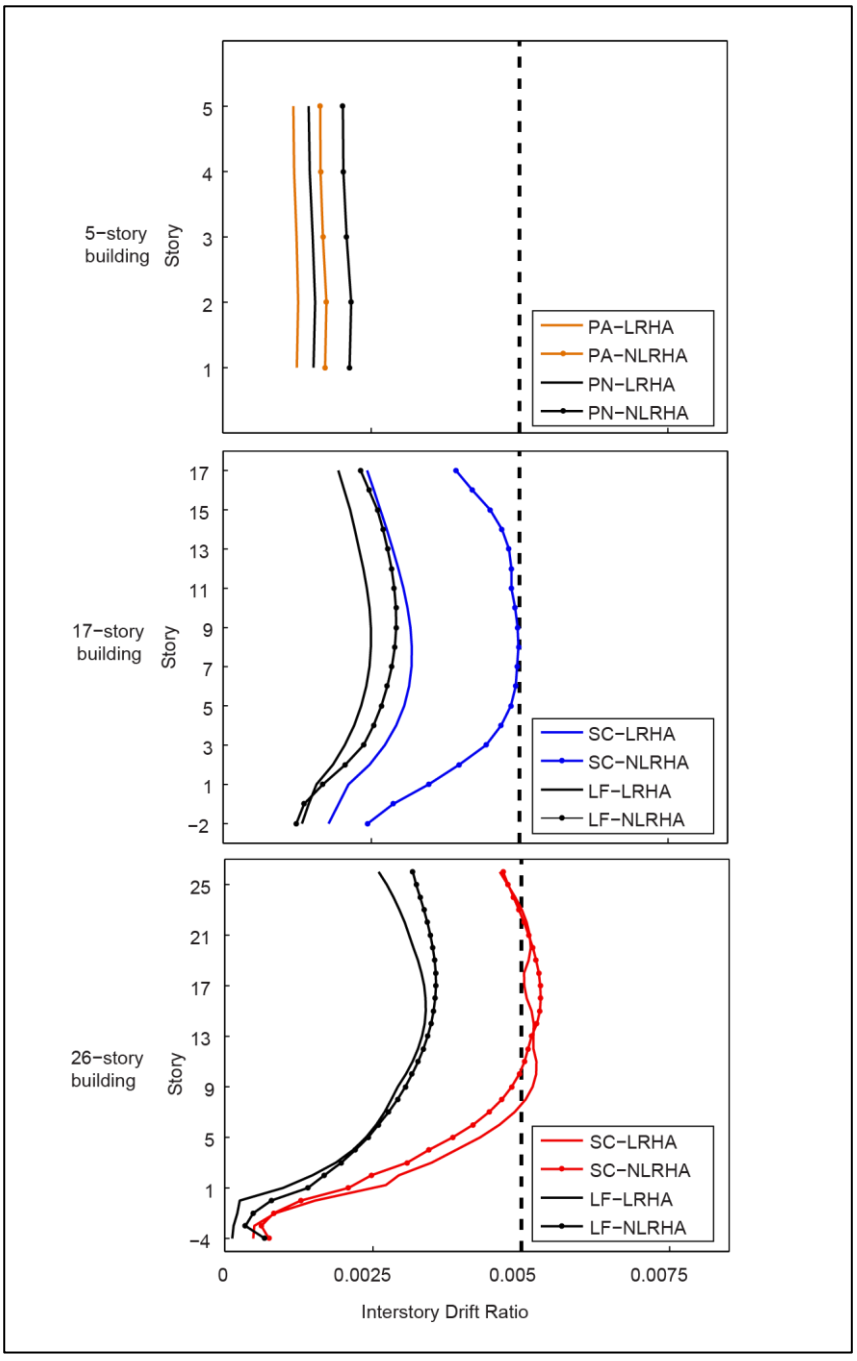

Fig. 2.9 – Linear (LRHA) and nonlinear (NLRHA) response history analysis: peak story drift response (in any direction).

Peak values of shear D/C ratios over all the walls at all stories and over the whole history of all records are illustrated in Fig. 2.10. For comparison purposes, peak D/C ratios obtained considering the shear capacity as evaluated in Section 2.6 are also shown. It can be seen that consideration of a sophisticated model (i.e., the model by Krolicki et al. 2011) leads to considerably smaller values of the peak shear D/C ratios. In particular, such values are now slightly less than unity in the 26-story building but still slightly above unity in the 17-story building. In this latter building, an inconsistency is noted in the sense that the story drift response indicates that damage is unlikely whereas the shear response indicates that damage is possible.

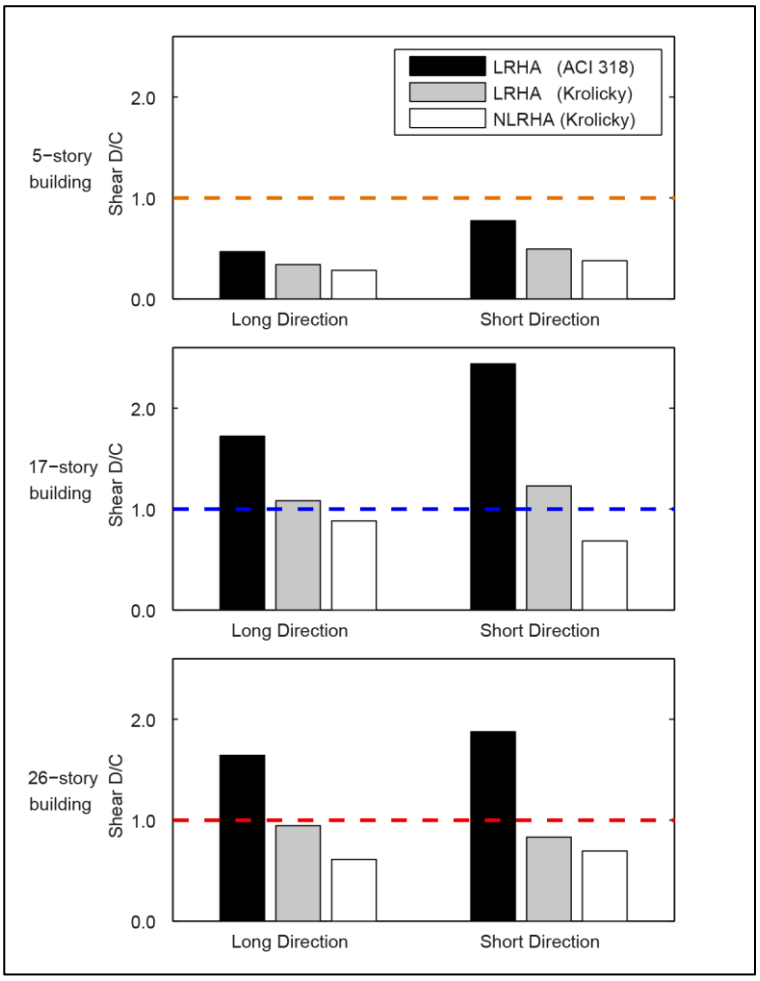

Fig. 2.10 – Linear (LRHA) and nonlinear (NLRHA) response history analysis: shear D/C ratio of the most demanded wall along the long and short directions.

Axial-flexural demands and capacities were evaluated in detail at the 15 walls indicated in Fig. 2.11. This set of walls is made up of 6 walls of the 17-story building, 6 walls of the 26-story building, and 3 walls of the 5-story building. The walls of the 17- and 26-story buildings were randomly selected among the most demanded walls along each principal direction. In the case of the 5-story building the analyses reported in Sections 5 and 6 give consistent results, hence only a few, randomly selected walls are included just for the sake of completeness and for comparison purposes. Complete histories of axial-flexural demands on 5 of the 15 selected walls are shown in Fig. 2.12, along with the corresponding capacity. This set of 5 walls is made up of: (a) the 2 most demanded walls out of the 6 previously selected walls of the 17-story building; (b) the 2 most demanded walls out of the 6 previously selected walls of the 26-story building; and (c) a randomly selected wall out of the 3 previously selected walls of the 5-story building. Results corresponding to the "planar approach" adopted so far are illustrated in the left-side plots. In each plot there is a graph at the top-right corner that shows the wall cross-section, and the rectangular portion considered in the analysis is filled with a solid color. It can be seen that the demand does not exceed the capacity at the 5-story building (wall W1), but it does at the 17-story building (walls W5 and W6) and at the 26-story building (walls W14 and W15). In order to examine the suitability of the "planar approach", demands and capacities were also evaluated considering the whole wall cross-section, which is denoted "non-planar approach". Results are shown in the middle plots of Fig. 2.12, and the graph at the top-right corner of each plot now shows the whole wall cross-section filled with a solid color. Interestingly, the capacity of the whole cross-section is now considerably larger at large compressive values of P, but not otherwise. While (logically) the demand changes as well (it is the demand on the whole cross-section), it still exceeds the capacity, and it does so at essentially the same location of the interaction diagram and essentially by the same margin. Peak axial-flexural D/C ratios at the 15 walls indicated in Fig. 2.11 are summarized in Fig. 2.13. Consistent with what was observed in Fig. 2.12, values shown in Fig. 2.13 indicate that the "non-planar" approach leads to D/C values that are slightly different from those corresponding to the "planar approach", and are usually (but not always) smaller. Again, D/C ratios at the walls of the 5-story building are well below

unity, but are still greater than unity at some walls of the 26- and 17-story buildings, the latter being again inconsistent with very low story drift demands.

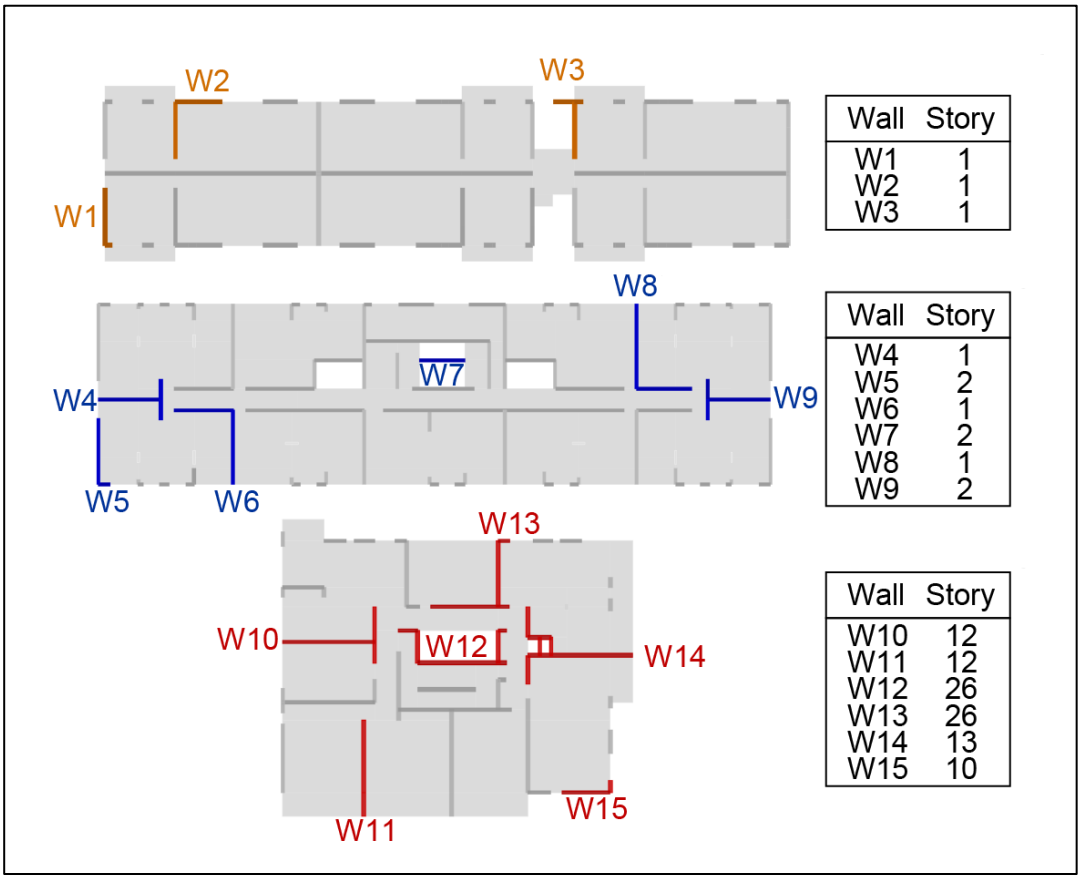

Fig. 2.11 – Selected walls for the analysis of axial-flexural behavior: (top) 5-story building; (middle) 17-story building; and (bottom) 26-story building.

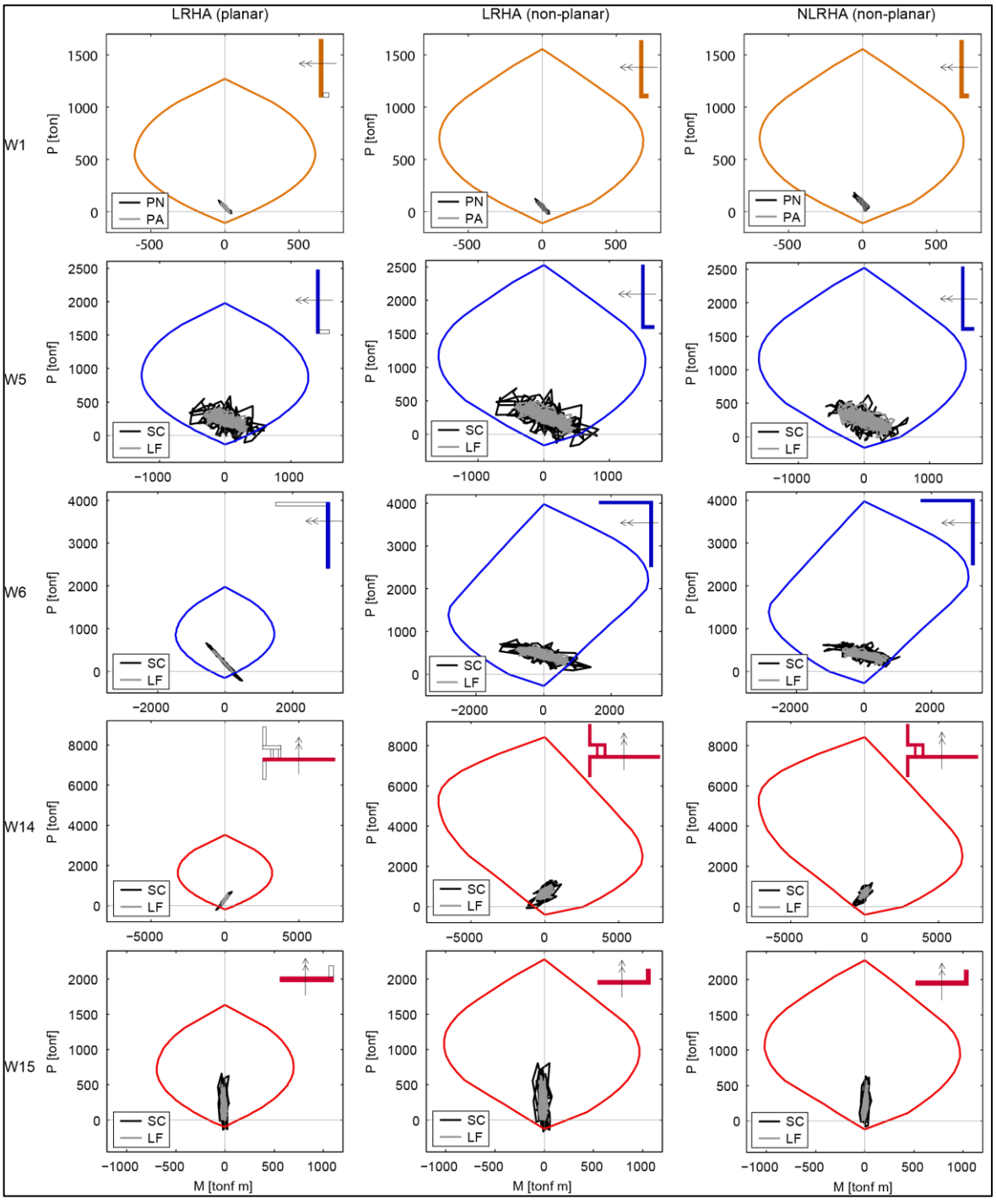

Fig. 2.12 – Linear (LRHA) and nonlinear (NLRHA) response history analysis: axial-flexural demands and capacity at 5 selected walls

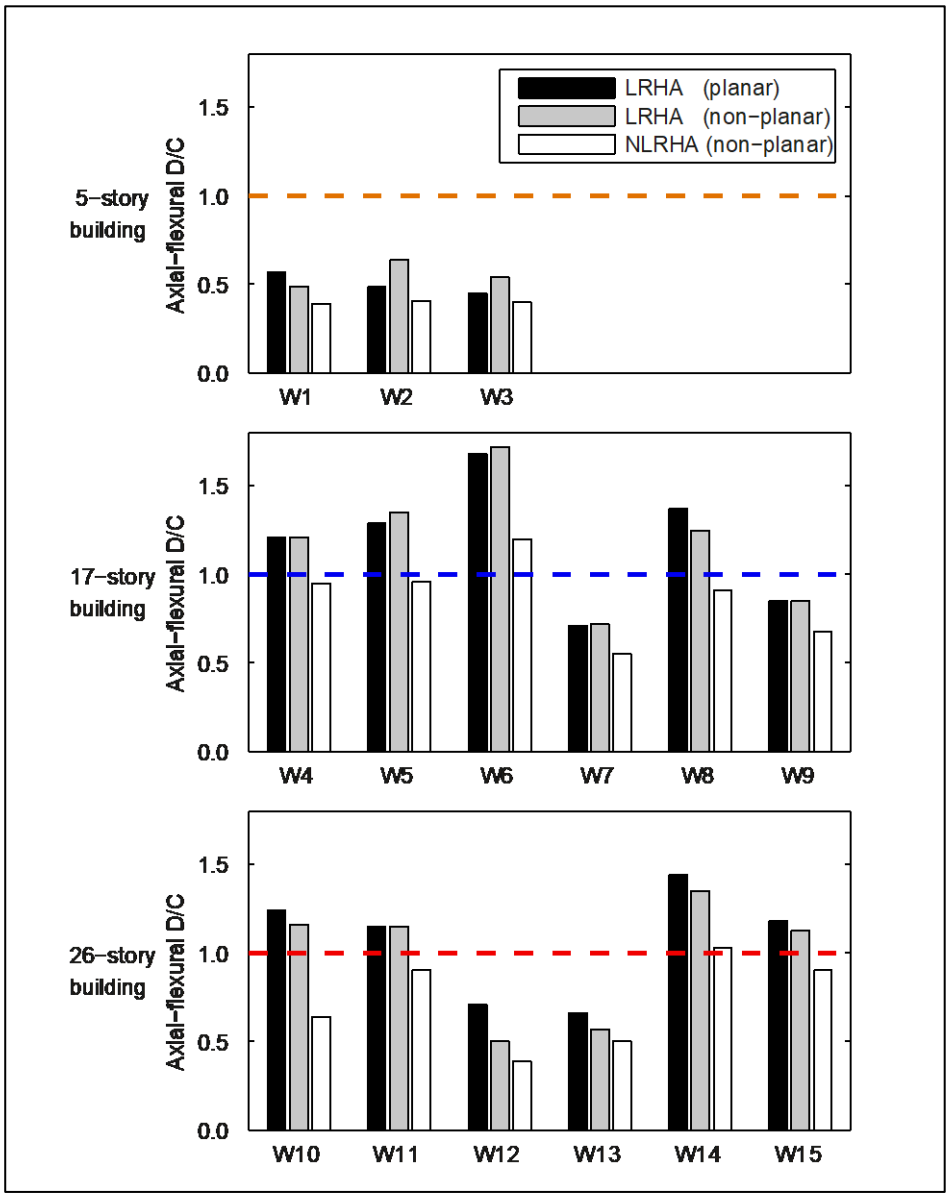

Fig. 2.13 – Linear (LRHA) and nonlinear (NLRHA) response history analysis: peak axial-flexural D/C ratios at the 15 walls indicated in Fig. 2.11.

2.7.2. Possible foundation uplift

Interestingly, it was observed in the former subsection that when the axial-flexural demand on walls exceeds the capacity it does so usually when the axial force is a tensile force. This

observation is further supported by the results shown in Fig. 2.14, which shows the peak "least compressive" axial force on each wall at the foundation level (if compressive forces are positive then the peak "least compressive" force is the minimum axial force over the entire response history). For comparison purposes the axial force on each wall due to gravity loads are shown as well. It can be observed that LRHA indicates that many walls are subjected to tensile forces, of considerable magnitude in some cases. Naturally, such observations raise a question on whether such tensile forces are actually real. Typical of buildings located in Santiago, the three buildings considered in this study are supported by shallow RC footings (see Appendix 1), which are not intended to withstand tension forces (although foundations might have some tensile capacity due to their self-weight and soil adherence, such capacity is not expected to be significant). Hence, at least in principle, foundation uplift might have occurred. Examples of post-earthquake observations related to foundation uplift in residential wall buildings are shown in Fig. 2.15. The left-side picture shows a 12-story building located in Concepcion that was severely damaged by the 2010 Chile earthquake. Post-earthquake inspections reported in Westenenk et al. (2012, 2013) suggest that the cracks at the surrounding floor are evidence of wall rocking. The right-side picture shows a 13-story building located in Coquimbo that was moderately damaged by the 2015 Illapel (Chile) earthquake (M_w 8.4). The residual deformation at the wall-to-floor intersection (70 mm) is evidence of relative vertical movement between the wall and the surrounding floor, possibly produced by wall rocking. Additional observations on the latter building can be found in Rivera et al. (2017). While foundation uplift is scarcely reported in the literature (it is difficult to notice, particularly in undamaged buildings that do not receive much attention after large earthquakes), the empirical evidence nevertheless indicates that it is possible. In the particular case of the 17- and 26-story buildings analyzed in this study no evidence of foundation uplift was observed.

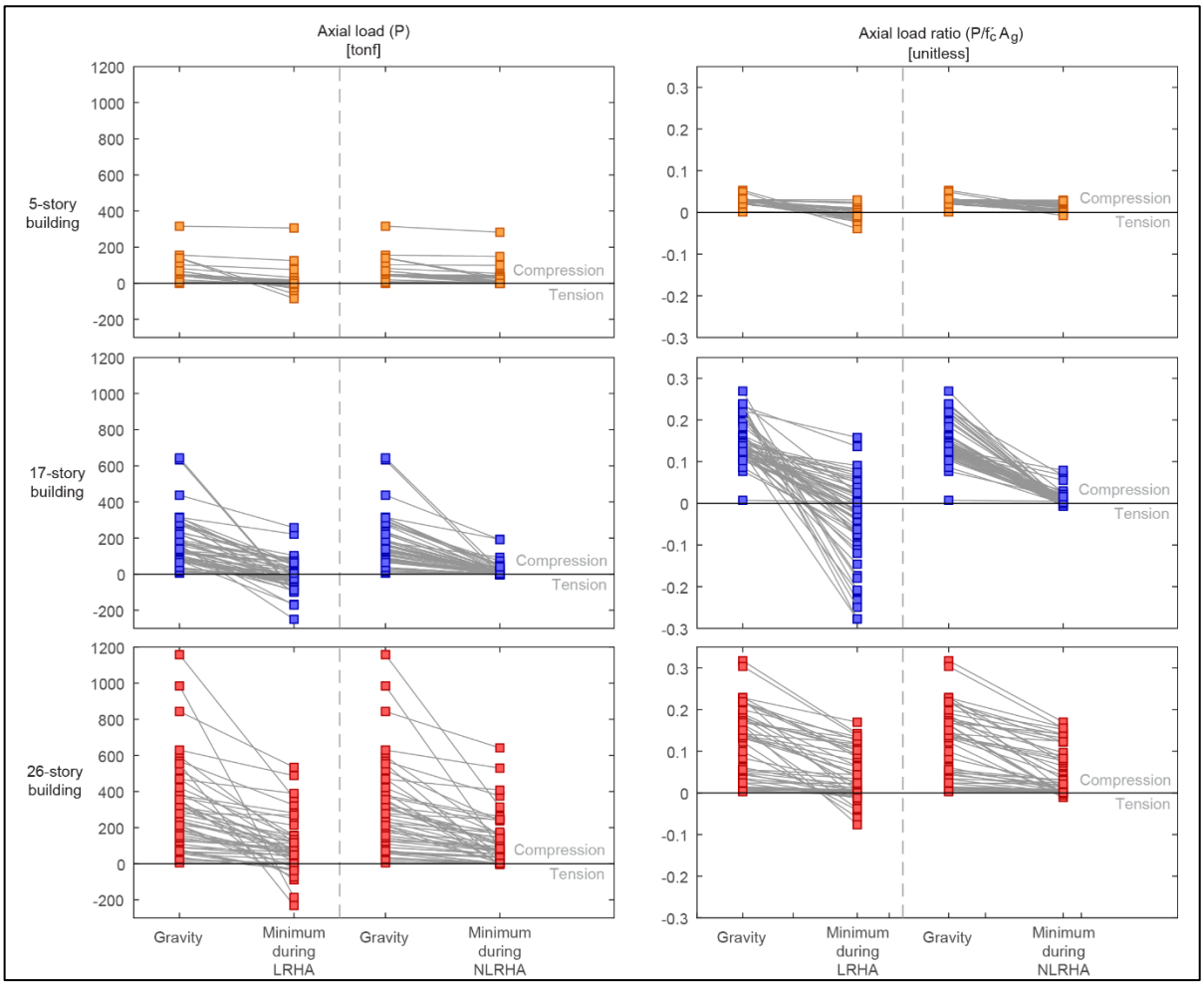

Fig. 2.14 – Axial force on each wall at the foundation level due to gravity loads and peak "least compressive" axial force on each wall due to linear (LRHA) and nonlinear (NLRHA) response history analysis. The right-side plots show axial forces normalized by $f'_c A_g$, where f'_c is the concrete compressive strength and A_g is the gross cross-section area.

Fig. 2.15 – Possible foundation uplift in damaged residential wall buildings located in Chilean cities: Concepcion (left, photo from [37]) and Coquimbo (right, photo by first author).

2.7.3. Nonlinear response history analysis

Motivated by the observations made in the former subsection, possible influence of foundation uplift is then examined. The structural models are the same models used to perform LRHA, except that: (a) the undamped linearly elastic springs that account for soil flexibility are replaced by undamped nonlinear elastic, compression-only springs; and (b) the seismic response is obtained by NonLinear Response History Analysis (NLRHA). Hence, from a conceptual perspective, LRHA is equivalent to "without foundation uplift" and NLRHA is equivalent to "with foundation uplift" (concrete behavior is linearly elastic in both LHRA and NLRHA). Similar to linear springs, the nonlinear springs are distributed along the wall length (Fig. 2.16a). Compression stiffness of the nonlinear springs was set equal to the tributary foundation area of each joint times the modulus of subgrade reaction (Fig. 2.16b).

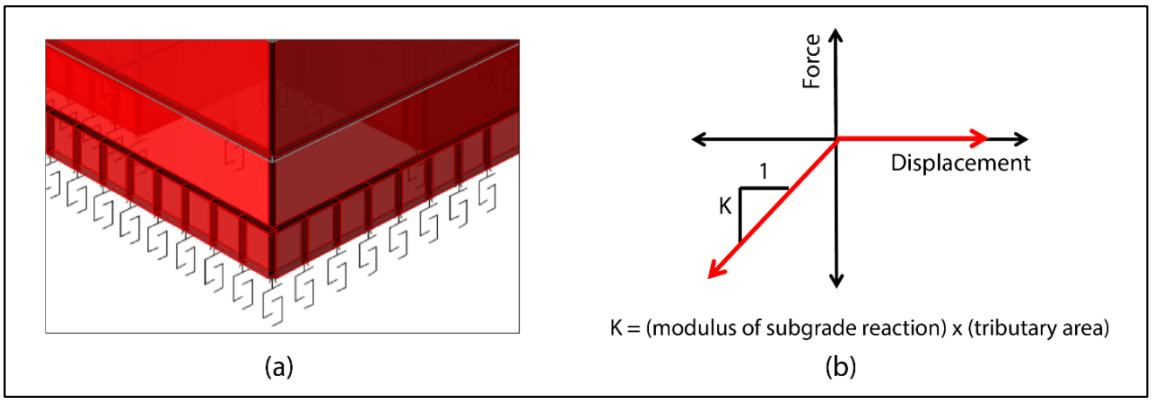

Fig. 2.16 – (a) Isometric view of one of the models with nonlinear support springs (b) Force-displacement relation of the nonlinear support springs.

A first glimpse of the relevance of foundation uplift (i.e., NLRHA) is provided by Fig. 2.14. As expected results given by NLRHA indicate that tensile forces are drastically smaller than those indicated by LRHA, very close to zero in all cases.

The story drift response is illustrated in Fig. 2.9. The 17-story building subjected to the La Florida record is the only case in which results given by NLRHA are significantly larger than those given by LRHA. In all other cases results given by NLRHA are either slightly larger than or essentially equal to those given by LRHA. Again, the response of the 5-story building is well within the range where no damage is expected, but now the response of both the 17- and 26-story buildings are essentially equal (at some stories) to the value commonly associated with the onset of damage (namely 0.005).

Peak values of shear D/C ratios (again, over all the walls at all stories and over the whole history of all records) are illustrated in Fig. 2.10. Values given by NLRHA are always less than those given by LRHA, considerably so in some cases. Further, values given by NLRHA are less than unity at the three buildings, significantly so at the 5-story building and marginally so at the other buildings. These latter values (i.e., the ones for the 17- and 26-story buildings) are consistent with the corresponding (i.e., given by NLRHA) story drift response.

Complete histories of axial-flexural demands on 5 walls are shown at the right-side plots of Fig. 2.12, along with the corresponding capacity (only the “nonplanar approach” was evaluated in this case). Demands given by NLRHA are always less than those given by LRHA, and either do not exceed the capacity or do so by a small margin. These results are consistent with those shown in Fig. 2.13, which indicate that peak axial-flexural D/C ratios given by NLRHA are always less than those given by LRHA, considerably so in some cases. Further, values given by NLRHA are significantly less than unity at the 5-story building, and marginally so or slightly greater than unity at the other buildings. Again, these latter values are consistent with the corresponding (i.e., given by NLRHA) story drift response.

Finally, the response of the most demanded vertical springs (in terms of vertical deformation) is shown in Fig. 2.17. Results are meaningful because they indicate that the significant changes in force demands described in the former paragraphs are the consequence of uplifts that are relatively small, at most (roughly) a dozen millimeters. Such small uplifts are deemed possible, and, if they indeed occur, are not likely to cause effects that might be observed in visual inspections.

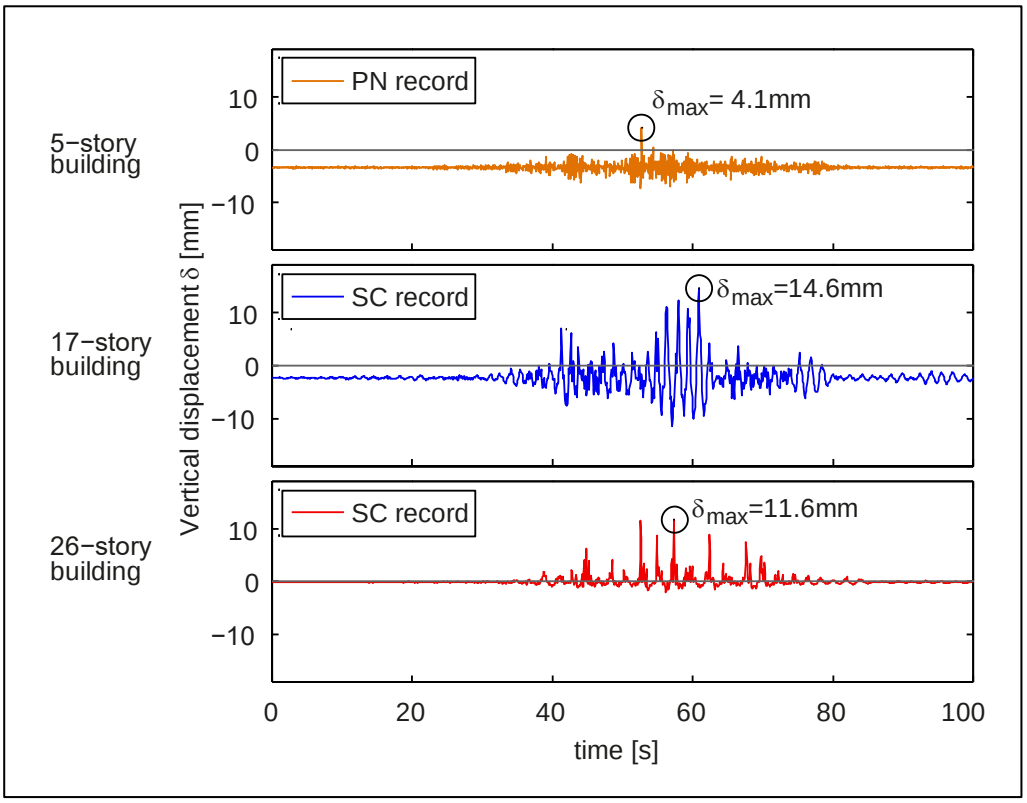

Fig. 2.17 – Nonlinear response history analysis (NLRHA): peak base uplift of the most demanded (in terms of vertical displacement) vertical spring at the foundation level.

Note: the conclusions of this chapter are presented in section 5.1.

---

3. PAPER II: ASSESSMENT OF THE SEISMIC CAPACITY OF TALL WALL BUILDINGS USING NONLINEAR FINITE ELEMENT MODELING

Note: This paper has already been published (Ugalde et al. 2019c). However the version presented in this chapter is slightly different from the published version due to dissertation format requirements and suggestions made by the members of the PhD committee.

3.1. Introduction

The M_w 8.8 2010 Chile earthquake (one of the strongest ever recorded) caused significant damage to only 2% of the affected inventory of buildings having 9 or more stories (Massone et al. 2012). This observation is somewhat surprising because, as it will be shown later, spectral ordinates of several recorded ground motions are in many cases (Naeim et al. 2011) much larger than the design spectrum specified in the Chilean seismic design code NCh433 (INN 1996a), which is the code the great majority of the medium and high rise buildings in 2010 was designed for. Hence, the 2010 Chile earthquake should have caused damage to a significant amount of multistory buildings, but such scenario did not occur (Naeim et al. 2011).

It is clear then that the actual seismic capacity of typical Chilean RC shear wall buildings is (much) larger than the strength required by the seismic design code, but the reasons for such larger-than-expected capacity have not been thoroughly evaluated. While several studies analyzed the response of multistory buildings damaged by the 2010 Chile earthquake (Carpenter et al. 2011; Rojas et al. 2011; Wallace 2011; Bonelli et al. 2012; Hube et al. 2012; Telleen et al. 2012b; Wallace et al. 2012; Song et al. 2012; Westenenk et al. 2013; Parra and Moehle 2014; Alarcon et al. 2015; Junemann et al. 2016), apparently only one study analyzed undamaged buildings (Junemann et al. 2015) and its sole finding is that the characteristics of damaged buildings are essentially not different from those of undamaged buildings. A research program was then initiated by the authors of this paper to obtain more insight into why undamaged buildings were indeed not damaged even though damage was

expected (due to current design damage-based design philosophy). It is emphasized that the objective of this research program is different from the objective of almost all post-earthquake studies, which focus on *damaged* buildings rather than on *undamaged* structures. In a strict sense the latter should be referred to as "buildings in which no damage was observed", but the expression "undamaged buildings" is nevertheless used just for the sake of brevity.

In the case of RC structures an important question related to the analysis of *undamaged* buildings is whether a linearly elastic model is appropriate. In favor of linearly elastic models, it can be argued that the number and extension of inelastic deformations must be very low (if any at all) in undamaged structures. Besides, linearly elastic models are also attractive because they require neither sophisticated modeling techniques nor large computational efforts. Against these models, however, it can be argued that the stress-strain relationship of concrete is intrinsically nonlinear both in tension (i.e., cracking) and in compression (i.e., nonlinear behavior even at low deformation levels), and such nonlinearity might significantly affect the overall structural response even in the absence of observable damage. Since no information was found in the literature on this issue (as mentioned before the literature focuses on damaged buildings rather than on undamaged structures) it was decided to consider both types of models (i.e., linear and nonlinear).

In former studies (Ugalde and Lopez-Garcia 2017a, b), three actual and representative residential RC shear wall buildings of 5, 17 and 26 stories that withstood undamaged the 2010 Chile earthquake were analyzed using linearly elastic models. In a first series of analyses it was found that the elastic capacity/demand ratio (denoted *elastic overstrength* in Ugalde and Lopez-Garcia (2017a)) is large enough to explain the lack of damage in the 5-story building but not in the other two buildings. These findings were ratified by results obtained in a second series of analysis (response history analyses, Ugalde and Lopez-Garcia 2017b), which also revealed that foundation uplift might be the reason for the lack of damage in the 17- and 26-story buildings. However, since very little evidence of foundation uplift was observed after the 2010 Chile earthquake, the results reported in Ugalde and Lopez-

Garcia (2017b), i.e., obtained considering linearly elastic models, were deemed somewhat inconclusive.

In this paper the seismic response of the same 17- and 26-story buildings analyzed in (Ugalde and Lopez-Garcia 2017b) is re-evaluated considering a fully nonlinear finite element model, i.e., a model in which a nonlinear concrete material model is adopted and other nonlinear features (such as the nonlinear behavior of reinforcement bars and PΔ effects) are also accounted for. In doing so the specific objectives of this study are: (1) to realistically evaluate the strength of typical Chilean residential RC shear wall buildings; (2) to identify the most relevant modeling issues for the analysis of RC shear wall buildings that did not suffer observable damage; and (3) to provide insight into why most Chilean residential RC shear wall buildings did not suffer observable damage during the severe 2010 Chile earthquake. Full 3D finite element models of the buildings were developed in PERFORM-3D (CSI 2016a), a commercial computer program that was deemed to provide an adequate balance between modeling capabilities and computational cost. The approach to model RC shear walls is presented and validated through comparisons with experimental results. The building structures are described in detail. The structural models are subjected to a series of pushover analysis to evaluate the impact of several nonlinear modeling considerations and to assess the seismic capacity of the structures. Finally, response history analyses were performed considering a ground motion recorded close to the location of the buildings. Particular attention is paid to examination of foundation uplift.

3.2. Description of the building structures

The buildings analyzed in this paper have 17 and 26 stories, respectively. They are actual, existing structures representative of medium- and high-rise Chilean shear wall buildings. The 17-story building (Fig. 3.1a) has two underground levels whereas the 26-story building (Fig. 3.1b) has four. Both buildings are apartment complex located in Santiago and in none of them noticeable damage was reported after the 2010 Chile Earthquake. Some relevant construction drawings of the buildings are presented in Appendix 1.

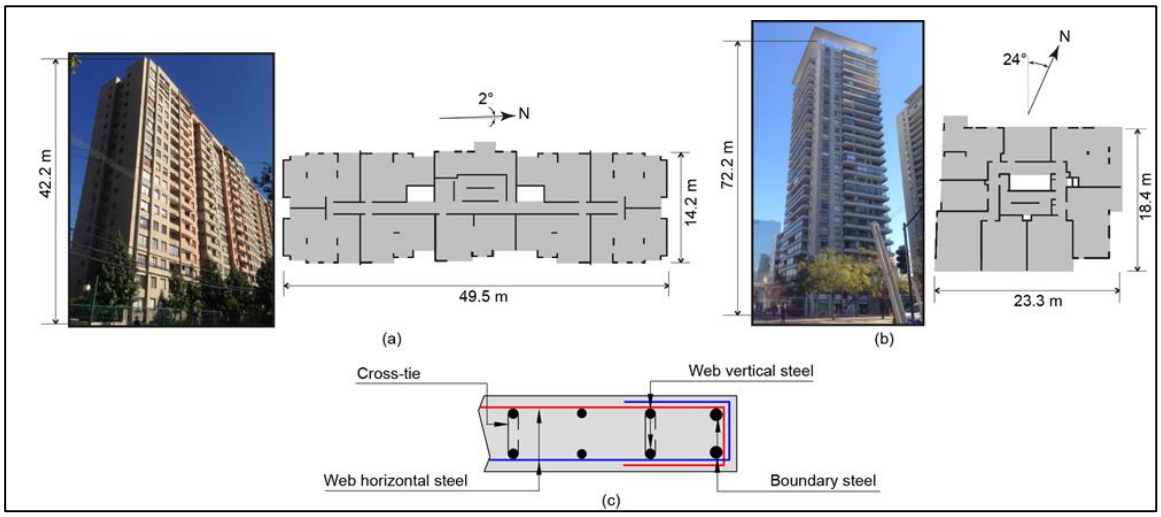

Fig. 3.1 – (a) Picture and plan view of 17-story building; (b) Picture and plan view of the 26-story building; (c) Typical detailing at boundaries of RC shear walls

Although there are a few columns at the bottom-most levels and beams at lintels and balconies, gravity and lateral forces are carried mainly by RC cantilever walls alone, i.e., without braces, coupling beams or moment frames. The typical floor plans of the buildings (Fig. 3.1) clearly show the significant number of walls, many of them with intricate cross sections. This structural configuration based on walls is typical of Chilean residential buildings and provides a large lateral stiffness (Lagos et al. 2012) compared to other lateral-force resisting systems such as moment frames or core walls. This large stiffness was deemed as the main reason for the little damage caused by past earthquakes (Wood 1991). The wall density of Chilean buildings, usually reported as the walls cross-section area over floor area on each story and along each principal direction, has a mean value of 2.85% (Junemann et al. 2015). This value is similar to the values of wall density of the buildings considered in this study (Table 3.1).

Table 3.1. Direction-dependent building properties

Building	5-story		17-story		26-story	
Number of modes in modal analysis	5		12		12	
Direction	Long	Short	Long	Short	Long	Short
Modal participating mass ratio recovered	0.97	0.97	0.99	0.99	0.91	0.93
Nominal fundamental period [(a)] [s]	0.11	0.25	0.47	1.1	1.39	1.62
Wall density A_w/A_f [%]	2.9	2.6	2.6	2.4	2.5	2.4
Code modification factor R*	2.30	3.52	7.45	9.46	9.89	10.13
Base shear coefficient before adjustment [%]	17.12	15.74	6.06	2.06	1.73	1.43
Base shear adjustment factor	0.74	0.80	1.00	2.42	2.90	3.50
Base shear coefficient after adjustment [%]	12.6	12.6	6.1	5.0	5.0	5.0
Effective modification factor R_{eff}	3.13	4.41	7.45	3.90	3.41	2.89

[(a)] The basis for computing these nominal fundamental period is presented in the first paragraph of section 2.5.

Wall thickness varies from 150 to 170 mm in the superstructure, while thicker walls (up to 250 mm) are found at the basement levels, either for shear or for soil retention. Typical of Chilean RC wall buildings, all nonstructural partitions are light partitions of negligible stiffness. The buildings were designed in accordance with the Chilean code NCh433, which refers to ACI 318 provisions for concrete design. However, motivated by the good performance of buildings without confined boundary elements in past earthquakes, the special boundary requirements were explicitly excluded when Chile formally adopted the

ACI-318 in 1993. Consequently, none of the RC walls in any of the selected buildings has confinement detailing. Typical detailing at wall boundaries is shown in Fig. 1(c). It is important to mention that both buildings satisfy by a wide margin the story drift requirement indicated in NCh433 (Ugalde and Lopez-Garcia 2017a).

Design forces for the buildings were obtained from NCh433, a code that, like many other seismic design codes worldwide, indicates that design forces are given by an elastic pseudo-acceleration spectrum reduced by a response modification factor R*. As commented in section 2.4, the base shear corresponding to this reduced spectrum (computed by Response Spectrum Analysis, RSA) must lay within certain limits; otherwise R* has to be scaled until the base shear meets the requirements. The modification factor after such scaling is the effective modification factor (R_{eff}) shown in Table 3.1. The design spectra for these structures, both elastic and reduced by R_{eff}, are presented in Fig. 3.2, along with the elastic response spectra of the ground motions recorded in the Greater Santiago Area on soil type II (stiff) or III (intermediate) during the 2010 Chile earthquake (both components). Design fundamental periods (i.e. the ones used to compute the design spectra as explained in section 2.5) along each direction are highlighted with vertical lines. As already reported by Naeim et al. (2011), it can be observed that spectral ordinates of the (reduced) design spectra are generally much smaller than those of the recorded ground motion, but even so no damage was reported. Further details of the buildings analyzed in this study can be found in Ugalde and Lopez-Garcia (2017a, b).

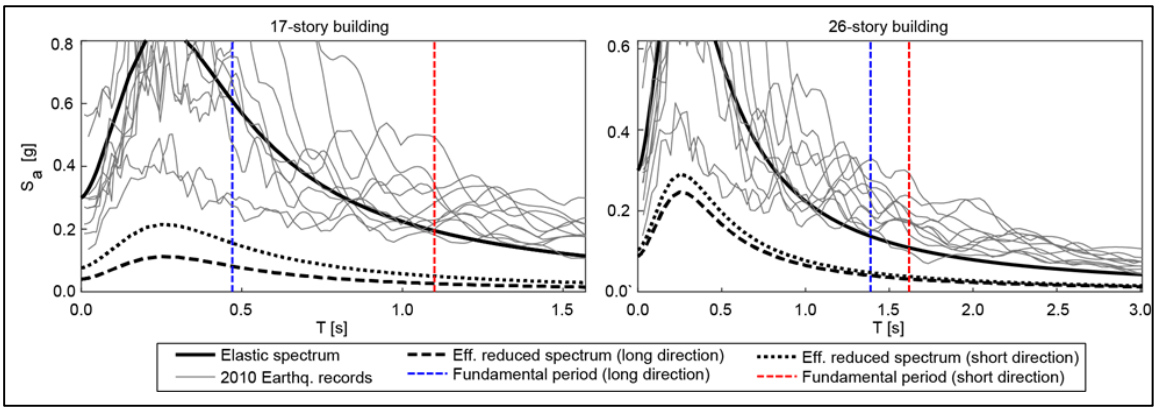

Fig. 3.2 – Comparison between design spectra compared and spectra of ground motions recorded during the 2010 Chile earthquake

3.3. Shear wall modeling and validation

Building models were developed using the commercial software PERFORM-3D (CSI 2016a), a structural analysis tool oriented to Performance Based Design (PBD) and currently the most commonly used for this purpose by practitioners. The software offers two types of elements to model shear walls: the Shear Wall element and the General Wall element. Both are 4-node finite elements specifically formulated to model RC walls, in which separate layers account for vertical axial load/bending interaction and in-plane horizontal concrete shear. Weak-axis shear and out-of-plane bending are elastically modeled. The General Wall element has one additional layer to model horizontal axial load/bending interaction and two additional layers to model diagonal shear related to strut-and-tie action. The General Wall element is then more sophisticated, but is computationally much more demanding and its parameters are also much more difficult to calibrate. Therefore, the General Wall element is recommended only in cases where horizontal axial-bending interaction or diagonal shear are relevant (e.g., to model squat walls or horizontal wall segments). On the other hand, the Shear Wall element offers reasonable accuracy in most cases, making it the preferred element in most building projects. This element was adopted for the analysis described in this paper.

In the Shear Wall element the vertical axial-bending behavior is accounted for using fiber cross sections, i.e., the wall is manually meshed into several Shear Wall elements, each with a cross section composed of concrete and steel fibers. The latter are given in terms of a vertical steel ratio (Auto Size cross-section) or in terms of area and coordinates of each bar (Fixed Size cross-section). Alternatively, bar groups can be explicitly modeled using Steel Bar/Tie/Strut elements (Kolozvari et al. 2017). The latter approach is advantageous to model boundary steel of walls that are not confined, such as the ones in the buildings analyzed in this study.

In the models, the vertical mesh is such that there are two vertical elements per story at locations where nonlinear response is expected, namely the underground stories and a few stories above grade level (2 and 5 stories in the 17- and 26-story buildings, respectively). Horizontal meshing was intended to set square-like elements at these stories. One vertical element per story was considered sufficient at all other stories, as recommended by the software documentation (CSI 2016b).

While PERFORM-3D documentation include guidelines on elements and analysis procedures, scarce information is available for material calibration, as this requires validation with experimental data. Such analysis has been presented in the literature along with modeling recommendations (Lowes et al. 2016; Kolozvari et al. 2017). Particularly, most of the recommendations given by Lowes et al. (2016) were implemented in the building models, including:

- Concrete elastic modulus defined per ACI 318-14 (ACI 2014) as $E_c=4700\sqrt{f'_c}$ (MPa units).

- Concrete compression stress-strain relationship follows a YURLX envelope (trilinear with strength loss, Fig. 3.3) whose parameters are summarized in Table 3.2. The quantity ε_{cmax} is given by Eq. 1 (Paulay and Priestley 1992). Variables ρ_h, f_{ym} and ε_{hm} are, respectively, the volumetric ratio, the yielding strength and the strain at maximum strength of the confining reinforcement. Confined concrete compressive strength (f'_{cc}) was computed according to Mander et al. (1988).

$$\varepsilon_{cmax} = 0.004 + 1.4\rho_h f_{yh}\varepsilon_{hm}/f'_{cc} \quad \text{(Eq. 1)}$$

Table 3.2 Concrete compressive stress-strain parameters according to Lowes et al. (2016)

Concrete	FY	FU	FR/FU	DU (mm/mm)	DL (mm/mm)	DR (mm/mm)
Unconfined	$0.75f'_c$	f'_c	0.00	0.002	0.00202	0.01
Confined	$0.75f'_{cc}$	f'_{cc}	0.20	0.004	0.00404	ε_{cmax}

- Steel stress-strain relationship follows a YURLX envelope adjusted to measured data (Fig. 3.3).

- Shear stiffness equal to 0.1 G_c A_{cv}, where G_c = 0.4 E_c as recommended by ATC (2010) and A_{cv} is the gross wall area.

- Concrete cyclic energy factors equal to those shown in Table 3.3.

Table 3.3 Concrete cyclic energy factors according Lowes et al. (2016)

Material State	Y (yield)	U (ultimate)	L (loss)	R (residual)	X (rupture)
Energy Factor	1.00	0.40	4.00	0.10	0.10

- Steel energy dissipation factor equal to 0.75 and steel unloading/reloading stiffness factor equal to 0.5.

- Regularization[a] of unconfined concrete envelope by reducing the compression strain at residual stress to the value given by Eq. 2, where unconfined crushing energy G_{fc} = 0.0876 kN/mm and L_{elem} is defined by the height of the element.

$$DR = \varepsilon_u = DU - \frac{f'_c}{E_c} + 2\,\frac{\left(\frac{G_{fc}}{L_{elem}}\right)}{f'_c} \qquad \text{(Eq. 2)}$$

- Regularization of confined concrete envelope by reducing the compression strain at residual stress to the value given by Eq. 3, where confined crushing energy G_{fcc} is given by Eq. 4 ("cc" subindex refers to confined concrete)

$$DR_{cc} = \varepsilon_{ucc} = DU_{cc} - \frac{0.8f'_{cc}}{E_c} + \frac{5}{3}\frac{\left(\frac{G_{fcc}}{L_{elem}}\right)}{f'_c} \qquad \text{(Eq. 3)}$$

$$G_{fcc} = 0.0876\,\frac{kN}{mm} < 0.4378\,\frac{kN}{mm}\left(\frac{f'_{cc}}{f'_c} - 0.85\right) < 0.2189\,\frac{kN}{mm} \qquad \text{(Eq. 4)}$$

- Simplified model for steel buckling, where the steel tensile stress is reduced to its residual value when the strain at the residual stress of concrete (given by Eq. 2 and Eq. 3) is reached.

---

[a] It has been documented in concrete tests that damage occurs within a zone of the specimen that has approximately the same size regardless of the size of the specimen. On the other hand, when one element of a finite element model reaches the yielding strain, the whole element yields. As the deformations are computed integrating strains along the length of the element, the deformations of the model depends on the size of the yielding element. This analytical behavior is called localization (Coleman and Spacone 2001). The regularization is a technique for preventing localization, in which the stress-strain relationship of materials is modified in order to make the response mesh-objective.

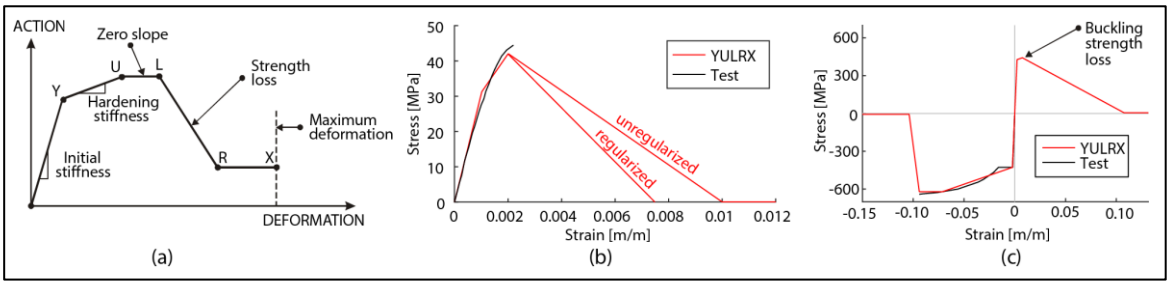

Fig. 3.3 – (a) General YURLX material model; (b) Unconfined concrete material model; (c) Steel material model

Shear force-deformation relationship was modeled as elastic, perfectly plastic. Shear strength was computed with Eq. 5. Since most of the walls are slender with aspect ratios greater than 2.0 parameter α_c was set equal to 0.17 (MPa units). Eq. 5 was adapted from equation 18.10.4.1 of ACI 318-14 but increased by 50% to approach ultimate conditions (Değer et al. 2015b). Variables ρ_t and f_y are the volumetric steel ratio and the yielding stress of transverse steel, respectively.

$$V_{ult} = 1.5\, V_n = 1.5\, A_{cv} \left(\alpha_c \sqrt{f_c'} + \rho_t f_y\right) \qquad \text{(Eq. 5)}$$

The modeling considerations previously presented were validated by reproducing the cyclic tests of wall specimens RW2 and TW2 reported by Thomsen and Wallace (1995). Fig. 3.4 (left) shows an elevation of the wall models developed in PERFORM-3D. Both wall specimens have confined boundary elements whose vertical steel could be modeled with fibers in the Shear Wall cross section. However, for consistency with the modeling approach implemented to analyze the buildings (which do not have walls with confined boundary elements), steel at boundary elements was explicitly modeled using bar elements, and therefore confined concrete elements do not have steel fibers (i.e., $\rho = 0$). In accordance with the study reported in Lowes et al. (2016), the specimens were assumed to have three stories, the first story was modeled with two vertical elements, and each of the other stories was modeled with one element. The vertical load was applied at the top nodes of the models,

distributed according to tributary length. PΔ effect was included. Other relevant parameters of the models are shown in Table 3.4.

In general, the global response of the walls is reasonably well predicted by the models (Fig. 4 center). Notably, the strength of specimen RW2 is slightly overestimated at low drift ratios but accurately predicted at larger displacements. Further, the strength of specimen TW2 is also very well predicted by the model when the flange is in compression. However, when the flange is in tension the model overestimates the strength, by 24% at peak strength. Analytical models of specimens RW2 and TW2 developed in PERFORM-3D have already been presented in ATC-72 (ATC 2010), but they were calibrated differently and results are less accurate (e.g., in ATC-72 the strength of specimen TW2 is overestimated by 53% when the flange is in tension). Even so, such results are deemed reasonable in ATC-72 given the wall geometries, loading histories, and particularly the simplified material models implemented in PERFORM-3D. More sophisticated models of specimens RW2 and TW2 developed with research-oriented software (Orakcal and Wallace 2006) give results that are only slightly more accurate than those shown in Fig. 4 (e.g., the strength of specimen TW2 is overestimated by 19% when the flange is in tension). Larger differences, on the other hand, are observed in local response quantities, e.g., concrete strains at the base of the walls (Fig. 4, right) measured with Deformation Gage elements at the base nodes. While the models predict well the experimental measurements at the center of the web, strains at the boundaries are overestimated in tension (34% on average) and underestimated in compression (54% on average). Again, the largest differences are observed in specimen TW2 when the flange is in tension. It must be noticed that the models assume constant strains between the end nodes of the Deformation Gage elements (located in this case between the base and mid-height of the first story), while actual strain gages implemented in the tests have much shorter spans.

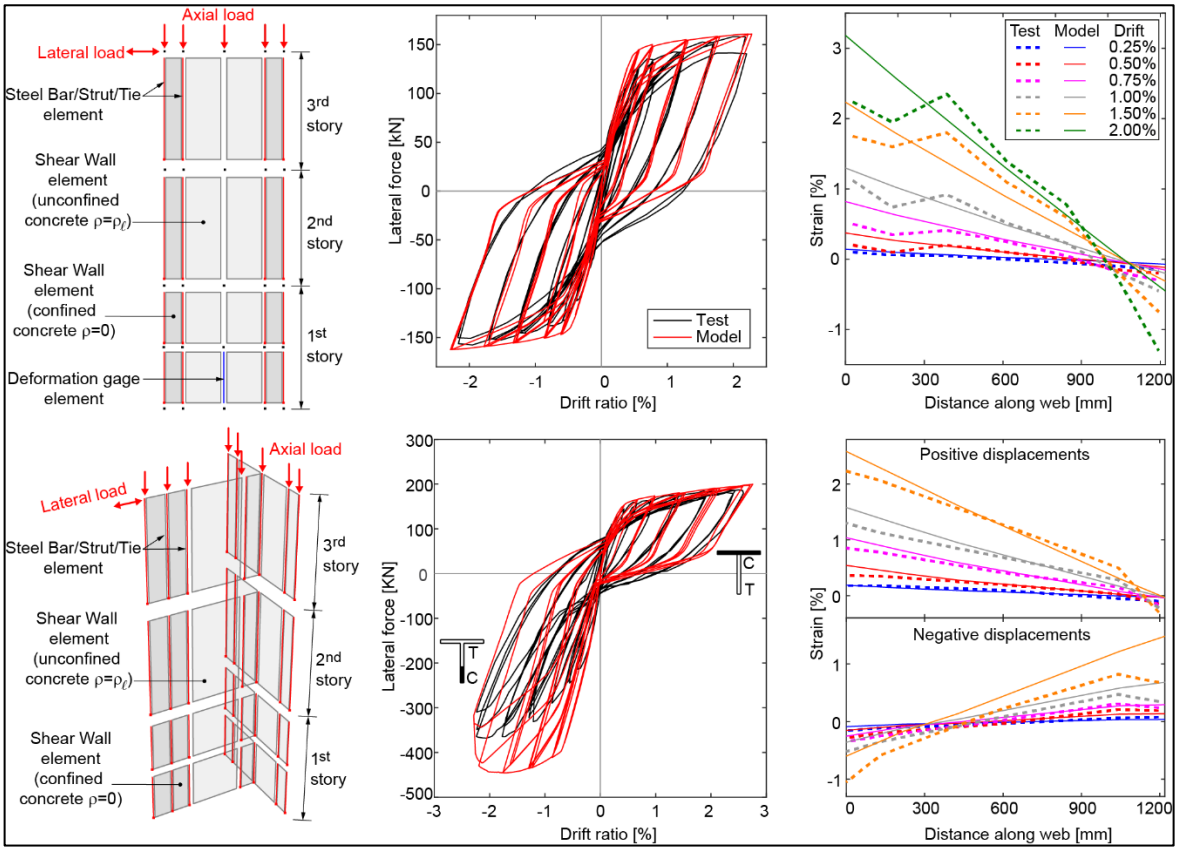

Fig. 3.4 – Specimens RW2 (top) and TW2 (bottom): (left) Model elevation (center) Measured hysteretic response vs. model prediction (right) Measured concrete strain vs. model prediction

Despite the limitations described in the former paragraph and despite other limitations as well (i.e., the lack of shear-flexure interaction, Kolozvari and Wallace 2016), results shown in Fig. 4 indicate that the Shear Wall element of PERFORM-3D is accurate enough for the purposes of this study. It is important to note that the "PERFORM-3D + Shear Wall element" modeling approach is possibly the most used of the few options currently available to perform nonlinear response history analyses of full 3D models of RC shear wall buildings.

Table 3.4 Model parameters of specimens RW2 and TW2 and of the walls of the buildings

	RW2	TW2	17-story building	26-story building
Wall width t (mm)	101.6	101.6	150 to 200	150 to 300
Concrete strength f'_c (MPa)	43.5	41.7	26	32.5
Concrete elastic modulus E (MPa)	31174	30541	24116	26962
Mander confined ratio K	1.095	1.3	1	1
Shear modulus G (Mpa)	12,470	12,216	9,646	10,785
Steel yielding stress f_y (MPa)	427.5	427.5	5,250	5,250
Steel ultimate stress f_u (Mpa)	620.5	620.5	6,840	6,840
Steel ultimate strain DU (mm/mm)	0.071	0.071	0.11	0.11
Steel loss strain DL (mm/mm)	0.094	0.094	0.16	0.16
Longitudinal steel ratio ρ_ℓ (%)	0.33	0.45	0.3 to 5.1	0.3 to 4.5
Transverse steel ratio ρ_t (%)	0.33	0.45	0.3 to 0.7	0.3 to 0.8

3.4. Model Implementation

The buildings presented in Section 2 were modeled in PERFORM-3D using the previously described model for the shear walls. This approach required identification of the dimensions and steel reinforcement of all walls in order to define the Shear Wall compound sections (it is recalled that this element is composed of one layer for vertical axial-bending and another layer for shear). In actual buildings like the ones considered in this study, the number of combinations of thickness, longitudinal steel ratio and transverse steel ratio is very large, which lead to numerous different Shear Wall compound sections whose definition and assignation to the model is cumbersome. Thus, longitudinal (web only) and transverse steel ratios were rounded to the third decimal number, e.g., two different walls having longitudinal web steel ratios (ρ_ℓ in Fig. 3.4) equal to 0.0028 and 0.0032 were both modeled with ρ_ℓ = 0.003. Results given by a separate sensitivity analysis (not shown here for brevity) confirmed

that the effects of such rounding are negligible. It is emphasized that only the web steel ratios (i.e., longitudinal and transverse) were rounded, areas of boundary steel were not. Even with this simplification, 53 different Shear Wall compound sections were required for the 17-story building, and 77 for the 26-story building. Once regularization of concrete material in compression was included, the number of Shear Wall compound sections increased to 62 and 91, respectively.

Three-dimensional views of the building models are shown in Fig. 3.5, where it can be observed that all boundary steel bars were explicitly modeled. Fig. 3.5 also shows an elevation of a resisting plane of each building to emphasize the finer vertical mesh in bottom-most stories, where 2 vertical elements per story were defined. Notice that the 26-story building has a podium (i.e., wider basement levels), which is intended for parking and storage units.

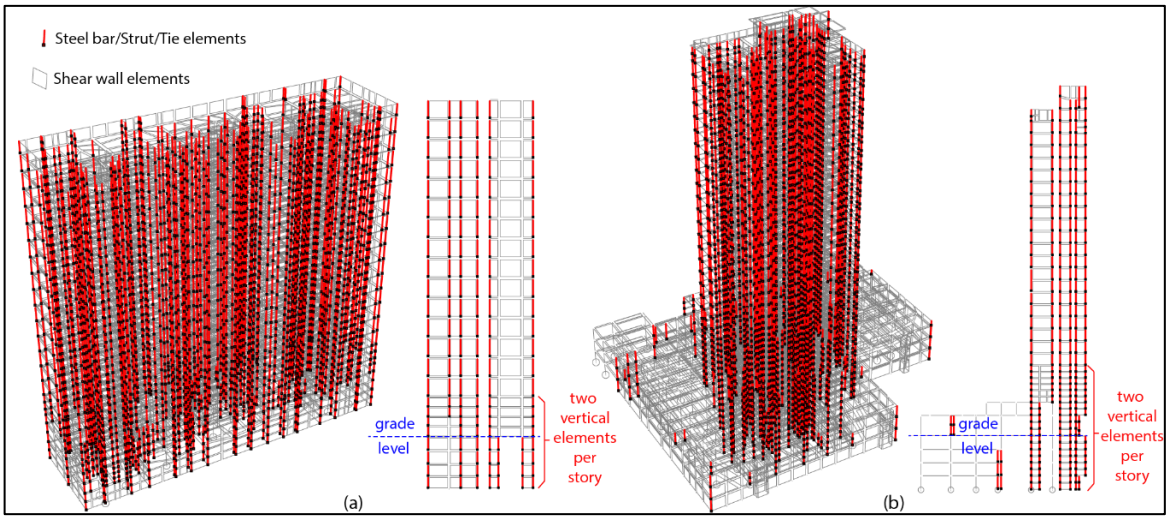

Fig. 3.5 – Three-dimensional view and plane elevation of models of the (a) 17-story building and the (b) 26-story building

Concrete beams were modeled using elastic frame elements with concentrated plasticity, i.e. moment-curvature hinges, located at a distance $L_p/2$ from each end, where L_p is the length assigned to the hinge (Fig. 3.6a). Concrete columns, whose behavior is affected by axial load

variation, were modeled using elastic frame elements with plasticity distributed along a distance L_p from each end, to which a fiber cross-section was assigned (Fig. 3.6b). For both beams and columns the length of the plastic hinge (L_p) was computed according to Priestley and Park (1987). Slabs were modeled using linear elastic area elements whose moment of inertia was reduced by 75% to account for stiffness reduction due to concrete cracking. This reduction is indicated in table 6.6.3.1(a) of ACI 318-14 (ACI 2014), and is intended for load factored design, near the ultimate strength of the lateral-force-resisting system. However, this value was deemed appropriate, as shaking table tests of full-scale wall buildings (Schotanus and Maffei 2008) found that the best analytical prediction of displacements is obtained with a reduction as large as 90%, even when the behavior of the building is "essentially elastic". Rigid diaphragm constraints were included to reduce the number of degrees of freedom and, consequently, to reduce the computational cost.

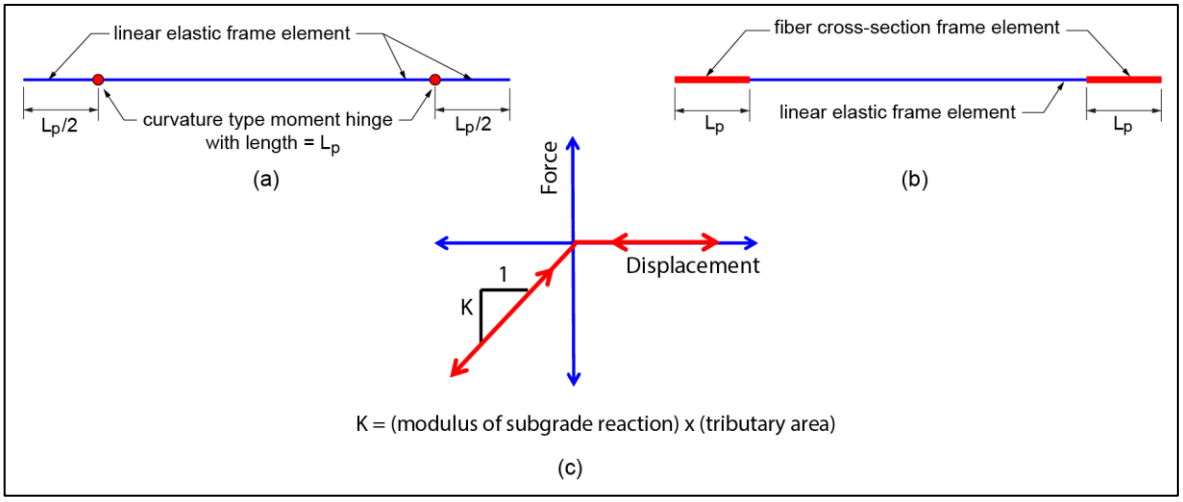

Fig. 3.6 – Modeling approach for (a) beams and (b) columns (c) support springs

Gravity loads and mass properties were modeled as concentrated loads and lumped nodal masses, respectively, and their values were set based on tributary areas. Following recommendations for PBD (LATBSDC 2015), the gravity loads include 100% of dead load and 25% of live load. On the other hand, seismic weight includes only the mass from dead load, i.e. live load was excluded from mass calculation (LATBSDC 2015; ASCE 2017). The models include PΔ effect in walls and columns. In the models, some features of the actual

floor layouts were slightly modified in order to simplify the structural models and computation of member capacities (for instance, walls having slightly separated parallel axes were assumed coaxial). Modified floor layouts are shown later in Fig. 3.10.

For concrete material, expected compressive strength was taken as 1.3 times the nominal strength (LATBSDC 2015) whereas the steel backbone curve was adjusted to match experimental test data of typical Chilean reinforcing bars available elsewhere (Alarcon 2013), which indicate yielding stresses 25% larger than the nominal value. These and other relevant material properties are listed in

Table 3.4. Ground supports were modeled using undamped nonlinear elastic, compression-only springs without energy dissipation (denoted Nonlinear Elastic Gap-Hook Bar elements in PERFORM-3D) in order to capture possible foundation uplift, as the shallow RC footings of the buildings were not designed to carry tension forces (foundation plan view and details taken from construction drawings are provided in Appendix 1). Compression stiffness of these nonlinear elastic springs was set equal to the foundation area times the modulus of subgrade reaction (Fig. 3.6c).

Modal damping was set equal to 2% for all modes. Besides, following recommendations given by the software documentation (CSI 2016c) a small amount of Rayleigh damping was provided in order to prevent undamped higher mode displacements. Thus Rayleigh damping was set equal to 0.1% at 0.2 T_1 and at 1.5 T_1 where T_1 is the first (elastic) mode period. These period values are recommended by Deierlein et al. (2010). With this damping model total damping remains below 2.3% in all the computed modes, i.e. below the maximum value of 2.5% stablished by ASCE (2017).

3.5. Incremental static (pushover) analysis

In order to evaluate their nonlinear response, the building models considered in this study were subjected to incremental static (pushover) analysis. The procedure was performed along both principal directions (short and long) following a lateral load distribution based on the first mode (i.e., the mode with the largest modal mass) along each direction. It is worth to mention that the standard pushover analysis may have limitations to accurately represent the dynamic response of tall buildings because the contribution of higher modes is underestimated. This fact could undermine the validity of the results, particularly for the 26-story building, as will be explored later. Bearing in mind that the pushover analysis is still the conventional procedure to calculate the overstrength as pretended here in chapter 3, this analysis will be applied to both buildings, but a cautious interpretation shall be given to the results. The overstrength (Ω) is defined as the ratio of the maximum lateral force reached during the pushover analysis (V_{max}) over the design base shear (V_d), computed using the effective reduced spectrum of NCh433 (Eq. 6). The overstrength is a measure of the capacity of a structure beyond that required by code specifications, and thus it is a quantitative descriptor of the structural behavior that can be realistically expected under a given earthquake scenario.

$$\Omega = \frac{V_{max}}{V_d} \qquad \text{(Eq. 6)}$$

The pushover curve and the overstrength of the models that include all the features described in Sections 3 and 4 are presented in Table 3.5 and Fig. 3.7 as model M1 = Fully nonlinear model. In these plots lateral forces are normalized by the seismic weight above the horizontal plane where the maximum and minimum base shear requirements were verified. This horizontal plane is located at the base of the 17-story building and at the grade level of the 26-story building. Roof drift ratio is measured from this horizontal plane up to the top concrete diaphragm. Buildings were pushed in 300 steps up to a roof drift ratio of 3% or until lack of convergence after 3000 nonlinear iterations, whichever occurred first.

Fig. 3.7 shows that in its short direction the 17-story building reaches a maximum strength equal to approximately 15% of the seismic weight, leading to an overstrength value of 3.11. This value is close to the 3.5 value reported for a similar 15-story building in Chile (Restrepo et al. 2017). On the other hand, the response of the 17-story building in the long direction does not exhibit strength degradation, and maximum strength is reached at a very large lateral displacement. A sharp stiffness degradation, however, is observed at a strength level roughly equal to 40% of the seismic weight. This large strength value is then assumed equal to the maximum strength and is used to compute the overstrength (= 6.34), which turned out to be much larger than that in the short direction because of the significant difference between horizontal dimensions (and therefore between lateral stiffness as well). In the case of the 26-story building, whose short and long directions are quite similar to each other, the response in both directions reaches a maximum strength of approximately 10% of the seismic weight, leading to similar overstrength values (2.03 and 2.12, respectively). The trends observed in these results, and also in those corresponding to the Chilean building analyzed by Restrepo et al. (2017), are consistent with those reported in several previous studies in the sense that overstrength decreases with increasing height (Jain and Navin 1995) and with increasing fundamental period (Humar and Rahgozar 1996). The 17- and 26-story buildings reach their maximum strength at a roof drift ratio that varies between 0.6 and 1.0%, and at that point the tangent stiffness is substantially smaller than the initial stiffness.

It was found that slabs between closely spaced walls are subjected to relatively large bending moment demands, which in turn is indicative of outrigger action (further evidence will be shown later, when describing results given by a model in which slabs are not included). Upon examination it was found that the bending moment demands on slabs exceed the capacity only at a very few locations (at less than 1% of the slab elements in each model).

The pushover analysis was also used to evaluate the influence of specific modeling issues on the global response. For this, series of additional pushover analyses were performed. In each additional analysis a single modeling issue was removed or modified from the reference model M1. The resulting models, denoted modified models, are summarized in Table 3.5

along with the corresponding modeling issue not accounted for. The pushover curves and overstrength values of each modified model are shown in Fig. 3.7 and summarized in Table 3.6. For comparison purposes, the pushover curve and overstrength value of the reference model M1 are shown as well. Since this paper deals with *undamaged* buildings, the analysis presented below focuses on the response up to maximum strength. The modified models and their corresponding modeling issues are:

M2 - Nonlinear soil-structure interaction: in these models the nonlinear elastic, compression-only support springs shown in Fig. 3.6c are replaced by linearly elastic springs (denoted Support Spring elements in PERFORM-3D) that do take tensile forces. In the case of the 17-story building this model leads to a strength along the short direction that is 18% larger than that of the reference model. In the other cases, however, no significant changes are observed, most likely because of the large dimension of the 17-story building along its long direction and because of the podium of the 26-story building, which increases overturning stability and reduces possible foundation uplift.

M3 - Soil flexibility: in these models the elastic nonlinear, compression-only support springs are replaced by fixed supports that restrain displacements and rotations in all directions. Differences with respect to the reference model are quite similar to those corresponding to model M2, i.e., there is an increase in the strength of the 17-story building (15%) along the short direction and very small variations in the other cases, suggesting that overturning stability reduces the relevance of soil-structure interaction.

M4 - PΔ effect: in these models the nonlinear geometric transformations for small deformations, i.e., the PΔ effect, is omitted. Thus all the elements use linear geometric transformations, and nonlinear behavior is due only to material nonlinearity. The analyses show that PΔ effect slightly reduces the strength, up to 4% in the 17-story building, and up to 7% in the 26-story building (Fig. 3.5). The influence of PΔ effect is even less at displacement levels smaller than that at maximum strength, suggesting that geometric nonlinearity has a very modest effect in stiff buildings such as the ones considered in this study.

M5- Bar buckling: in these models the compression strength of steel was not reduced to account for bar buckling. Instead, the steel constitutive relationship is symmetric and based on rebar tensile tests. The pushover curves of these models are virtually identical to those of the reference models up to large displacements levels, indicating that bar buckling (at least in the context of the simplified approach used herein) has a negligible effect on the stiffness and strength of the buildings.

M6- Nonlinearity in frame elements: in these models the inelastic features in beams and columns (Fig. 3.6) were removed and these members were modeled using linearly elastic frame elements. This simplification turned out to be relevant only along the long direction of the 17-story building, in which case leads to a significant increase in stiffness at strength levels greater than 20% of the seismic weight. In the other three cases it is relevant only after maximum strength is attained. (it must be noticed that in these three latter cases the maximum strength is less than 20% of the seismic weight). The lack of relevance of inelastic deformations in beams and columns at relatively low strength levels was somehow expected because most of the lateral forces are carried by the walls.

M7- Shear capacity: in these models the elastic-perfectly plastic constitutive relationship for shear in walls was replaced by a linearly elastic relationship whose stiffness is equal to the initial (elastic) stiffness of the nonlinear relationship. In both buildings these models result in a slight increase of strength (around 5%) in the long direction but do not cause appreciable differences (with respect to the reference models) in the short direction. These observations suggest that the seismic response of the walls of the buildings under study is dominated by axial-flexure rather than by shear.

M8- Effective shear stiffness: in these models the shear stiffness is equal to $0.4\ E_c\ A_{cv}$ (i.e., it is not reduced) rather than equal to just 10% of $0.4\ E_c\ A_{cv}$ as in the reference models M1 (Section 3). The reduction of the shear stiffness adopted in the reference models is recommended by ATC (2010) on the basis that the shear stiffness computed assuming isotropic conditions greatly overestimates the actual stiffness of cracked RC walls. Similar recommendations for stiffness reductions can be found in the literature (Gerin and Adebar 2004; Powell 2007; Değer et al. 2015b) but they are often omitted in practice.

Results indicate that unreduced shear stiffness leads to a significant overestimation of global stiffness. It must be noted, however, that the actual shear stiffness most likely degrades progressively as cracks develop, evolving from a value similar to that based on the gross cross-section properties at low deformation levels to a relatively small (effective) value at maximum strength. In other words the actual pushover curve probably evolves progressively from that of model M8 to that of model M1 as lateral displacements increase. In any case these results clearly indicate that shear stiffness is definitely relevant even in buildings like the ones considered in this study whose walls are slender and the contribution of shear deformations is expected to be small, and even when the displacement demand is smaller than that at maximum strength (i.e., even when there is no significant incursion into the inelastic range).

M9- Material Regularization: in these models the compressive constitutive relationship of concrete was not regularized to account for mesh sensitivity (regularization is not common in practice). Results indicate that the maximum strength is overestimated by 2%-6% when regularization is not included, while the lateral stiffness is not affected. Larger differences are observed in the descending branch of the pushover curves. This result was somehow expected because regularization affects only the descending branch of the compressive constitutive relationship of concrete.

M10- Slab elements: in these models the elastic slab elements were removed, leaving only a rigid diaphragm constraint to account for in-plane slab stiffness (slab self-weight was modeled as nodal loads). This is a common approach in practice because explicit modeling of slabs highly increases the computational cost. As it can be observed in Figure 7 this modification has by far the largest impact on the pushover curves as stiffness and strength are drastically reduced when the slabs are removed. It is recalled that the flexural stiffness of the slabs in the M1 reference models is relatively very low to account for cracking (equal to just 25% of the gross cross-section stiffness), hence even so the slabs greatly influence the global response by coupling the walls to each other. Qualitatively, the relevance of the slabs in the type of buildings analyzed in this study (i.e., typical Chilean multistory residential buildings having a seismic force-

resisting system made up exclusively of RC shear walls) has already been mentioned in Zhang et al. (2017) and in Restrepo et al. (2017). The analyses performed in this study provide a clear quantitative measure of such relevance, which turned out to be much larger than expected.

Table 3.5 Identification of modeling issues not included in the modified models

	Model ID									
Modelling feature not included	M1	M2	M3	M4	M5	M6	M7	M8	M9	M10
Nonlinear soil structure interaction		X								
Soil flexibility			X							
PΔ effect				X						
Bar buckling					X					
Nonlinearity in frame elements						X				
Shear capacity							X			
Effective shear stiffness								X		
Material regularization									X	
Slab elements										X

Table 3.6 Overstrength values for the reference model (M1) and the modified models (M2-M10)

		Overstrength (Ω)									
Building	**Direction**	**M1**	**M2**	**M3**	**M4**	**M5**	**M6**	**M7**	**M8**	**M9**	**M10**
17-story	Short	3.11	3.66	3.58	3.22	3.11	3.22	3.12	3.23	3.31	1.84
	Long	6.34	6.69	6.31	6.53	6.35	7.06	6.68	5.27	6.48	2.57
26-story	Short	2.03	2.03	2.00	2.18	2.04	2.07	2.01	2.31	2.11	1.04
	Long	2.12	2.11	2.00	2.23	2.12	2.16	2.20	2.21	2.20	1.32

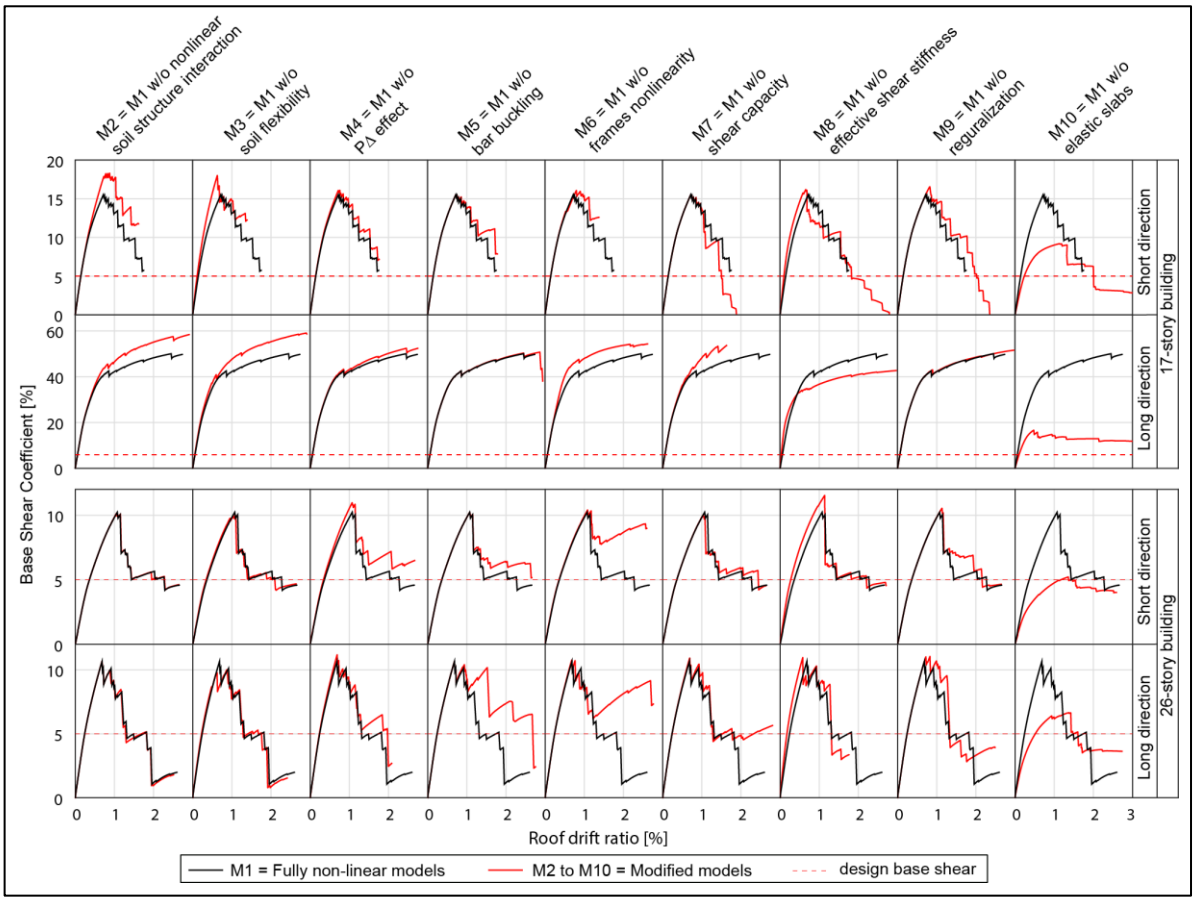

Fig. 3.7 – Pushover response of the reference model (M1) and the modified models (M2-M10)

3.6. Response history analysis

The fully nonlinear models M1 were subjected to Response History Analysis (RHA) to study the seismic performance of the 17- and 26-story buildings. RHA was also performed in models M2 (i.e., omission of nonlinear soil-structure interaction) because results given by previous RHA of linearly elastic models of the superstructure (Ugalde and Lopez-Garcia 2017b) suggested that foundation uplift could significantly affect the seismic demands on the walls. The models were simultaneously subjected to both horizontal components of the ground motion recorded at the Santiago Centro station during the 2010 Chile Earthquake (Table 3.7). This station is located nearby the buildings in similar soil conditions according

to data reported by Kayen et al. (2014) and in seismic zone II (A_0=0.3g according to NCh433). The horizontal components of the record were applied in the principal directions of the buildings according to their approximate geographic orientation (Fig. 3.1), i.e. the North-South component was applied in the long direction of the 17-story building and in the short direction of the 26-story building. PERFORM-3D uses the step-by-step constant-average-acceleration time integration method (Newmark 1959), which is unconditionally stable. When this method is applied to multi degree-of-freedom structures the time step should be smaller than the period of the highest mode that significantly contributes to the response divided by 12 in order to obtain sufficient accuracy. Thus, the time step for all the analyses was set equal to 0.01 s, which satisfies the previous recommendation. In any case this time step was in many instances reduced even further as the event-to-event solution strategy implemented in PERFORM-3D automatically reduces the time step wherever there is a nonlinear event, i.e., a change in stiffness. Due to the large size of the models the maximum number of nonlinear events per time step was set equal to 500, and while the output of the analyses indicates that the vast majority of the steps were solved with less than 250 sub-divisions (nonlinear events) a few time steps needed up to 473.

Table 3.7 – Properties of the ground motion used in RHA

Station name	Soil type	PGA North-South [g]	PGA East-West [g]	Record duration [s]	Distance to 17-story building [km]	Distance to 26-story building [km]
Santiago Centro	II	0.21	0.31	140	4.8	9.1

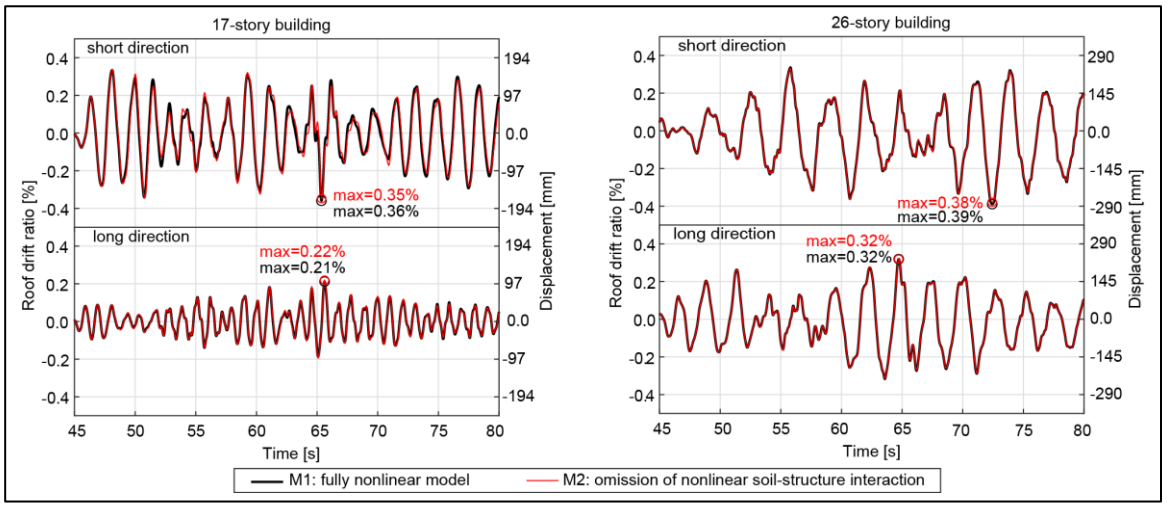

Fig. 3.8 – Roof drift ratio for short and long direction of both buildings

Fig. 3.8 shows a portion of the roof drift response history to emphasize the comparison between models M1 and M2 around the time of maximum response. Notice that the difference between the response of the models is modest as their curves technically overlap each other. This result is consistent with the static analyses as the pushover curves of models M1 and M2 also overlap at roof drift ratios similar to those given by RHA (the maximum values of the latter are highlighted in Fig. 3.8). Besides, at these levels of roof drift ratios (i.e., less than 0.4% in all cases) the pushover curves indicate little stiffness degradation, which is consistent with the empirically observed lack of damage.

Although the difference between the roof displacement response of the models with (M1) and without (M2) nonlinear soil-structure interaction is negligible (Fig. 3.8), results given by models M1 indicate that significant foundation uplift does occur at some support joints, particularly in the 17-story model. Fig. 3.9a shows the peak upwards vertical displacement of each support joint during the RHA. Notice that model M1 gives uplift values as large as 60 mm, which are drastically reduced when the support springs are linear (model M2). A similar comparison is presented in Fig. 3.9b in terms of the corresponding vertical reactions, which show unrealistically large tensile forces given by model M2.

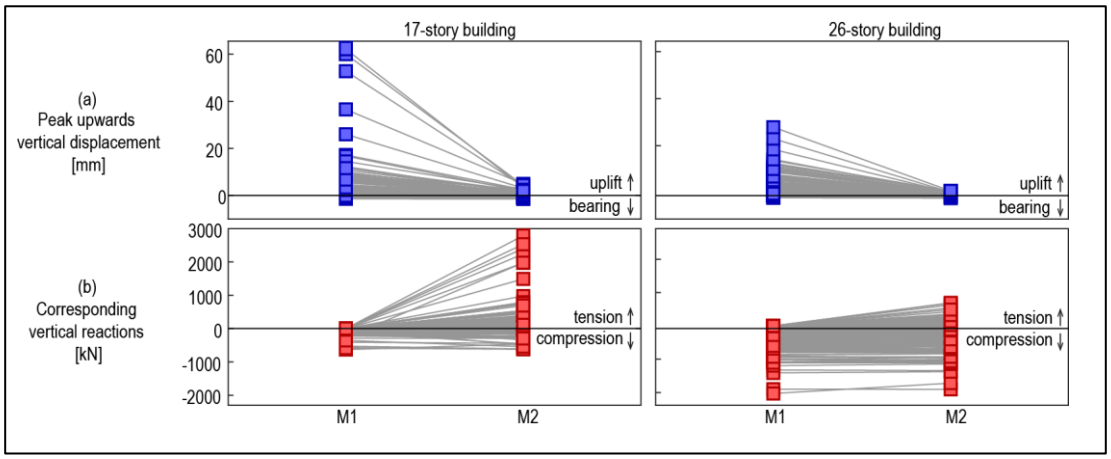

Fig. 3.9 – Variation of vertical (a) displacements and (b) reactions with and without nonlinear soil-structure interaction

PBD guidelines offer some criteria to assess the seismic performance by means of drift ratios. For instance ASCE 41-13 (ASCE 2014) establishes that at immediate occupancy walls do not exceed a 0.4% drift ratio, whereas LATBSDC (2015) establishes, indistinctly, a maximum drift ratio of 0.5% for performance acceptance. These requirements are expressed in terms of total story drift ratios, which could be substantially different from roof drift ratios like those indicated in Fig. 3.7 and Fig. 3.8. Thus, six walls in each building, distributed along the floor plan and oriented in both directions (Fig. 3.10), were selected to evaluate total story drift ratios. This quantity is defined as the horizontal displacement between two vertically aligned joints at consecutive floors (Fig. 3.10c) divided by the (undeformed) vertical distance between the same joints. Total story drift ratio, which is the quantity typically addressed in design codes, has a component due to panel distortion (shear and flexural deformations) and another component due to rigid body rotation, which is not expected to produce damage in walls. Then, an additional evaluation was performed using the tangential drift (ATC 1996) which, rather than horizontal displacement, considers the displacement perpendicular to the wall slope (Fig. 3.10c). Tangential drift accounts only for shear and flexural deformations, which are related to wall damage, and is a better indicator of structural performance in mid- to high-rise buildings (FIB 2003). However, tangential

drift calculation requires more input data than the total drift, and is usually omitted in design guidelines.

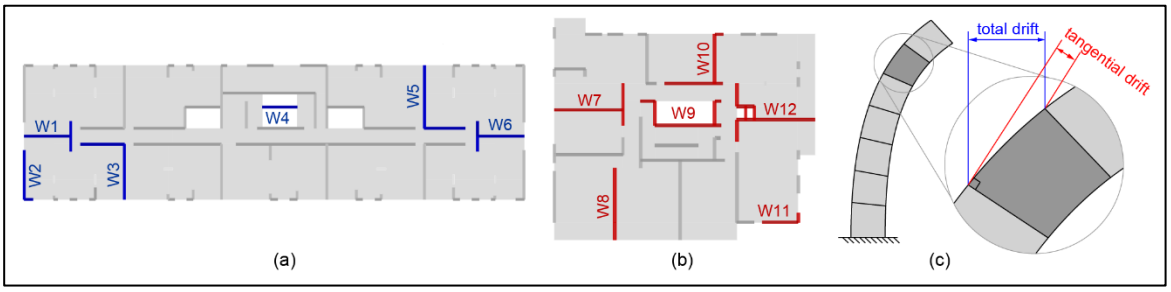

Fig. 3.10 – Selected walls distributed along the (modified) floor plan of (a) the 17-story building and (b) the 26-story building. (c) Difference between total and tangential story drift ratios

Peak values of total and tangential story drift ratios at each story of the selected walls are presented in Fig. 3.11 (peak values at different stories do not necessarily occur at the same time). Only results of models M1 are included. At each wall, story drifts were measured along the horizontal direction parallel to the web of the wall, which is aligned to the wall label in Fig. 3.10. Results in terms of total drift ratios indicate that 8 out of 12 walls exceed the ASCE 41-13 limit and 5 also exceed the LATBSDC limit, which would be typically associated with some degree of damage. Notice, however, that tangential drifts are quite smaller and rarely exceed 0.2%. It is acknowledged that total story drift limits are intended for other purposes such as to control chord rotation in beams and to limit non-structural damage, which could be left unattended if limits were expressed in terms of tangential story drift. However, in a post-earthquake evaluation scenario (rather than in a design scenario) the tangential story drift ratio is a much better indicator of damage, and results shown in Fig. 3.11 are definitely consistent with the observed lack of damage in the buildings.

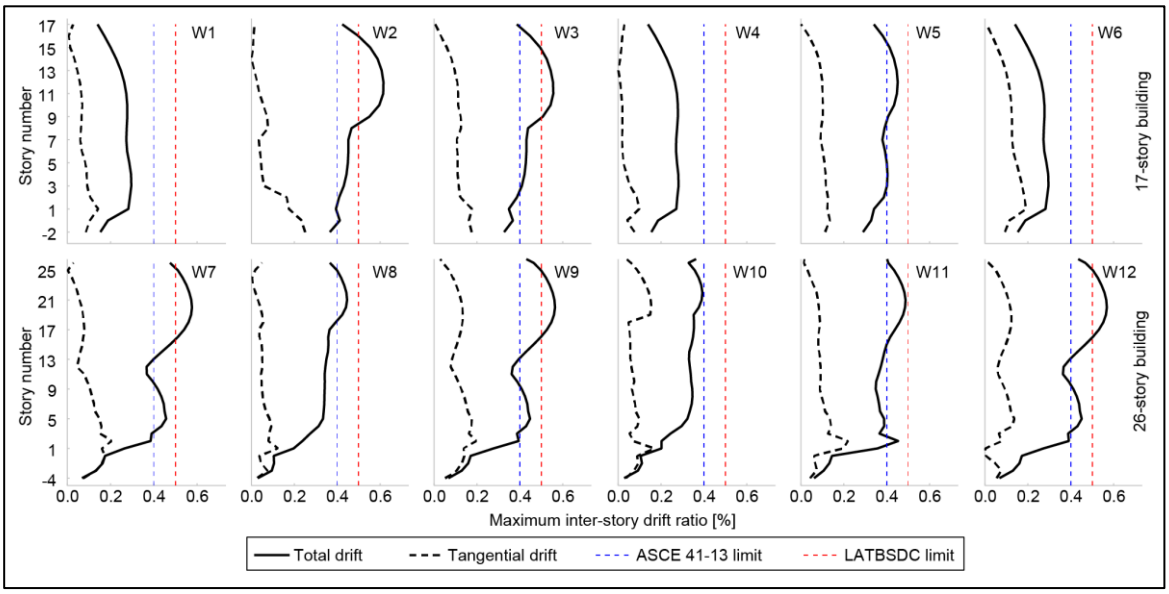

Fig. 3.11 – Maximum total and tangential story drift ratios of the monitored walls (model M1)

A similar analysis is presented in Fig. 3.12, which shows the peak compression and tension strains at the two Steel Bar/Strut/Tie elements used to model the boundary steel of each selected wall. The strain at the onset of strength loss of unconfined concrete and the yielding strain of a 420 MPa grade steel (both equal to 0.2%) are presented as limit values. Notice that according to this local response little damage (if any at all) is expected as strain values remain below the established limits. It is recalled that according to the validation analysis presented in Section 3 the modeling approach adopted in this study, on average, overestimates the tension strains by 34% and underestimates the compression strains by 54%. These values can be used to "correct" (i.e., to calculate a more realistic estimation of) the strain curves, and the "corrected" values are also presented in Fig. 3.12. In doing so concrete strains become close to that at the onset of strength loss in several walls but exceed the limit value in only one wall (W11). However, considering that compression strains decrease along the web, such exceedance affects only the fibers at the end of the wall and hardly translates into noticeable damage.

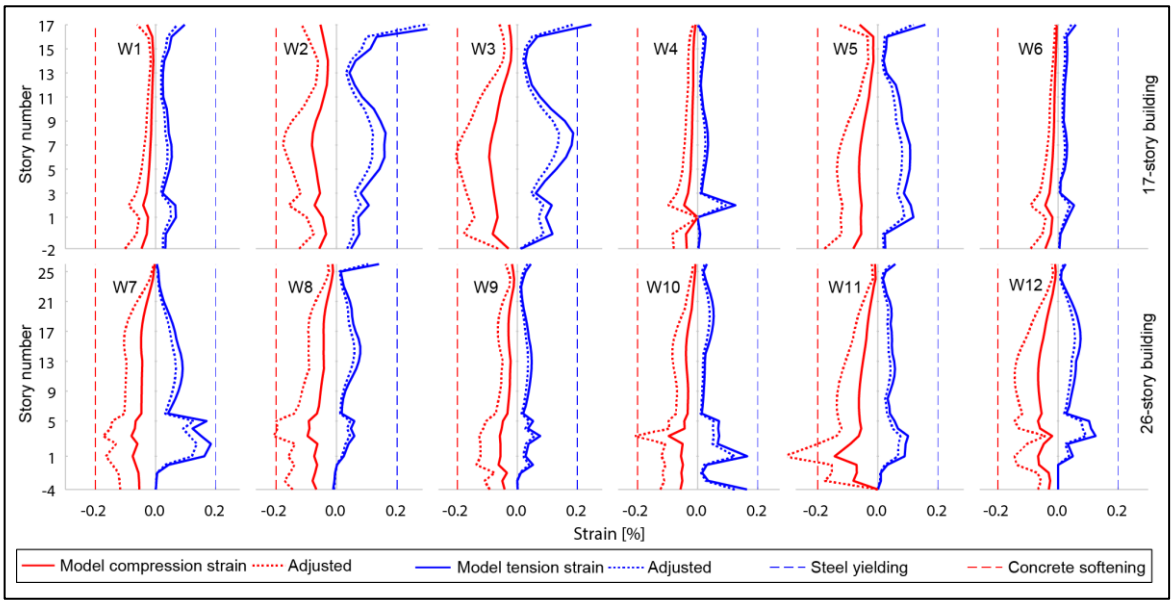

Fig. 3.12 – Maximum boundary strains in the monitored walls (model M1)

Finally, the peak demand/capacity (D/C) ratios for axial-bending and shear at the most demanded story of the selected walls were computed using results given by models M1 and M2. The axial-bending D/C ratios were computed according to the graphical approach presented in the interaction diagram of Fig. 3.13a, i.e., demands and capacities were not measured from the unloaded condition but from the internal forces due only to gravity loads. For consistency, shear D/C ratios were computed in the same way. In order to account for the non-rectangular cross-section of the walls, the interaction diagrams were obtained through series of moment-curvature analyses using fiber cross-sections defined in OpenSees (McKenna et al. 2000). Shear capacity was computed according to Chapters 11 and 18 of ACI 318-14, and such capacity was amplified by 1.5 to account for ultimate conditions (Değer et al. 2015b). Both axial-bending and shear analyses used expected material properties (Table 3.4) and strength reduction factor (ϕ) equal to 1.0. Results are presented in Fig. 3.13b. Notice that no relevant difference is observed between the D/C ratios of models M1 and M2, confirming the modest effect of foundation uplift on the response of the buildings. All shear D/C ratios are less than unity (by a wide margin in the 26-story building), which is consistent with the lack of relevance of the shear capacity already observed in

pushover analysis (model M7). On the other hand, larger D/C ratios are observed in axial-bending behavior, particularly in the 26-story building where the capacity is exceeded in two walls (W7 and W12). The interaction diagrams of these walls and the corresponding demand histories are presented in Fig. 3.13c, where it can be observed that there is one incursion outside the capacity diagram in wall W7 and two very subtle incursions in wall W12. It must be kept in mind, however, that according to the validation analysis presented in Section 3 the wall model adopted in this study might overestimate the bending moment demand up to 24%. Further, the incursions occur at the lower bound of the interaction diagram where a ductile failure is expected due to steel yielding, specifically at the unflanged end of these walls. Thus, in the real structure it is possible that steel bars at this location actually yielded but the tension cracks eventually closed and were not noticeable after the earthquake, as it has been observed in shake-table test of walls (Panagiotou et al. 2010).

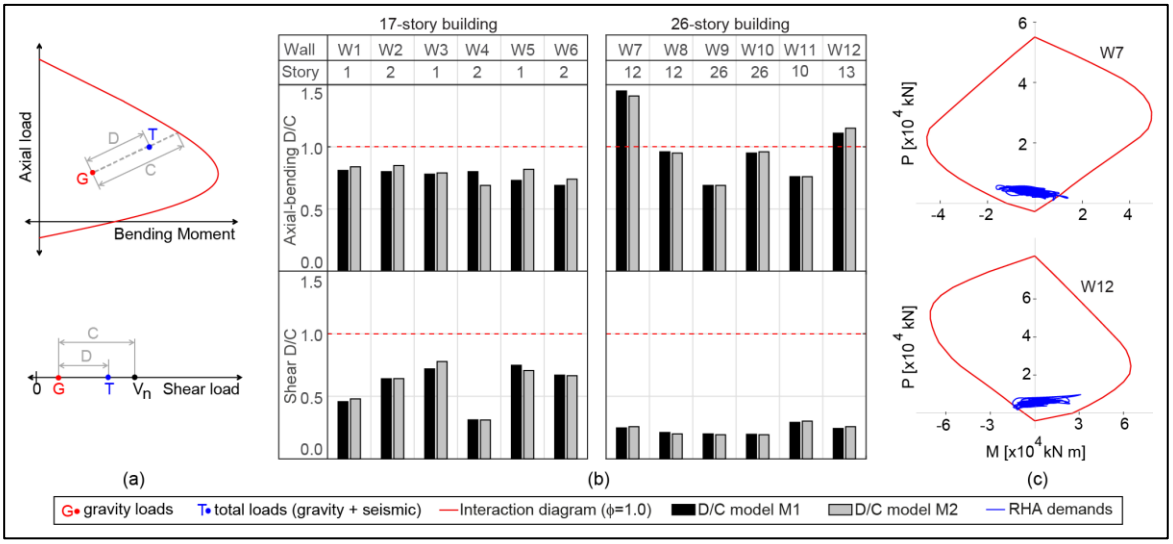

Fig. 3.13 – (a) Criteria to compute demands D and capacities C; (b) Axial-bending and shear D/C ratios for the monitored walls; (c) Interaction diagram of walls W7 and W12

3.7. Evaluation of the effect of stiffness degradation on the seismic performance

In the former section it was found that results given by RHA of fully nonlinear models are essentially consistent with the empirically observed lack of damage. When stiffness

degradation (even at relatively low levels of roof drift ratio) is taken into account to determine the dynamic properties of the buildings, more qualitative insight into the reasons for the lack of observable damage can be obtained by comparing seismic demands and capacities in terms of Acceleration-Displacement Response Spectra (ADRS).

The pushover curves shown in Fig. 3.7 (reference models M1) were converted into capacity spectra using the following equations (ATC 1996):

$$S_a = \frac{V}{\alpha_1} \quad \text{(Eq. 7)}$$

$$S_d = \frac{u_{roof}}{\Gamma_1 \phi_{1,roof}} \quad \text{(Eq. 8)}$$

where S_a = pseudo-acceleration, V = base shear, α_1 = first mode mass coefficient, S_d = spectral displacement, u_{roof} = lateral roof displacement, Γ_1 = first mode participation factor and $\phi_{1,roof}$ = first mode ordinate at the roof level. The resulting capacity spectra in the short direction (critical, particularly in the 17-story building) are shown in Fig. 3.14 along with the same elastic response spectra already shown in Fig. 3.2 (recorded ground motions). The response spectrum of the short-direction component of the record used in RHA (Section 3.6) is highlighted in red color. Strictly speaking, the point at the intersection of the capacity spectrum and the response spectrum is not really the performance point because at such point the capacity spectrum is not strictly linear any more. However, such point is located well before the point at maximum strength of the capacity spectrum, which means that the level of ductility at the intersection point must be very low (if any at all). Therefore, the intersection point is assumed as a very good approximation of the actual performance point.

Consistent with results given by RHA, Fig. 3.14 clearly shows that at the performance point the demand imposed by the Santiago Centro record is less than the capacity (i.e., peak strength) of the buildings. Further, the same can be said about the demands imposed by the other records. At the performance point of the Santiago Centro record the effective period (i.e., the one based on secant stiffness) is equal to 1.85 s (17-story building) and 2.49 s (26-

story building). These periods roughly coincide with the periods than can be inferred from the roof displacement responses (short direction) shown in Fig. 3.8. The effective periods are substantially larger than the nominal periods reported in Table 3.1 and shown in Fig. 3.2. The nominal periods are the ones that were considered in the actual design of the buildings (i.e., the ones with which the design seismic loads were determined), and were calculated following the standard practice in Chile. They were obtained from linearly elastic 3D models in which shear and bending stiffness of all members are based on gross cross-section properties, walls and slabs were modeled with shell elements, and diaphragm constraints were incorporated at each floor level. Such practice is believed to be conservative, and is widely adopted because of simplicity and also because effective stiffness properties are not considered in the local seismic design codes. Pseudo-acceleration ordinates at the nominal periods are equal to 0.29 g (17-story buildings) and 0.18 g (26-story building), but at the effective periods are significantly smaller, 0.11 g and 0.12 g, respectively. Hence, the significant amount of stiffness degradation even at a displacement level smaller than that at peak strength leads to significant period elongation, which in turn leads to demands that are substantially smaller than those at the nominal periods.

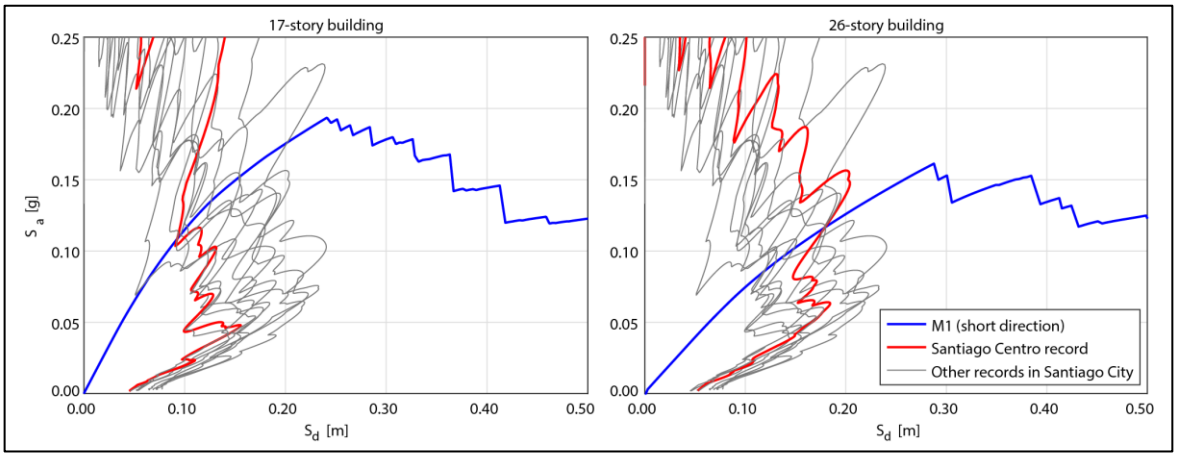

Fig. 3.14 – Comparison between capacity and response spectra in ADRS format

Note that the response predicted by the pushover analysis in Fig. 3.14 is quite similar for both buildings in terms of stiffness reduction close to the performance point. However, the

results of RHA presented in Fig. 3.13 showed that, in general, the axial/bending D/C ratios of the taller building were higher, and two of its walls slightly exceeded the nominal capacity at intermediate stories. This could be the result of higher mode effects during the dynamic analysis that are not reflected in the static pushover analysis.

Note: the conclusions of this chapter are presented in section 5.2.

---

4. PAPER III: FRAGILITY-BASED ANALYSIS OF THE INFLUENCE OF EFFECTIVE STIFFNESS OF REINFORCED CONCRETE MEMBERS IN SHEAR WALL BUILDINGS

4.1. Introduction

In Chile the frequent occurrence of severe earthquakes has led to the adoption of a somewhat unique structural system in multistory *residential* buildings. Such structural system, rarely found elsewhere, consists almost exclusively of a large number of Reinforced Concrete (RC) shear walls (NIST 2012). This structural system has been deemed the most likely reason for the satisfactory performance of most Chilean residential buildings in recent major seismic events such as the M_W 8.0 1985 Algarrobo Earthquake (Wood 1991) and the M_W 8.8 2010 Maule Earthquake (Saito et al. 2011). In the latter event the small number of damaged buildings is remarkable given that the (reduced) design spectra prescribed by the Chilean seismic design code were exceeded (by a large margin in many cases) by the spectra of many ground accelerations recorded at several stations (Naeim et al. 2011). This observation motivated a previous study conducted by the authors (Ugalde et al. 2019c) where Static Pushover (SPO) analysis was used to quantify the overstrength of residential wall buildings. The study strongly recommended further research on two modeling issues that were found to have a significant impact on the analytical non-linear response. Those modeling issues, deeply analyzed in this paper, are: (a) the in-plane shear stiffness of the shear walls, hereafter called the wall shear stiffness; and (b) the out-of-plane bending stiffness of the slabs, hereafter called the slab bending stiffness.

When a RC structure is subjected to increasing levels of external forces the stiffness of its members decreases progressively due to concrete cracking and the parabolic stress-strain relationship of concrete. This gradual stiffness degradation can be correctly accounted for only by non-linear models. In practice, such non-linear models are typically macroscopic. They account for the non-linear stiffness of the members that most contribute to the global response, and the stiffness of the remaining members is often modeled simply as linearly elastic or sometimes not modelled at all. For instance, most of the non-linear models

currently implemented in Performance-Based Design (PBD) of slender walls use either concentrated or distributed plasticity to model the axial and in-plane bending behavior, while the out-of-plane bending and shear behavior (deemed less relevant) have linear constitutive relationships. Similarly, slabs are modeled by linear shell elements when they are explicitly included, and in many cases they are not even modeled and are instead (partially) accounted for simply by a rigid diaphragm constraint.

Some novel models have shown promising capabilities to model the non-linearity of the wall shear stiffness (Kolozvari et al. 2015) and the slab bending stiffness (Lu et al. 2014), but their implementation in large building models is still cumbersome. Consequently, both the wall shear stiffness and the slab bending stiffness are still linearly modeled in most cases. In such simplification, the gross cross-section stiffness is reduced to a constant (effective) value intended to be consistent with the expected stiffness degradation at the demand level considered in the analysis. However, given the simplified nature of this approach, the value of the effective stiffness is affected by a large degree of uncertainty, and (as it will be shown later) there is a wide range of values recommended in the literature. This lack of consensus motivated the analyses presented in this paper, which are intended to assess the influence of the effective value of the wall shear stiffness and the slab bending stiffness on the analysis of models of RC Chilean residential shear wall buildings subjected to seismic loading.

Currently, a robust method widely implemented to study the seismic performance of structures consists of developing fragility curves. The structural models are typically subjected to Incremental Dynamic Analysis (IDA) (Vamvatsikos and Cornell 2002) using several earthquake records. For each record, series of Response History Analysis (RHA) are performed at increasing values of a given Intensity Measure (IM), and the response value of a given Engineering Demand Parameter (EDP) is monitored. It is then possible to find, for a given value of the IM, the number of records that causes the EDP to exceed a given threshold typically associated with a given limit state (such as, for instance, immediate occupancy). Probabilities of exceedance, conditional to given values of the IM, are then obtained directly, and such information is then presented as fragility curves. This

comprehensive procedure, however, requires numerous non-linear RHAs that might not be feasible to perform because of the very large computational cost. This limitation is particularly relevant for full 3D models of structures with complex configurations, such as tall residential RC Chilean wall buildings, and this is likely the reason why, to the best of the authors' knowledge, there are no published studies on fragility curves for this specific kind of buildings. Consequently, there is a motivation to implement simplified methods to develop fragility curves. One of these simplified methods is Static Pushover to Incremental Dynamic Analysis (SPO2IDA) (Vamvatsikos and Cornell 2006), which uses empirical equations to simulate IDA from results given by SPO. This procedure was recently extended to Static Pushover to Fragility (SPO2FRAG) (Baltzopoulos et al. 2017), with which it is possible to develop (in an approximate manner) fragility curves accounting for several sources of uncertainty.

In this paper, the influence of effective values of the wall shear stiffness and the slab bending stiffness on the analytical seismic performance of Chilean RC residential wall buildings is evaluated through fragility curves developed by the SPO2FRAG procedure. A validation analysis of the SPO2FRAG procedure was performed first. The seismic fragility of a 16-story Chilean office building (already presented in the literature) was compared with that given by the SPO2FRAG procedure, and the latter was found to be a reasonable approximation to the former. The SPO2FRAG procedure was then implemented to develop seismic fragility curves of two actual and representative residential buildings of 17 and 26 stories located in Santiago (Chile). Full 3D non-linear models of the buildings were developed in the software PERFORM-3D and were subjected to SPO analysis. Several fragility curves were obtained considering several values of effective stiffness recommended in the literature, and the influence of the effective value of the wall shear stiffness and the slab bending stiffness was then evaluated.

4.2. Wall Shear Stiffness and Slab Bending Stiffness

According to the small-displacement theory of beams with shear flexibility the bending moment (M) and the shear force (V) in a frame element can be expressed as follows (Krenk 2001):

$$M = EI\,\kappa \tag{1}$$

$$V = GA_s\,\gamma \tag{2}$$

where EI and GA_s are the bending and shear stiffness, respectively. The curvature κ is the ratio of the distance between two sections (ds) measured along the beam axis to the angle between those sections ($d\theta$) (Fig. 4.1a). The average shear strain, γ, is the angle between the beam axis and the line perpendicular to a beam section (Fig. 4.1b). A_s is the shear area that takes into account the non-uniform distribution of shear stresses over the beam section.

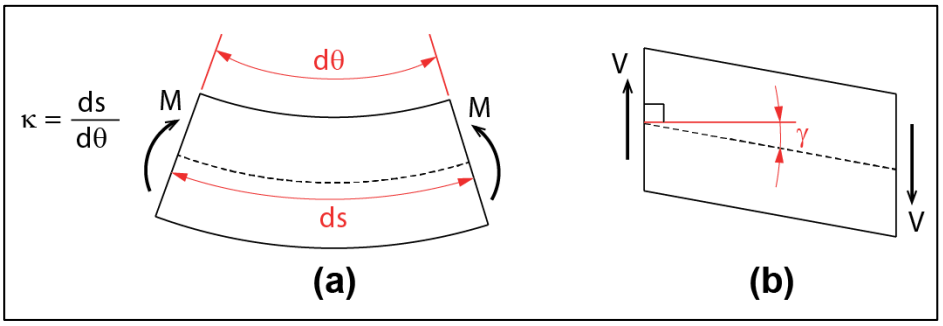

Fig. 4.1 – Deformed beam section in: (a) bending; and (b) shear.

Using equilibrium and kinematics considerations the relations presented in Eqs. (1) and (2) can be extended to relate displacements with forces at a given degree of freedom of a structure. For instance, Fig. 4.2a shows that the lateral displacement at the top of a laterally loaded cantilever wall has a component related to the shear stiffness and a component related to the bending stiffness. If the wall is slender, the term L^3 makes the bending component more relevant than the shear component. Similarly, Fig. 4.2b shows the relationship between the end rotation of a slab bent between two walls and the end moments of the slab (obtained

according to Bernoullis beam theory when vertical displacement are zero). The latter expression is valid only when the slab span is much larger than the slab thickness because in such a case the shear component is negligible. In general the force-displacement relationships depend on the kinematics of the structural system, but in all cases the terms EI and GA_s appear in the resulting expressions.

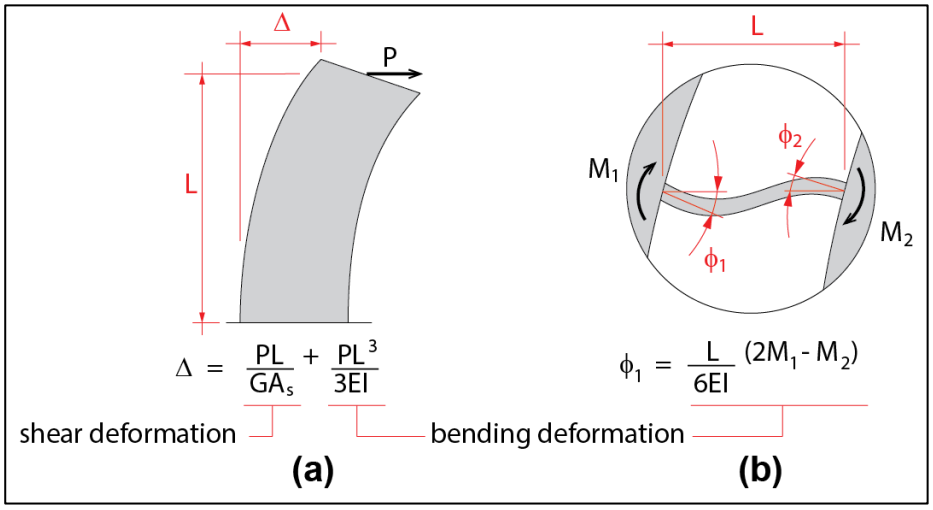

Fig. 4.2 – Deformation components for: (a) a cantilever wall; and (b) a slab between two walls

In RC structures the uncracked shear modulus is computed assuming isotropic behavior and a Poisson ratio (ν) equal to 0.2, as presented in Eq. (3). The (uncracked) gross shear stiffness of RC walls is then given by Eq. (4), where A_w is the gross area of the wall web.

$$G = \frac{E}{2(1+\nu)} = 0.4\,E \tag{3}$$

$$GA_s = GA_w = 0.4EA_w \tag{4}$$

However, the isotropic material assumption is not accurate for cracked concrete. As a result, the shear stiffness of cracked walls might be considerably smaller than that given by Eq. (4). According to ATC-72 (ATC 2010), the effective shear modulus of a RC wall at yield varies between 0.05 G and 0.10 G depending on the shear strength. In the context of PBD,

LATBSDC (2015) recommends a shear area equal to 1.0 A_w under service conditions and equal to 0.5 A_w under Maximum Considered Earthquake (MCE) conditions. It is interpreted that this reduction of cross-section is equivalent to a reduction of the shear modulus.

Some studies on specific RC wall buildings have assumed different values of the wall effective shear stiffness (GA_{eff}) based on judgment. For instance, Powell (2007) used 0.25 GA_w, Değer et al. (2015) used 0.20 GA_w, and Beiraghi et al. (2015) used 0.14 GA_w. Hagen (2012) used a secant shear stiffness in a trilinear backbone curve, approximated using a moment distribution assumption, and obtained secant stiffness values between 0.07 GA_w and 0.08 GA_w. Validation of any of these criteria to provide a single recommendation would require either experimental data or sophisticated microscopic models. Unfortunately, the test data necessary to assess the shear stiffness is scarce due to practical limitations to accurately measure shear deformations. Some analytical models have found that the values of effective stiffness more appropriate to reproduce experimental tests are 0.1 GA_w for relatively slender cracked walls (Tran 2012) and 0.025 GA_w for slender cracked walls (Gogus 2010). In an analysis of a relatively slender wall Kolozvari and Wallace (2016) compared a fiber model (in which the shear stiffness was accounted for through a constant (linear) effective value) with a shear-coupled model whose shear stiffness degraded through the analysis. They found that setting $GA_{eff} = 0.1\ GA_w$ improves the response matching at the plastic hinge region (1st story), while setting $GA_{eff} = 0.5\ GA_w$ improves the matching at the other stories. This finding highlights the limitations of assuming a single GA_{eff} value at all stories. The large dispersion of the GA_{eff} values available in the literature raises questions on whether this variation is relevant for the seismic fragility of tall wall buildings.

Regarding the slab effective bending stiffness (EI_{eff}), there is a similar scenario in the sense that several guidelines provide different reduction factors. ACI 318-14 (ACI 2014) specifies an effective moment of inertia equal to 0.25 I_g for the prescriptive design of buildings (I_g is the gross cross-section moment of inertia). ASCE 41-13 (ASCE 2014) recommends 0.33 I_g for the analysis of existing buildings (with non-posttensioned slabs) while LATBSDC (2015) recommends a sensitivity analysis using 0.2 I_g and 0.5 I_g. Schotanus and Maffei

(2008) conducted a parametric study where results obtained by shaking table tests of a wall building were compared with results given by analytical models. They found that analytical displacement predictions improved when the slab effective bending stiffness EI_{eff} was set equal to 0.1 EI_g in both linear and non-linear models. Other researchers (Powell 2007; Moehle et al. 2011) did not include the slab elements and instead used a rigid diaphragm constraint in their models. This practice (equivalent to setting EI_{eff} = 0.0 EI_g) is commonly observed in non-linear analysis of core wall buildings (i.e., buildings having only a small number of shear walls, plus perimeter frames). However, other studies (Zekioglu et al. 2008; Yang et al. 2010; Melek et al. 2012) have shown that slabs can significantly affect the seismic response of this kind of structures, which raises questions on the validity of models in which the slabs are not explicitly accounted for.

Some analytical models (Junemann et al. 2016; Restrepo et al. 2017; Zhang et al. 2017) and post-earthquake observations (Telleen et al. 2012a; Westenenk et al. 2012) of residential RC wall buildings in Chile have shown that slabs do provide an unintended coupling effect that substantially influences the seismic performance. However, the use of an slab effective bending stiffness is not addressed in the Chilean seismic design code NCh-430 (INN 2008b). It is indeed mentioned in the recently published Chilean PBD guideline (ACHISINA 2017), but this last document is a reference guideline that is not yet part of the Chilean seismic design regulations. Therefore, the prescriptive seismic design of wall buildings in Chile consists of using linearly elastic models in which the slabs are explicitly modeled with shell elements whose bending stiffness is equal to the gross cross-section stiffness (i.e., EI_{eff} = EI_g). This approach could lead to underestimation of lateral displacements, but such issue is rarely of concern in Chilean residential wall buildings because they are usually very stiff structures.

Fig. 4.3 shows the effective stiffness values mentioned in the former paragraphs. It can be observed that there is a large dispersion of values. This dispersion is a consequence of the numerous factors the stiffness of RC members depends on, such as member dimensions, reinforcement ratio, and level of demand. The values marked with a star are the values

considered in this paper to analyze the influence of the wall shear stiffness and the slab bending stiffness on the analytical seismic response of two residential RC wall buildings. A set of models was created using different values of the wall shear stiffness (GA_{eff}/GA_w = 0.05, 0.1, 0.2 and 1.0) and another set of models was created using different values of the slab bending stiffness (EI_{eff}/EI_g = 0.0, 0.1, 0.25, 0.5 and 1.0). Each model was subjected to SPO analysis and then the SPO2FRAG procedure was applied.

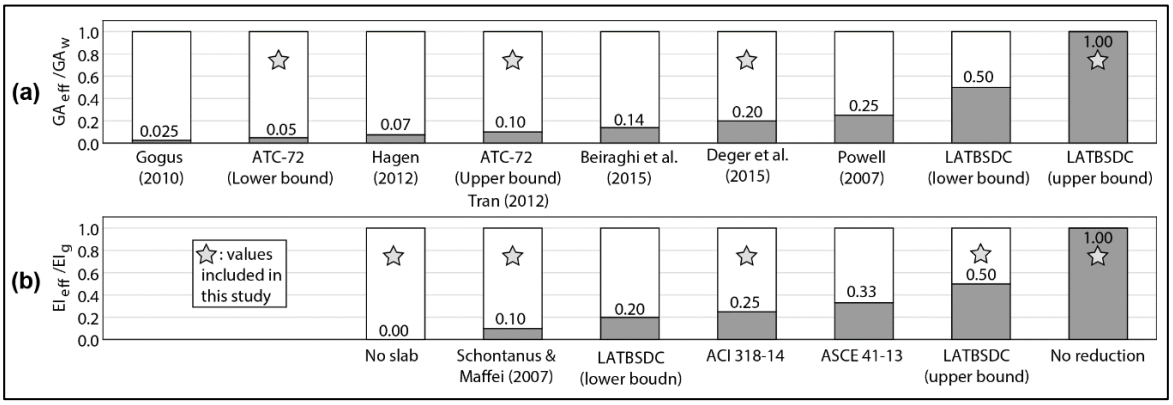

Fig. 4.3 – Effective values found in the literature for: (a) wall shear stiffness; and (b) slab bending stiffness

4.3. SPO2IDA and SPO2FRAG procedures

SPO2IDA is a methodology presented by Vamvatsikos and Cornell (2006) to provide estimates of IDA curves based on results given by SPO analysis. The capacity curve obtained by SPO is converted into a simplified piece-wise curve completely defined by a few parameters. The empirical SPO2IDA equations that relate the IDA curve with the period of the structure and the parameters of the SPO curve were derived from results given by a large number of IDAs of single degree-of-freedom (SDOF) oscillators having a wide range of periods and types of force-displacement relationships (Vamvatsikos and Cornell 2006). SPO2IDA provides empirical equations for the 16, 50 and 84% fractile curves, which are the curves above the 16, 50 and 84% of the IDA curves. These percentages are relevant because they are the probabilities of exceedance associated to the mean, plus/minus one

standard deviation of a normal distribution (assumed below for the logs of the IM) and then they can be used to find the best-fitting cumulative distribution function of a fragility curve.

The SPO2FRAG procedure presented by Baltzopoulos et al. (2017) is an extension of the SPO2IDA procedure. It incorporates the estimation of fragility functions considering different limit states and sources of uncertainty. The procedure is implemented in an open source software also called SPO2FRAG. It contains algorithms for the automatic conversion of the SPO curve into the piece-wise backbone of an equivalent SDOF system. With this information, the IDA curves are computed in an R vs. μ format and are then automatically converted into a traditional IM vs. EDP format (Baltzopoulos et al. 2017). Then, the threshold EDP value associated with a given limit state defines a vertical line whose intersection with the IDA fractile curves defines the IM values at probabilities of exceedance equal to 16%, 50% and 84%, denoted $IM_{16\%}^{LS}$, $IM_{50\%}^{LS}$ and $IM_{84\%}^{LS}$, respectively (Baltzopoulos et al. 2017). It is assumed that the IDA curves follows a lognormal distribution, i.e., the logs of the IM follows a normal distribution and then the logs of the 16% and 84% fractile curves are one standard deviation away from the log of the 50% fractile curve. In other words, as presented in Eq. 5 and 6, the mean of the logs (η) is given by the log of the 50% fractile curve and the logarithmic standard (β) deviation is given by the distance between the logs of the 16% and 50% fractile curves (or alternatively, by half the distance between the logs of the 16% and the 84% fractile curves) (Baltzopoulos et al. 2017):

$$\eta = \ln\left(IM_{50\%}^{LS}\right) \tag{5}$$

$$\beta = \ln\left(\frac{IM_{50\%}^{LS}}{IM_{16\%}^{LS}}\right) \quad \text{or} \quad \beta = \frac{1}{2}\ln\left(\frac{IM_{84\%}^{LS}}{IM_{16\%}^{LS}}\right) \tag{6}$$

Additional sources of uncertainty, such as record-to-record variability at nominal yield due to higher-mode effects (β_y) and model uncertainty (β_u) can also be accounted for (Baltzopoulos et al. 2017). In doing so, the value of parameter β increases.

4.4. Case Studies

The case studies are two RC wall buildings located in Santiago, the capital city of Chile. The first building (Fig. 4.4a), built in 2006, has 17 stories and 2 basement levels. The second building (Fig. 4.4b), built in 2005, has 26 stories and 4 basement levels. Typical of residential buildings in Chile, the structural system is entirely made up of cantilever walls, i.e., there are no frames or coupling beams. RC walls resist all the gravity and earthquake loads. The thickness of most walls ranges between 150 and 170 mm, and some thicker walls are found at the basement levels. Table 4.1 summarizes these and other relevant building properties. The buildings showed no observable damage after the severe 2010 Chile Earthquake (M_w 8.8) and their functionality was not interrupted (i.e., they kept continuous occupancy).

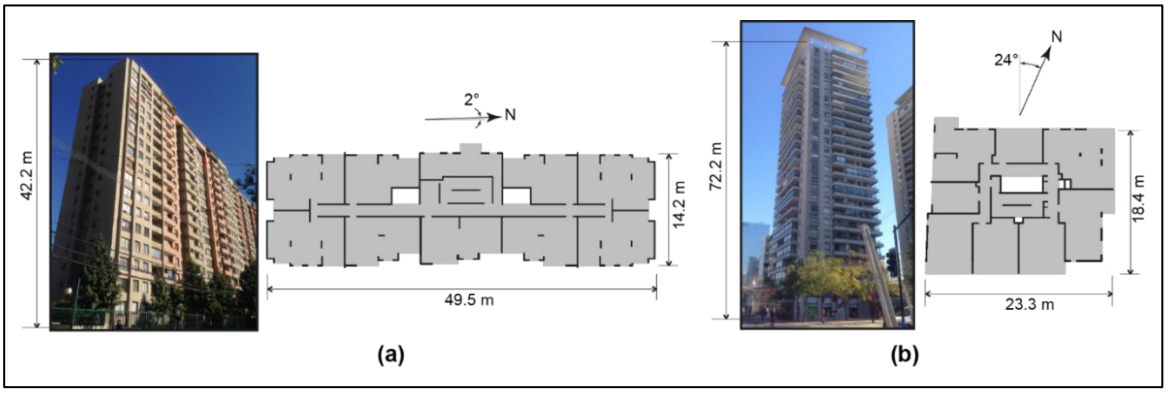

Fig. 4.4 – Picture and plan view of typical story for: (a) the 17-story building; and (b) the 26-story building

Table 4.1 – Properties* of the case study buildings

Building	Direction	Period [s]	1st mode effective modal mass [%]	Effective reduction factor R_{eff}	Design base shear coefficient	Wall Density
17 stories	Long	0.43	0.60	7.48	0.061	0.026
	Short	1.11	0.73	3.88	0.050	0.024
26 stories	Long	1.49	0.47	3.68	0.050	0.025
	Short	1.73	0.45	3.17	0.050	0.024

*Nominal properties considered in the actual design of the buildings (i.e., the ones with which the design seismic loads were determined), and calculated following the standard practice in Chile. They were obtained from linearly elastic 3D models in which shear and bending stiffness of all members are based on gross cross-section properties, walls and slabs were modeled with shell elements, and diaphragm constraints were incorporated at each floor level.

Most Chilean residential buildings are regarded as stiff structures (Lagos et al. 2012) due to their large wall density (total cross-section area of walls over floor area), which typically ranges from 2.5 to 3.5% along each of the main directions (Junemann et al. 2015). The case study buildings are not an exception (Table 4.1). As shown in Fig. 4.4, the typical floor of both buildings have a significant amount of walls, and some of them are closely spaced to each other and have intricate cross sections. None of the walls has confined boundary elements because confinement requirements were explicitly removed when Chile adopted ACI-318 in 1996. Fig. 4.5 shows a typical detail of wall boundaries taken from the construction drawings of the buildings. Further information on the case study buildings can be found in the previous chapters and some relevant construction drawings of the buildings are presented in Appendix 1.1.

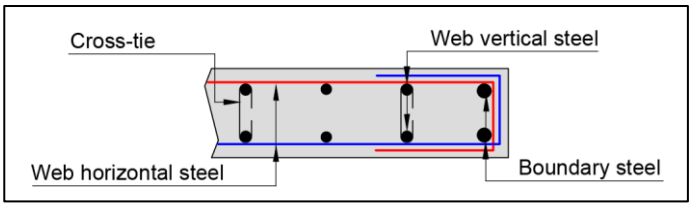

Fig. 4.5 – Construction detail of wall boundaries

4.5. Non linear structural modeling

Full 3D non-linear models of the case study buildings were developed in the software PERFORM-3D (CSI 2016d). Shear walls were modeled using the 4-node "Shear Wall" element, which is a somewhat simplified non-linear area element intended for the specific purpose of modeling RC walls. The cross section is defined by fibers that account for axial-bending interaction, which is uncoupled from the shear response. Material properties are defined separately for shear, out-of-plane bending and in-plane bending. Recommendations available in the literature for this element (Lowes et al. 2016; Kolozvari et al. 2017) were implemented in this research as explained next.

Concrete material and distributed shear reinforcement of the walls were modeled as fibers in the "Shear Wall" element, while reinforcement at wall boundaries was explicitly modeled using the inelastic "Steel Bar/Tie/Strut" element (one per end). Following PERFORM-3D guidelines (CSI 2016b) two vertical area elements per story were used at the levels where non-linear behavior was expected. At all other levels each wall was modeled using one element per story (Fig. 4.6). Horizontally, areas were meshed in such a way that the aspect ratio is in all cases smaller than 5 (i.e., square-like elements were intended) (Kolozvari et al. 2017).

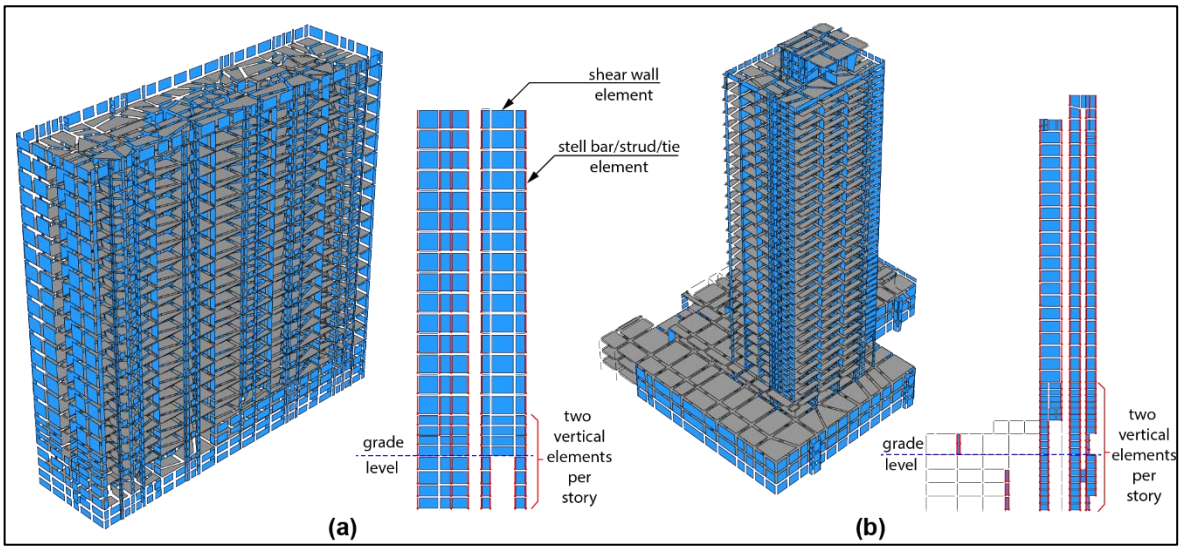

Fig. 4.6 – Full models of: (a) the 17-story building; and (b) the 26-story building

Unfortunately, measured material properties were not available, and tests were not allowed by the owners. Hence expected concrete strength was adopted. This was assumed equal to 1.3 times the nominal concrete strength ($f'_{expected} = 1.3\ f'_c$) (LATBSDC 2015). A 4-segment piece-wise backbone curve was used for concrete material following the calibration suggested in Lowes et al. (2016). The concrete constitutive law neglects the tensile capacity, but such neglect has very small influence on the overall behavior (Kolozvari et al. 2017). The resulting backbone curve is presented in Fig. 4.7a next to a well-known curve (Karthik and Mander 2011) for comparison purposes. Confined concrete was not considered because, as mentioned before, the walls of the case study buildings do not have confined boundary elements. A 5-segment piece-wise backbone curve was used for reinforcing steel. This curve was defined based on data obtained from tests of bars used in Chile (Fig. 4.7b). Buckling of reinforcing steel was accounted for by the simplified approach presented in Pugh et al. (2015) and illustrated in Fig. 4.7b. Cyclic degradation of steel and concrete was calibrated according to Lowes et al. (2016).

Material regularization was performed as recommended in Lowes et al. (2016). This regularization procedure depends on the vertical size of the area elements (L_{elem}). As each

wall was modeled by either one or two elements per story, there are roughly two sizes of elements in each building, and such sizes were used for the regularization shown in Fig. 4.7a.

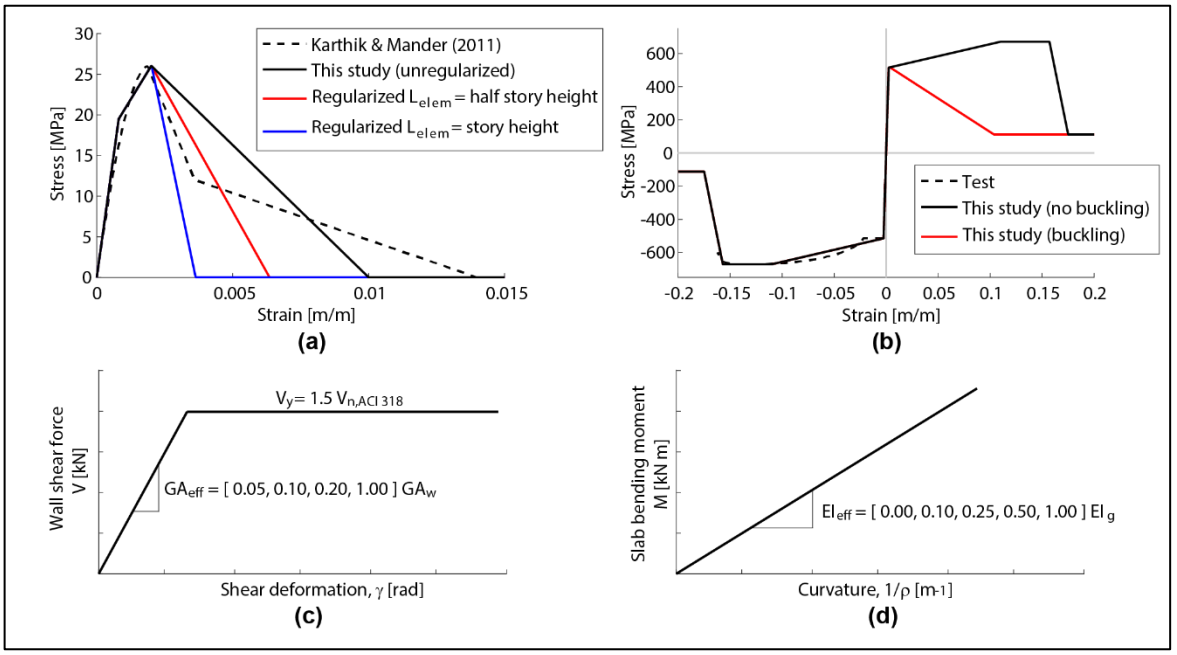

Fig. 4.7 – Force-deformation relationship of: (a) unconfined concrete fibers; (b) steel fibers; (c) wall shear stiffness; and (d) slab bending stiffness

As adopted in Değer et al. (2015) the in-plane shear response of walls was defined by an elastic, perfectly plastic force-deformation relationship (Fig. 4.7c), where the yielding shear strength was set equal to 1.5 times the nominal capacity according to ACI 318-14 (ACI 2014). The pre-yielding shear stiffness was set equal to the GA_{eff} values highlighted in Fig. 4.3a. The slabs were modeled using linearly elastic 4-node area elements whose bending stiffness (Fig. 4.7d) was set equal to the EI_{eff} values highlighted in Fig. 4.3b. EI_{eff} = 0.0 in fact indicates the case in which the slab elements were not included in the model. All the models have a rigid diaphragm constraint in order to reduce the number of degrees of freedom, which in turn reduces the computational cost of the analyses. In the set of models with variable values of EI_{eff} the value of GA_{eff} was set equal to 0.1 GA_w. In the other set of models (i.e., variable values of GA_{eff}) the value of EI_{eff} was set equal to 0.25 EI_g. In other words, GA_{eff} = 0.10 GA_w and EI_{eff} = 0.25 EI_g are deemed "reference" values.

The very few columns of the buildings were modeled with frame elements that have fiber sections only at both ends (length of expected plastic hinges), and an elastic section was adopted in between. Non-linearity in beams was modeled using (point) moment hinges. Masses and gravity loads were distributed among wall and slab joints according to tributary areas. Supports were modeled using non-linear springs that account for the soil stiffness in compression but have no tensile stiffness. In doing so the models account for possible foundation uplift. P-Δ effect was included in all wall and frame elements. Accidental torsion was not included because, as shown in Table 2.4, it has little influence on the response of these buildings.

4.6. Validation of the SPO2FRAG Methodology

Published studies in which the SPO2FRAG procedure was implemented are either on frame structures or on dual wall-frame buildings (Baltzopoulos et al. 2017; Pavel et al. 2018; Nazri et al. 2019). To the best of the authors' knowledge there are no published studies on "pure" wall buildings such as the case study buildings considered in this paper. Since, as mentioned before, no IDA-based fragility curves of pure wall building systems such as the Chilean residential wall buildings were found, a validation analysis was performed considering a Chilean office building that was subjected to a full IDA in a previous study (Araya-Letelier et al. 2019). The "validation" building actually has a dual frame-wall lateral force-resisting system, but it is nevertheless considered the best possible choice for validation because: a) it was also designed per the current Chilean seismic design regulations for RC structures; and b) its walls are the main lateral force-resisting members (they take more than 75% of the base shear). The "validation" building has 16 stories and 3 underground levels. The structural layout is representative of that typical of current office buildings in Chile, and the soil type at its location is the same soil type at the locations of the case study buildings. The "validation" building (Fig. 4.8a) was modeled in PERFORM-3D following essentially all the modeling considerations presented in Section 4.5. The wall effective shear stiffness was set equal to 0.1 GA_w. As usual in core wall buildings the slabs were not modeled, hence (implicitly) the slab effective bending stiffness was set equal to 0.0 EI_g. The IDA was

performed using 45 records caused by eight different Chilean major subduction earthquakes that occurred along the boundary between the Nazca and South America plates. The selected earthquakes have magnitudes (M_w) between 6.3 and 8.8. They were recorded at rupture distances as large as 500 km, on rock or firm soil sites with $V_{s30} > 300$ m/s, and PGA greater than 0.15 g. Frequencies outside the range 0.1–25 Hz were filtered from the records. For each hazard level, the records were scaled to match the target spectral pseudo acceleration at the fundamental period $S_a(T_1)$ with increments of 0.1 g until collapse was triggered. The bisection method was then used to find the value of $S_a(T_1)$ at collapse with a tolerance of 0.01 g. Even though the slabs were not included in the model, a total running time equivalent to approximately 6 months was necessary to perform the complete IDA. Such computational cost certainly justifies the development of alternative (albeit approximate) procedures such as the SPO2FRAG method adopted in this paper. Further information regarding the design, modeling and IDA of the "validation" building is available in Araya-Letelier et al. (2019).

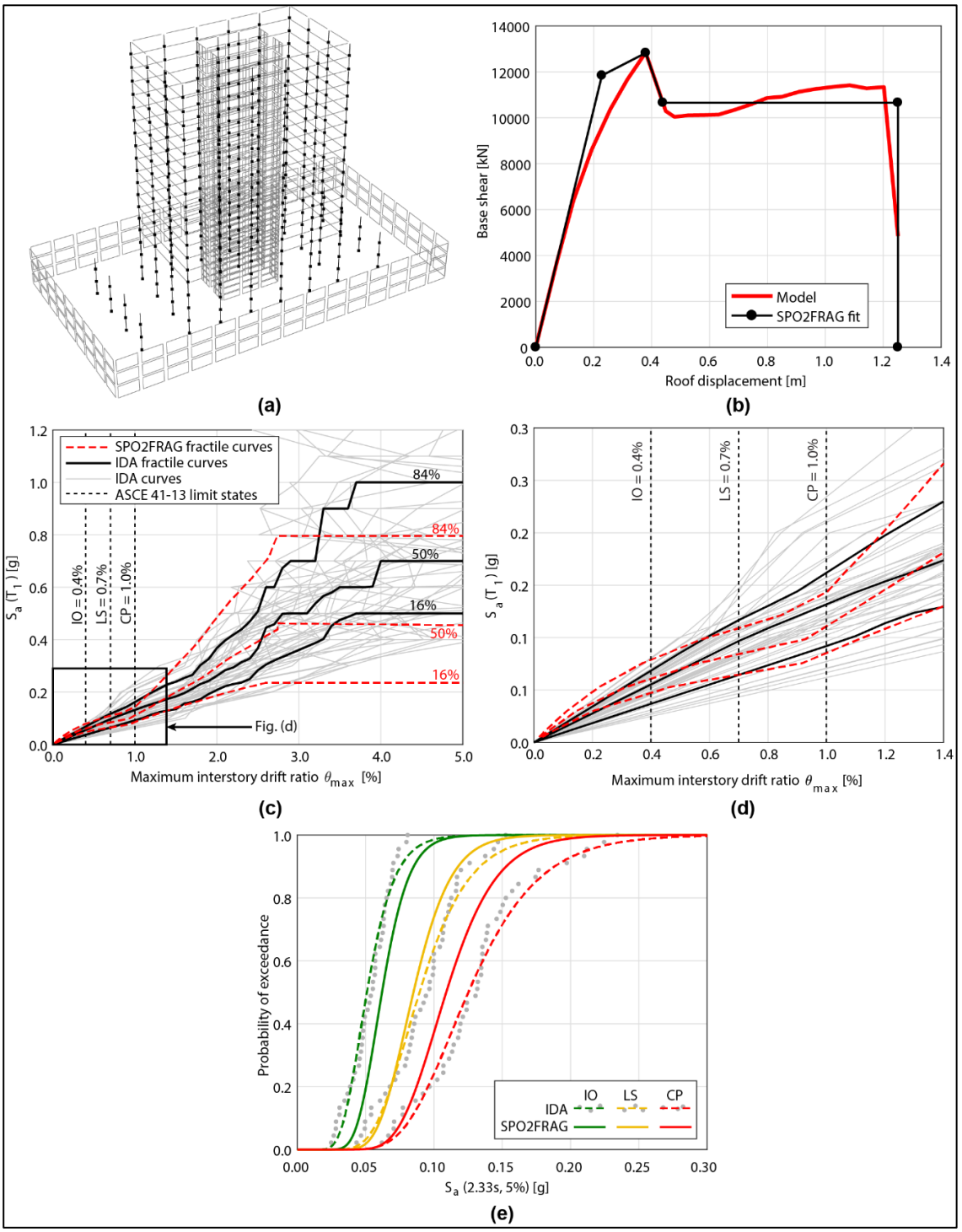

Fig. 4.8 – Structural model of the 16-story building considered in the validation analysis and comparison between fragility curves given by SPO2FRAG and by full IDA

The “validation” building was subjected to SPO analysis following the procedure described in detail later in Section 4.7. The resulting pushover curve is presented in Fig. 4.8b along with the piece-wise fit automatically computed by SPO2FRAG. It can be observed that the 5-segment fit matches the pushover curve reasonably well. Particularly, the initial stiffness is correctly captured, which is critical for limit states related to relatively low levels of lateral displacement. The residual strength is also well fitted. Right before the peak strength, however, the match is of somewhat lesser accuracy.

With all the necessary input data (i.e., the pushover curve, physical and modal information on the building, and the level of uncertainty) the SPO2FRAG procedure provided the 16%, 50% and 84% fractile curves presented in Fig. 4.8c and Fig. 4.8d. For comparison purposes, the actual IDA curves and their corresponding fractile curves are also presented in the same plot. It can be observed that at large values of the EDP the SPO2FRAG curves do not match the actual IDA curves very well. Nevertheless, at smaller values of the EDP the match is quite better, particularly at the values that define the three limit states considered in this study (indicated by vertical dashed lines). Detailed information on how the SPO2FRAG tool was configured and how the limit states were defined is provided later in Section 4.8. Finally, the SPO2FRAG fragility curves were computed using Eq. (6) and are presented in Fig. 4.8e along with the results (and fitted lognormal curves) obtained from the actual IDA. A good match is observed between the SPO2FRAG curves and the IDA fragility curves at the limit states associated with smaller values of the EDP (i.e., Immediate Occupancy and Life Safety). On the other hand, matching at the Collapse Prevention limit state is moderate, particularly at probabilities of exceedance greater than 0.15. However, as shown later, such collapse fragilities are hardly achieved by the case study buildings under seismic demands comparable with that imposed by the 2010 Maule earthquake (i.e., the situation that will be considered later to evaluate whether SPO2FRAG results are realistic or not). In summary, bearing in mind that the computational cost of the SPO2FRAG method is affordable and significantly less (an order of magnitude) than that necessary to perform a full IDA, results given by the SPO2FRAG method were deemed satisfactory for the purposes of this study.

4.7. Static Pushover (SPO) Analyses of the case study buildings

Two sets of models of each case study building were subjected to SPO analysis. Lateral forces were applied along the direction in which the building is more flexible, which coincides with the shorter plan dimension. The distribution of lateral forces was consistent with the first mode in the direction of analysis. The models were pushed in 500 steps up to a roof drift ratio equal to 5.0% or until lack of convergence after 2000 nonlinear iterations, whichever occurred first. Fig. 4.9a shows the results of the first set of models (i.e., $EI_{eff}=0.25EI_g$ and different effective values of wall shear stiffness GA_{eff}), whereas Fig. 4.9b shows the results of the second set of models (i.e., $GA_{eff}=0.10GA_w$ and different effective values of the slab bending stiffness EI_{eff}). In these plots, lateral forces are normalized by the total seismic weight.

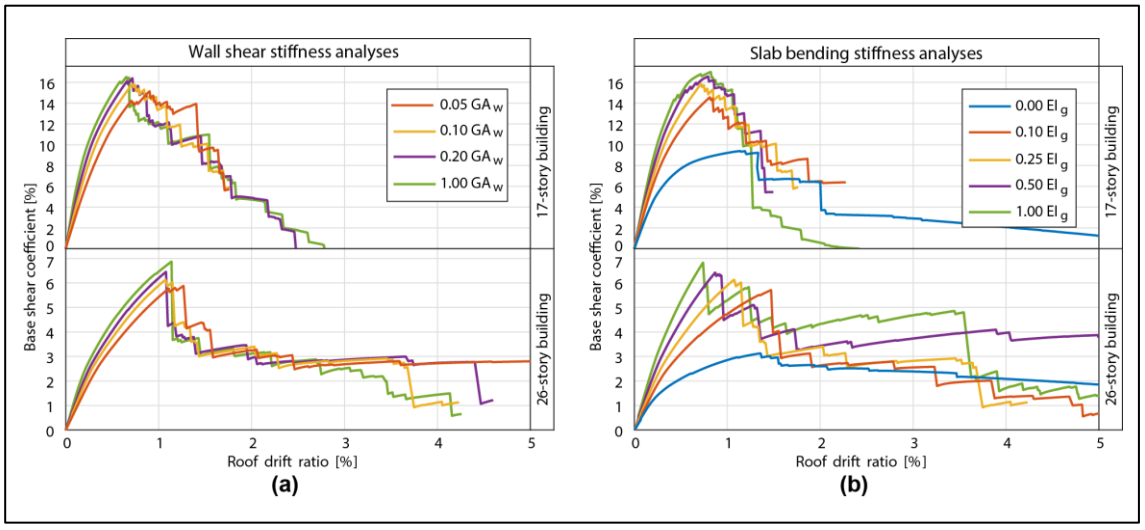

Fig. 4.9 – SPO curves of the sets of models with: (a) different wall effective shear stiffness; and (b) different slab effective bending stiffness

The characteristics of the pushover curves up to the peak strength are analyzed first. In can be observed in Fig. 4.9 that the degree of stiffness reduction (considerable in all cases), the peak strength, and the roof drift ratio at peak strength are moderately influenced by the value of GA_{eff} (Fig. 4.9a) and heavily influenced by the value of EI_{eff} (Fig. 4.9b), particularly in the models of the 26-story building. It is also observed that the response of the models in

which the slabs were not explicitly included (i.e., $EI_{eff} = 0.0\ EI_g$) is markedly different from that of all other models, even from that of the model having a very small value of EI_{eff} (i.e., $0.1\ EI_g$).

The characteristics of the pushover curves at roof drift ratios larger than that at peak strength are, quantitatively (but not qualitatively), again slightly influenced by the value of GA_{eff} (Fig. 4.9a) and heavily influenced by the value of EI_{eff} (Fig. 4.9b). Qualitative differences are found to actually depend on the building. While the strength of the 17-story building diminishes progressively, the strength of the 26-story building diminishes abruptly after the peak strength, and then takes a somewhat constant value at what could be defined as a plateau of residual strength. These qualitative differences are attributed to structural features such as the larger number of walls of the 17-story building in the direction of analysis (see Fig. 4.4) and the large podium of the 26-story building (see Fig. 4.6).

4.8. Seismic Fragility Analysis of the case study buildings

The SPO results shown in Fig. 4.9 provide the input data for the SPO2FRAG tool. With this information, the piece-wise backbone curve is automatically defined by SPO2FRAG. SPO displacements at each story were also provided to SPO2FRAG because in this study the EDP is the peak story drift ratio (as noted later, limit states were defined in terms of peak story drift ratio). Additional input data include story heights and masses, and the modal participation factor of the first mode (Γ_1), obtained from the modal analysis of the full model with modes normalized with respect to the roof displacement (values of Γ_1 obtained using the SPO2FRAG internal approximation were found to be quite similar because the SPO load pattern was consistent with the first mode). With the input data mentioned up to this point SPO2FRAG computes the equivalent SDOF periods (T_{eq}), which are shown in Table 4.2 where the fundamental period of the full 3D models are also presented for comparison purposes. Note that for the 17-story building the equivalent SDOF periods are virtually equal to the fundamental periods of the 3D models, while for the 26-story building the SDOF periods are slightly larger. Also notice that, despite being slender buildings, smaller values

of GA_{eff} significantly increase the value of T_{eq} (in other words, contrary to what is assumed in common practice the wall shear stiffness is also relevant in slender wall buildings such as the case study buildings). At this stage, the first and second mode periods (again, obtained from modal analysis of the building models) are also provided for the subsequent computation of the missing variability at nominal yield (β_y). The effective modal participation factor (Γ_{eff}) computed internally by SPO2FRAG was implemented in this analysis to account for higher-mode contributions (without such implementation the validation procedure described in Section 4.6 would have given much less accurate results).

With the data input described in the former paragraph the SPO2FRAG software computes the 16%, 50% and 84% fractile curves of the IDA. Then, values of the EDP for each limit state must be defined. Three limit states are considered in this study, i.e., Immediate Occupancy (IO), Life Safety (LS) and Collapse Prevention (CP). These limit states were defined in terms of the peak story drift ratios indicated in Table 10-22 of ASCE 41-13 (ASCE 2014). This table is intended for walls controlled by shear while Table 10-21 is intended for walls controlled by flexure. The geometry of these buildings suggests that they are controlled by flexure, which means (at least in principle) that Table 20-21 is applicable. However, it was nevertheless decided to use the values indicated in Table 20-22 (intended for walls controlled by shear) for the following reasons:

1 - The limits indicated in Table 20-21 are expressed in terms of plastic hinge rotation, but SPO2FRAG only accepts limits in terms of story drift.

2 - Even though the geometry suggests that these buildings are controlled by flexure, the empirical evidence (i.e., post-earthquake observations) indicate that walls such as the ones in the buildings analyzed in this dissertation have definitely a brittle behavior and have very limited (if any at all) ductility. Further, this observation is consistent with the pushover curves shown in Fig. 4.9a, which show little (or none at all) ductility. Table 20-21 of ASCE 41-13, on the other hand, is intended for ductile walls such the ones presented in Figure 4-

16 of ATC-76-1 (NIST 2010), i.e. pushover curves exhibiting a significant degree of ductility.

It was considered that the limits indicated in Table 20-22 are definitely more appropriate for the walls of pre-2010 Chilean buildings, which do not have boundary elements at their ends. Some typical shear failures were documented in the 2010 Chile earthquake (Rojas et al. 2011), although it is acknowledged that the brittle behavior of pre-2010 Chilean walls is not necessarily caused by shear failures.

The limit values of Table 20-22 of ASCE 41-13 are given for two levels of axial load (namely, high and low). Upon examination both buildings were found to comply with the high axial load condition. The corresponding thresholds of story drift ratio are 0.40% for IO, 0.75% for LS and 1.00% for CP. Finally, additional variability was included through the already mentioned factors β_y and β_u. As recommended in Baltzopoulos et al. (2017) the value of the latter was set according to Table 5-3 of FEMA P-695 (FEMA 2009). The accuracy and robustness of the models were ranked "medium", which recognize the somewhat simplified modeling of the material stress-strain relationships and of the shear walls (it is recalled that the "Shear Wall" element is a somewhat simplified element). On the other hand, considering that the SPO analyses are building-specific, the representation of collapse characteristics was ranked "high" according to Appendix F of FEMA P-695. Thus, the value of β_u was set equal to 0.2 (side-sway collapse limit state). The value of β_y is automatically computed by SPO2FRAG.

Table 4.2 – Equivalent SDOF periods T_{eq} [s] for different values of GA_{eff} and EI_{eff}

	Building	**AG_{eff}**				**EI_{eff}**				
		0.05 AG_c	**0.10 AG_c**	**0.20 AG_c**	**1.00 AG_c**	**0.00 EI_g**	**0.10 EI_g**	**0.25 EI_g**	**0.50 EI_g**	**1.00 EI_g**
Equivalent SDOF period	17-stories	1.91	1.62	1.50	1.30	1.99	1.76	1.62	1.59	1.51
	26-stories	3.39	3.06	2.84	2.54	3.65	3.35	3.06	2.84	2.78
3D model fundamental period	17-stories	1.89	1.65	1.49	1.29	1.95	1.74	1.65	1.58	1.50
	26-stories	3.16	2.85	2.63	2.33	3.00	3.08	2.85	2.65	2.46

The fragility curves provided by SPO2FRAG are presented in Fig. 4.10a (sensitivity analysis of the wall effective shear stiffness GA_{eff}) and in Fig. 4.10b (sensitivity analysis of the slab effective bending stiffness EI_{eff}). These curves suggest that both GA_{eff} and EI_{eff} have a relevant influence on the seismic performance of the buildings, definitely more so in the 17-story building than in the 26-story building. Further, the seismic fragility of the 17-story building is more sensitive to the value of GA_{eff} than to the value of EI_{eff} (the opposite sensitivity was observed in the SPO curves). This is most likely due to the fact that the equivalent SDOF period is more sensitive to the value of GA_{eff} than to the value of EI_{eff}.

According to Fig. 4.10 the 17-story building has a better seismic performance than the 26-story building in the sense that its fragilities are smaller. To get a deeper insight into this observation the fragilities at the equivalent-period spectral accelerations (i.e., $S_a(T_{eq})$) of the ground motion recorded at the Santiago Centro station during the 2010 Chile earthquake are also indicated in Fig. 4.10 with solid-colored dots. Santiago Centro is the closest station to both buildings with similar soil conditions. It is located 5 and 9 km away from the 17- and the 26-story buildings, respectively, on soil type II (firm soil). This analysis should be carefully interpreted because it combines a deterministic input (i.e., only one ground motion) with a probabilistic assessment (i.e., fragility curves). Nevertheless, it provides a rough idea of the performance of the buildings, and should be consistent (at least in a broad sense) with

empirical observations. It can be observed in Fig. 4.10 that under the demand imposed by the 2010 Maule earthquake the fragilities of the 17-story building are smaller than those of the 26-story building, particularly those associated with the LS and CP limit states. This result contradicts the empirical evidence in the sense that damage due to the 2010 Maule earthquake in residential wall buildings having 10 or more stories was not observed to depend on the number of stories. Unfortunately no accurate empirical fragilities exist for the class of buildings considered in this study. However, based on published reports and their own post-earthquake observations the authors of this study estimate that the percentage of tall residential wall buildings affected by the 2010 Maule earthquake in which the IO, LS and CP thresholds were exceeded are roughly equal to 25%-40%, 2%-10% and less than 1%, respectively. These empirical fragilities agree reasonably well with the analytical fragilities associated with the LS and CP limit states of the 17-story building, but the analytical fragilities of the 26-story building are significantly larger. This inconsistency suggest that the fragility curves provided by the SPO2FRAG procedure might not be accurate for structures as tall as the case study 26-story building. It must be mentioned that in fact the SPO2FRAG software did report a warning message indicating that results for the 26-story might not be accurate.

Each plot in Fig. 4.10 shows a comparison between the fragilities of different structural models. In all cases the IM is the pseudo-spectral acceleration at the equivalent period $S_a(T_{eq})$, which is the only IM available in the SPO2FRAG tool. Spectral acceleration is a widely adopted IM because it correlates better with most limit states than other IMs such as the Peak Ground Acceleration (PGA) (Mackie and Stojadinovic 2004) and is compatible with most seismic hazard curves. It must be noted, however, that in each plot of Fig. 4.10 each structural model has a different value of equivalent period T_{eq}, hence their fragilities are, in a strict sense, not really comparable to each other (Hueste and Bai 2007). This last observation has been sometimes overlooked in the literature (Ellingwood et al. 2007; Park et al. 2009). A more robust assessment requires either a period-independent IM or combination with seismic hazard curves (Kinali and Ellingwood 2007; Li and Ellingwood 2007).

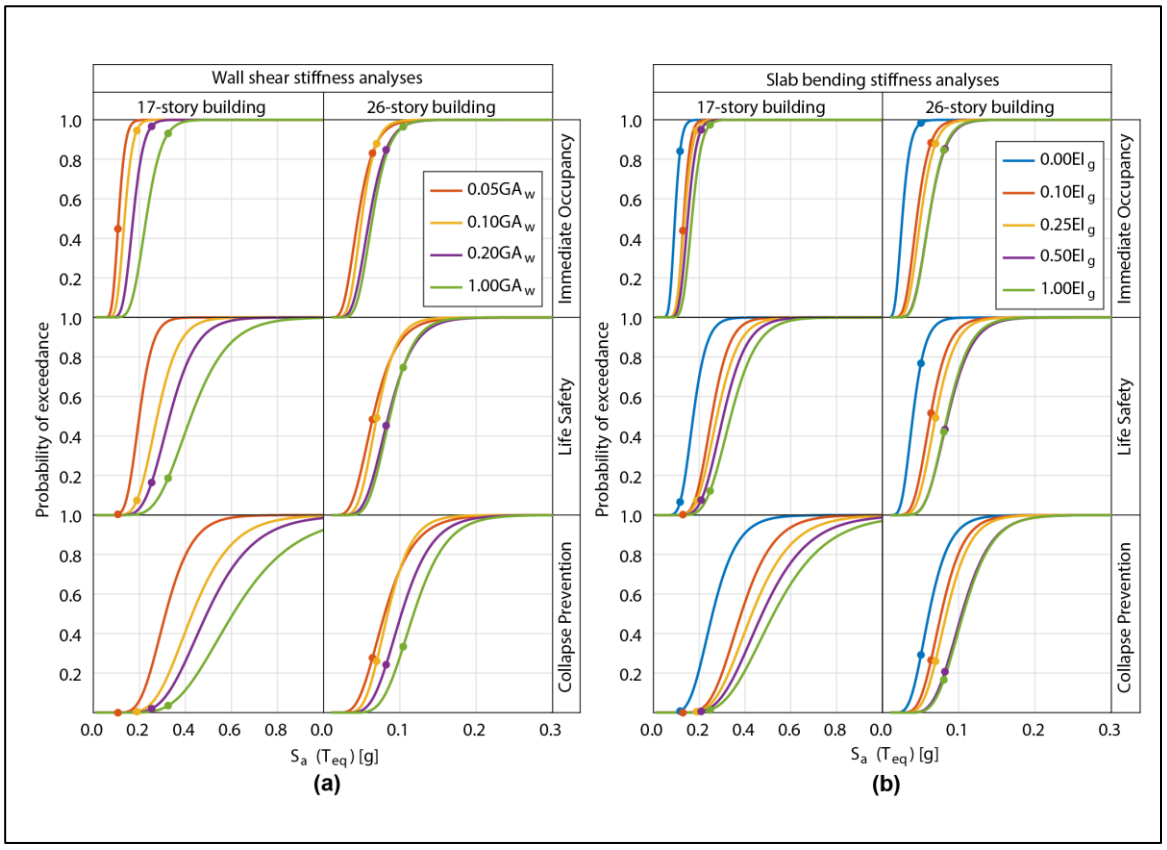

Fig. 4.10 – Fragility curves provided by SPO2FRAG for the sets of models with: (a) different wall shear stiffness; and (b) different slab bending stiffness. Dots indicate the fragilities at $S_a(T_{eq})$ values of the ground motion recorded in Santiago Centro station during the 2010 Maule earthquake.

In order to overcome the limitation commented in the previous paragraph the IM of the fragility curves was converted from $S_a(T_{eq})$ into mean return period (T_r) using the seismic hazard curves shown in Fig. 4.11. These curves were generated by the seismic hazard analysis tool developed by Candia et al. (2018). The hazard curves were generated for east Santiago and account for inter- and intra-plate seismic sources within a 500 km radius. Hazard curves were computed for each value of T_{eq} reported in Table 4.2.

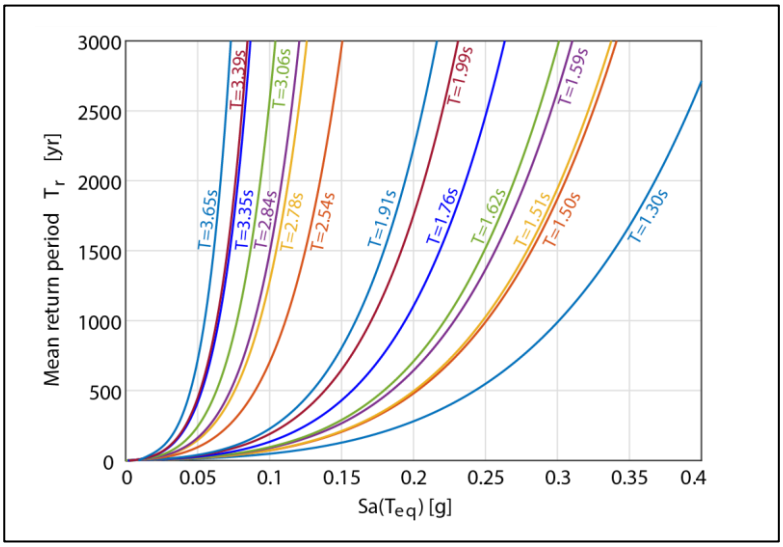

Fig. 4.11 – Seismic hazard curves at east Santiago (stiff soil) for several values of period T_{eq}

The procedure to convert the IM of the fragility curves is schematically presented in Fig. 4.12 and includes the following steps: (1)-(2) the probabilities of exceedance are projected on the fragility curves to get the corresponding values of $S_a(T_{eq})$; (3)-(4) these values of $S_a(T_{eq})$ are projected on the associated hazard curve (i.e., the one valid for the same value of T_{eq}) to get the corresponding values of T_r; (5)-(6) these values of T_r become the abscissas of the corresponding probabilities from steps (1)-(2).

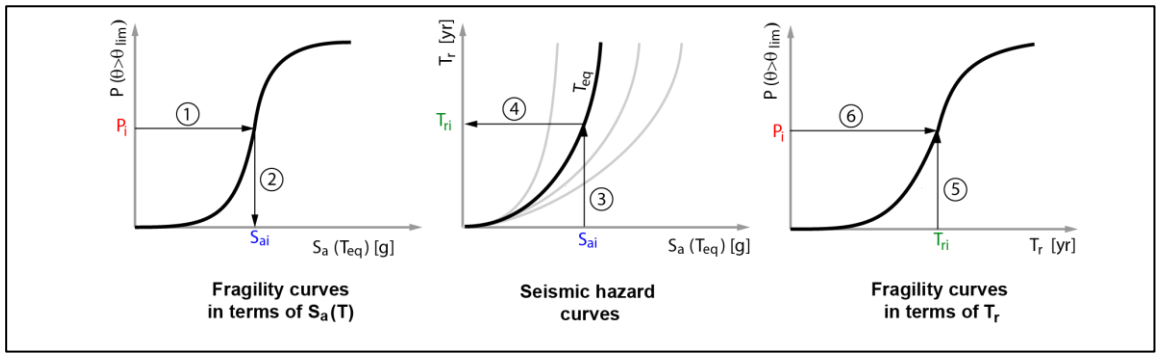

Fig. 4.12 – Conversion of IM from $S_a(T_{eq})$ into T_r using seismic hazard curves

The resulting fragility curves with T_r as IM are presented in Fig. 4.13. Interestingly, the influence of the value of GA_{eff} on the seismic fragility of the 17-story building is now significantly less than that on the seismic fragility in terms of $S_a(T_{eq})$. As for the influence of EI_{eff}, it can be observed that the fragilities for $EI_{eff} \neq 0.0\ EI_g$ are essentially equal to each other and significanlty different from the fragilities for $EI_{eff} = 0.0\ EI_g$. Further, the value of the fragilities for $EI_{eff} = 0$ are always greater than those for $EI_{eff} \neq 0.0\ EI_g$.

As a reference, two relevant values of T_r used in seismic design (500 yr and 2500 yr) are higthlighted in Fig. 4.13, and the fragilities associated with the 500 yr event are presented in Table 4.3. With the hazard curves shown in Fig. 4.11 the value of T_r of the Santiago Centro spectral accelerations was obtained for each value of T_{eq} shown in Table 4.2. The average value of T_r is 739 yr. If the values of GA_{eff} and EI_{eff} are set equal to $0.10\ GA_w$ and $0.25\ EI_g$ (i.e., the reference values mentioned in Section 5), the equivalent periods of the 17- and 26-story buildings are equal to 1.62 s and 3.06 s, and the corresponding values of T_r are 593 yr and 692 yr, respectively. In other words the demand imposed by the 2010 Maule earthquake is similar (although somewhat greater) to that associated with a hazard level consistent with a 500 yr mean return period. Again, the LS and CP analytical fragilities of the 17-story building at 500 yr agree reasonably well with the already mentioned estimates of empirical fragilities, but the analytical fragilities of the 26-story building are significantly larger. It is also observed that the IO fragilities of the 17-story building at 500 yr are more consistent with the empirical evidence when the value of GA_{eff} is relatively large, which makes sense

because the value of GA_{eff} is expected to be relatively large at a relatively low response level such as that associated with the IO limit state. Such consistency was not found in the fragility curves expressed in terms of spectral accelerations.

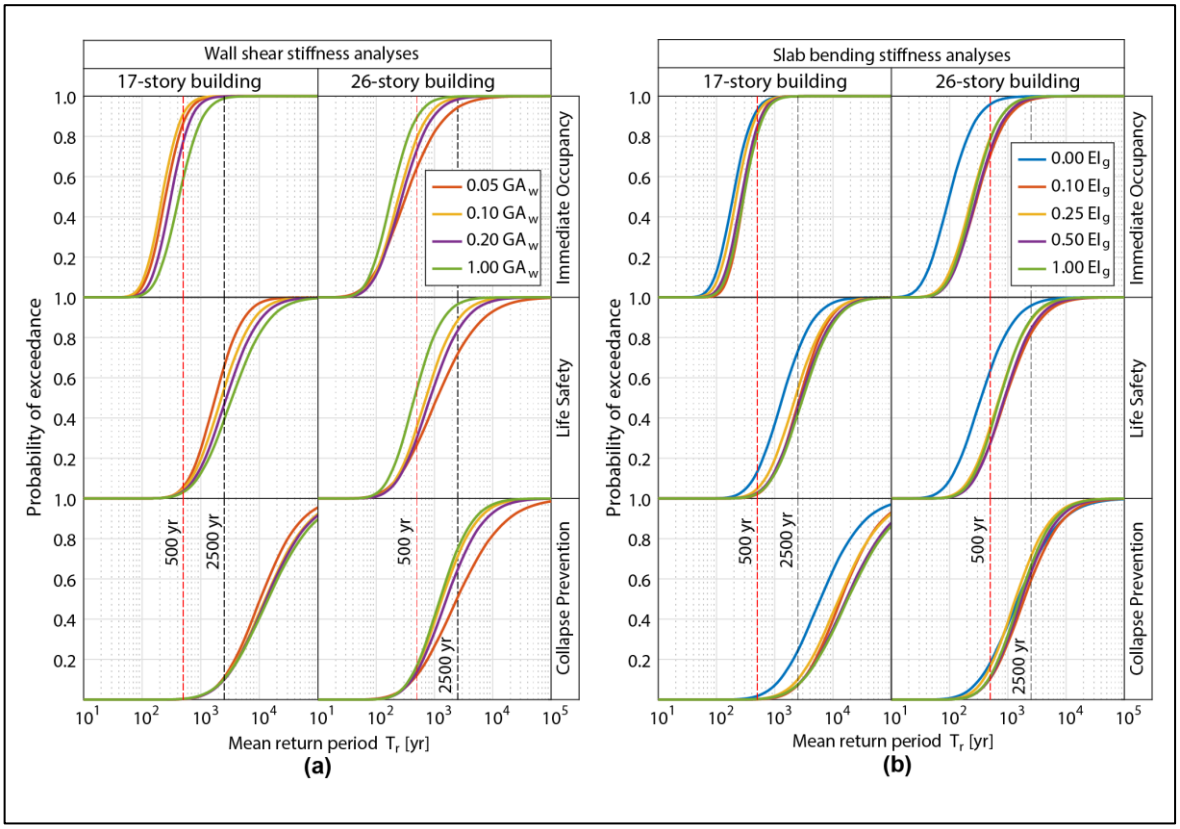

Fig. 4.13 – Fragility curves in terms of mean return period for the sets of models with: (a) different wall effective shear stiffness; and (b) different slab effective bending stiffness

Table 4.3 – Probabilities of exceedance for a 500-year mean-return-period event

		GA_{eff}				EI_{eff}				
Limit State	**Building**	**0.05 GA_w**	**0.10 GA_w**	**0.20 GA_w**	**1.00 GA_w**	**0.00 EI_g**	**0.10 EI_g**	**0.25 EI_g**	**0.50 EI_g**	**1.00 EI_g**
IO	17-story	86.6	91.0	77.2	59.0	93.2	83.9	91.0	84.9	81.0
	26-story	64.5	79.5	73.4	89.5	96.0	70.7	79.5	73.1	78.5
LS	17-story	5.7	5.0	3.7	3.1	13.4	2.2	5.0	2.9	2.5
	26-story	26.8	35.9	30.4	54.5	63.7	27.5	35.9	27.6	33.5
CP	17-story	0.2	0.3	0.3	0.4	1.8	0.1	0.3	0.2	0.2
	26-story	12.2	16.4	13.9	17.0	18.4	10.5	16.4	10.9	11.7

Note: the conclusions of this chapter are presented in section 5.3.

---

5. CONCLUSIONS

5.1. Analysis of residential Chilean buildings using linear analysis

In chapter 2, the seismic capacity of three existing Chilean RC shear wall buildings of 5, 17 and 26 stories was analyzed. The three buildings are located in Santiago, and are typical examples of Chilean residential buildings. The spectral ordinates of the ground motions recorded during the 2010 Chile earthquake at stations close to the buildings exhibit spectral ordinates that are (much) higher than the spectral ordinates of the corresponding (reduced) design spectra, yet the three buildings withstood the 2010 Chile earthquake with no observable damaged. The seismic response was assessed using models in which concrete behavior is linearly elastic.

In a first series of analyses nominal procedures were adopted to estimate the seismic capacity of the buildings. The elastic overstrength, defined in this chapter as the ratio of the actual elastic capacity to the code-required capacity, was assessed. The analyses considered different values of material properties and different modeling issues, ranging from those typical of the Chilean seismic design practice to those deemed more realistic and typically adopted when evaluating (with state-of-the-practice procedures) the seismic capacity of an existing structure. In what is deemed as the most accurate scenario (within the scope of nominal procedures) it was found that the elastic overstrengh is very large in the case of the 5-story building (i.e., greater than 4), significant (i.e., roughly equal to 2) in the case of the 17-story building, and somewhat less significant (roughly equal to 1.5) in the case of the 26-story building. Further, no single property or modeling issue was identified as the most important source of elastic overstrength. Rather, the elastic overstrength was found to be a consequence of the simultaneous effect of several analysis/modeling issues. The seismic capacity of the 5-story building was found indeed greater than the demands imposed by the 2010 Chile earthquake, which is consistent with the observed behavior. However, the seismic capacity of the 17- and 26-story buildings turned out to be *not* greater than the

demands imposed by the 2010 Chile earthquake, which is *not* consistent with the observed behavior.

In a second series of analyses the buildings were subjected to response history analysis considering the recorded ground motions deemed most similar to the ones the buildings were actually subjected to during the 2010 Chile earthquake, and member capacities were evaluated by state-of-the-art procedures. Results given by linear response history analysis indicate that the seismic capacities of the 17- and 26 story buildings are still of lesser magnitude than the demands. Since these analyses indicate relatively large tensile forces at the foundation level, nonlinear response history analysis was also performed to account for possible foundation uplift (the only nonlinear elements in the model were the vertical springs modeling soil flexibility at the foundation level). The resulting peak demands were found essentially equal to (or at most slightly greater than) the seismic capacity, in terms of both force demands and story drift demands. Such consistency between force demands and story drift demands was not observed in results given by linear response history analysis (i.e., without accounting for foundation uplift).

It is then further concluded that either:

a) foundation uplift *did* occur (and was not noticed or did not cause observable effects) and had a significant influence on the response in the sense that it caused an important reduction of seismic demands; or

b) foundation uplift *did not* occur, hence the inconsistencies described before indicate that linearly elastic concrete models are simply not suitable for the analysis of RC buildings subjected to strong seismic demands even in the absence of observable damage.

The structures analyzed in this study are representative of the vast building inventory in Santiago, and although the analyses indicate that foundation uplift is feasible, it was not reported after the 2010 earthquake. Hence, while foundation uplift might have occurred (and not noticed) in a few buildings, it is deemed unlikely to be the actual reason why the 17- and

26-story buildings analyzed in this study (and by extension many other similar buildings) did not exhibit damage after the 2010 Chile earthquake. Much more likely, linearly elastic concrete models might simply not be capable of accurately assessing the response of RC buildings subjected to large seismic demands even in the absence of observable damage. This issue was the main motivation of the research effort presented in chapter 3, in which the 17- and 26-story buildings considered in this study are analyzed using nonlinear concrete models.

5.2. Analysis of residential Chilean buildings using nonlinear analysis

In chapter 3, two existing RC shear wall buildings of 17 and 26 stories representative of Chilean residential buildings were analyzed using fully nonlinear finite element models, i.e., models in which a nonlinear concrete material model is adopted and other nonlinear features (such as the nonlinear behavior of reinforcement bars and PΔ effects) are also accounted for. The buildings are located in Santiago, Chile and have a large number of walls to carry seismic and gravity loads. Although the ground accelerations recorded during the 2010 Chile Earthquake widely exceeded the code-specified design spectra, the buildings did not suffer observable damage, suggesting (at least in principle) that their response was essentially linear. However, in former studies that considered linear models of the buildings (Ugalde and Lopez-Garcia 2017a, b) the seismic demands were found larger than the capacity. Only when foundation uplift was accounted for using a nonlinear soil-structure interaction model, the seismic demands did not exceed the capacity. However, no evidence of foundation uplift was observed in the buildings analyzed in this study after the 2010 Chile earthquake, and very little evidence was observed elsewhere after this earthquake. This inconsistencies between analytical results and empirical evidence were the main motivation for the study described in this chapter.

The buildings were modeled using the structural analysis computer program PERFORM-3D. Shear walls were modeled using Shear Wall and Steel Bar/Strut/Tie elements calibrated according to recommendations available in the literature. The modeling approach adopted

in this study was validated through comparisons with results experimentally obtained from a cyclic static test conducted on isolated wall specimens. A good match was found in terms of force-displacement hysteretic cycles but strains were predicted with a lesser degree of accuracy.

Incremental static (pushover) analyses were performed first. The overstrength of the 17-story building was found roughly equal to 3 and 6 in the short and long directions, respectively, and the overstrength of the 26-story building was found roughly equal to 2 in both directions. In all cases the maximum strength is attained at a roof drift ratio that varies between 0.6% and 1.0%. The influence of soil-structure interaction was found relevant only in the short direction of the 17-story building. In this case the pushover curve of the model that accounts for nonlinear soil-structure interaction deviates from that of the model that considers fixed support conditions at a roof drift ratio roughly equal to 0.2%, and deviates from that of the model that considers linear soil-structure interaction at a roof drift ratio roughly equal to 0.4%. In all other cases the influence of soil-structure interaction was found negligible at roof drift ratios that are smaller than that at maximum strength.

Response History Analysis (RHA) was performed considering a ground motion recorded during the 2010 Chile earthquake in Santiago. In terms of global response, peak roof drift ratios were found in all cases less than 0.4%, well below the values at maximum strength obtained from pushover analysis. Also consistent with pushover analysis, the roof drift ratio response was found essentially insensitive to soil-structure interaction, even though the model that considers nonlinear soil-structure interaction indicates considerable uplift levels (up to 60 mm). In terms of local response, the *total* story drift deformation was found to take considerable values at some walls, especially at the upper stories where the limits established by ASCE 41-13 and LATBSDC were in some cases exceeded. This is not consistent neither with the lack of observable damage nor with the expected location of peak demands on walls in multi-story buildings (typically the first few stories above the grade level). This seems to indicate that the *total* story drift deformation is not really an appropriate parameter to evaluate the seismic performance of slender walls. Values of *tangential* story drift

deformation, on the other hand, were found to take values that are smaller than the established limits, which is indeed consistent with the lack of observable damage in the buildings analyzed in this paper. Further, the *tangential* story drift deformation was indeed found to take its maximum value at the grade level. These results indicate that in fact the *tangential* story drift deformation relates much better with seismic damage (or lack of) in slender walls, and therefore it should be considered for accurate assessments of the seismic demand on tall RC wall buildings. While shear demands were found smaller than the capacity, axial-flexural demands and strains at wall boundaries do take values slightly greater than that at onset of damage at a few locations. Such demands, however, seem to affect only the boundary of a few walls and are deemed unlikely to produce visible damage. Hence, in general it is concluded that results given by the nonlinear models considered in this study are consistent with the observed lack of damage, hence nonlinear concrete material models are indeed necessary for the analysis of RC shear wall buildings even in the absence of observable damage. It was also found that the strength of the buildings considered in this study is such that they might withstand earthquakes somewhat greater than the 2010 Chile earthquake without significant damage. It is noticed, though, that the models also reveal that foundation uplift is indeed possible, and even though uplift does not seem to significantly affect the seismic response it nevertheless deserves further study.

The pushover curves were converted into capacity spectra. The performance point consistent with the response to the 2010 Chile earthquake was assumed equal to the point at the intersection of the capacity spectrum and the response spectrum of the same recorded ground motion used in RHA (both plotted in ADRS format). The effective periods (i.e., based on secant stiffness) at the performance point turned out to be significantly longer than the nominal periods considered for design, and at such long periods it was found that the strength of the buildings (including overstrength) is in fact larger than the demand imposed by the 2010 Chile earthquake. Hence the main motivation for this study (i.e., lack of observable damage despite demands larger than capacities) turned out to be not really true at the effective periods consistent with the response to the 2010 Chile earthquake. Effective periods longer than the nominal were certainly expected, but not as long as those found in this study.

Future research on this issue should obviously include data from building instrumentation to quantify this finding with greater precision.

Pushover analyses were also performed to analyze the influence of several modeling issues. It was found that PΔ effect, bar buckling, inelastic deformations in beams and columns, nonlinear constitutive law for shear (elastic perfectly plastic for this study) and regularization of the concrete material model do not seem to be relevant to the seismic analysis of undamaged RC shear wall buildings having a large number of walls such as the ones considered in this study. However, two modeling issues were indeed found to have a considerable influence on the analysis (even in the absence of damage) and are deemed worthy of further research. The first issue is the shear stiffness of the walls, which was found to be relevant even when the walls are slender and subjected to demands that are well below the full strength. The value of shear stiffness adopted in this study (10% of the gross cross-section stiffness) is the value recommended in the literature for the analysis of *damaged* structures. Further research is needed to accurately determine the actual effective shear stiffness at relatively low deformation levels. The second issue is the influence of the slabs. The response of the models in which the slabs are explicitly modeled (even with an effective flexural stiffness that is 25% of that of the gross cross-section) is vastly different from those in which the slabs are not explicitly modeled and only a rigid diaphragm constraint is imposed. The quantitative differences shown in this study are much larger than the differences qualitatively suggested in former studies. For the class of buildings analyzed in this study (i.e., lateral force-resisting system made up of a large number of RC shear walls having intricate C, L, and T shapes) further research on this issue was found essential.

5.3. Analysis of residential Chilean buildings using an approximate fragility analysis

In chapter 4, the influence of the wall effective shear stiffness (GA_{eff}) and the slab effective bending stiffness (EI_{eff}) on the analytical seismic performance of a specific class of buildings was evaluated. The structures considered in this study are tall Chilean residential shear wall buildings, in which the lateral-force resisting system consists entirely of a large number of

slender reinforced concrete shear walls. The seismic performance was evaluated in terms of fragility curves. However, due to the large computational cost necessary to analyze full 3D nonlinear building models, the fragility curves were not obtained from results given by nonlinear response history analysis but by the simplified SPO2FRAG methodology, which provides fragility curves from results given by the computationally more affordable incremental static (pushover) analysis. When applied to a 16-story Chilean dual wall-frame reinforced concrete office building, fragility curves given by the SPO2FRAG methodology were found to agree reasonably well with fragility curves obtained from more rigorous results given by incremental dynamic analysis. The SPO2FRAG methodology was then applied to two buildings representative of the class of structures of interest in this study. These two case study buildings (17 and 26 stories, respectively) are actual, existing buildings located in Santiago, Chile. Two intensity measures were considered for the fragility curves: spectral acceleration at the fundamental period (in fact the equivalent SDOF period in the SPO2FRAG methodology, denoted $S_a(T_{eq})$) and mean return period, denoted T_r. The latter intensity measure makes possible valid comparisons between structures having different fundamental periods (different values of GA_{eff} and/or EI_{eff} change the stiffness and, consequently, the fundamental period and the equivalent SDOF period of the building models).

It was found that the degree of influence of the wall effective shear stiffness GA_{eff} on the seismic fragility of the 26-story building is non-negligible but moderate in all cases. That of the 17-story building, however, was found to depend on the intensity measure. It is very important when the intensity measure is $S_a(T_{eq})$, but only moderate when the intensity measure is T_r. As for the slab effective bending stiffness EI_{eff} it was found that results for $EI_{eff} = 0.0\ EI_g$ (i.e., the case in which the slabs are not explicitly modeled) are always clearly different from results for all other values of EI_{eff} (these latter values are often similar to each other). In other words results indicate that what really matters is the explicit inclusion of the slabs in the models; the exact value of EI_{eff} is of lesser relevance. It was also found that $EI_{eff} = 0.0\ EI_g$ leads to conservative assessments (by a large margin in some cases) in the

sense that the resulting fragilities are greater (significantly so in some cases) than those for $EI_{eff} \neq 0.0\ EI_g$.

The case study buildings and many other similar buildings were affected by the 2010 Maule earthquake. A comparison was then made between estimates of empirical fragilities and fragilities given by SPO2FRAG. Although not entirely conclusive because of its simplicity and roughness, the comparison clearly indicate that the fragility assessments provided by SPO2FRAG seem to be indeed realistic for the 17-story building (particularly for the Life Safety and Collapse prevention limit states) but overly conservative for the 26-story building. It must be mentioned that, when applied to the 26-story building, in fact the SPO2FRAG software reported a warning message indicating that results for the 26-story might not be accurate. Findings of this study confirms that such warning seems to be indeed correct.

5.4. Overall Conclusions

After analyzing the results obtained in the three articles of this dissertation, it is possible to integrate the main conclusions and confront them with the objectives and hypothesis initially raised.

First, the hypothesis that linearly elastic concrete models are appropriate to evaluate the reasons why most buildings did not suffer noticeable damage after the 2010 Chile Earthquake could only be corroborated for the low-rise building. On the contrary, the reasons why the medium and high-rise buildings were not damaged could not be found by linearly elastic concrete models.

Validation of the performance of medium- and high-rise residential wall buildings during the 2010 Chile Earthquake, even without noticeable damage, requires non-linear models, since it is precisely the non-linear response the reason why severe damage was not widespread. The analyses showed that the non-linear response of the models even at early stages of loading (due to the parabolic stress-strain relationships of concrete) entails a period

elongation and consequently a reduction of the seismic demands. It is very important that structural monitoring be implemented in this kind of buildings in order to validate this behavior during future earthquakes. The results of the nonlinear models numerically supports the good performance of two typical Chilean residential buildings, because regardless of the aforementioned reduction in stiffness, critical levels of tangential story drift, strains, or D/C ratios are not achieved, with some minor exceptions. These exceptions suggest that the buildings were close to reaching the limit states related to noticeable damage (as those observed in many buildings in Concepción city where seismic demands were larger). It is worth noting that these two buildings, of which at least the taller one was apparently at the limit of noticeable damage, were designed for the minimum seismic base shear. The design base shear initially obtained with the seismic code equations was much lower than the required minimum (in this case, 5% of the seismic weight). Therefore, it is inferred that this requirement played an important role in preventing widespread damage.

Fig. 5.1 shows the values of overstrength found in this study as a function of the number of stories. Only the overstrength in the short direction of each building is shown. Given that the 5-story building was not subjected to pushover analysis, the value shown in Fig. 5.1 is the elastic overstrength found in chapter 2, the "conventional" overstrength is larger. In order to extend the number of samples, the overstrength found by Restrepo et al. (2017) for another Chilean residential wall building is added and the best fit linear regression for these 4 buildings is presented. For comparison purpose, the values presented in table 4-15 of ATC-76-1 for archetypes RC wall buildings in high seismic zone (D_{max}) are presented as well. Those archetypes were design according to ASCE/SEI 7-05 and chapter 21 of ACI 318-08, following the requirements for Special RC shear walls. They have a configuration different from that of the pre-2010 Chilean residential buildings in the sense that they have less but ticker walls with a rectangular cross-section and boundary confinement when necessary. In general terms, these archetypes are intended to represent buildings like the one presented in Fig. 1.2 below. Notice the significantly larger overstrength found in the Chilean buildings. While ATC-76-1 also reports larger values in Table 4-15, they belong to archetypes with lower seismic design category, which usually tend to have larger overstrength as reported

by Jain and Navin (1995). Because of this observation, they were not included in Fig. 5.1. These results confirm that, as proposed in the hypothesis, Chilean residential wall buildings have an important reserve of strength, at least when compared with similar buildings having similar demands.

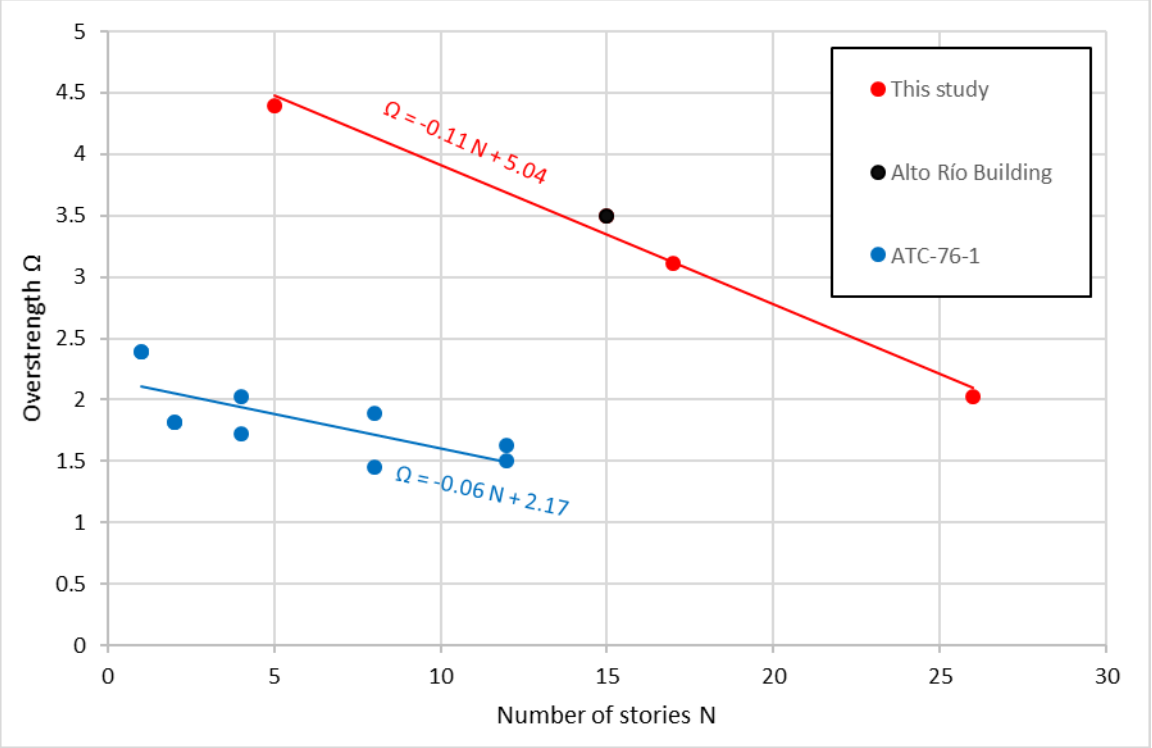

Fig. 5.1 Overstrength values for RC shear wall buildings in high seismic zone

The overstrength values found in this study can hardly be linked to specific issues of the Chilean seismic design code (except for the aforementioned minimum base shear), as the main reserve of capacity (or reduction of demand) is related to the nonlinear behavior of the materials and the redundancy provided by the structural configuration of Chielan residential wall buildings. Nevertheless, it was found that, in general, for medium- or high-rise buildings the modeling issues that tend to overestimate stiffness lead to overestimation of seismic demands and, consequently, they increase the overstrength. Such is the case of using non-reduced moment of inertia on the walls or overestimating the modulus of elasticity. The use

of non-reduced moment of inertia for slabs seems to follow the same line, however, overestimating the bending stiffness of the slabs reduces the flexure demands on the walls, and may not be conservative. After the 2010 Chile Earthquake, the use of reduced moment of inertia of the slabs, has been implemented by some Chilean engineers. But this is not a requirement of the design code NCh430, since the current version (2008) indicates that non-reduced moments of inertia for all the elements "may" be used. It is recommended that future investigations develop models with non-linear slab elements in order to obtain deeper insight into the role of the slabs and provide recommendations for effective slab bending inertia.

Finally, during this investigation it became evident that the structural complexity of Chilean residential wall buildings and the sophistication of wall models are a great limitation for implementing robust seismic evaluation methodologies in actual 3D building models. Therefore, pending the development of computational capabilities and the numerical efficiency of the models, there is a need to validate simplified methodologies. In this line, the SPO2FRAG tool allowed to approximate fragility curves that validate the good performance shown at least by the medium-rise building and somewhat less by the high-rise building. This tool showed that the wall shear stiffness and the slab bending stiffness have a moderate relevance in the fragility assessment of residential wall buildings. The only exception was the model with no slab bending stiffness that, similar to the pushover analysis, confirmed the great contribution of the slabs to prevent damage by coupling the walls.

Future investigations may explore the use of simplified building models such as the coupled shear-flexural beam (Miranda and Taghavi 2005) to better characterize the influence of the building height on relevant global parameters. That could also be applied to reproduce the comparison presented in Fig. 5.1 in terms of Collapse Margin Ratio (rather than in terms of overstrength) because it is a better indicator of overstrength under dynamic conditions. Another research opportunity would be to explore recent models that account for the non-linear response of wall shear (Kolozvari et al. 2015) and slab bending (Lu et al. 2014), in order to validate the results of chapter 4. Currently, such analysis will probably require the use of academic-oriented models, i.e. 2D models or partial building models. With them, it

could also be possible to study the unexpected drop of overstrength when the rigid diaphragm is omitted, as documented in Table 2.4. Finally, while in this research the conventional pushover analysis was implemented, it would be interesting to study other static procedures such as the modal pushover analysis, particularly for the taller buildings.

6. REFERENCES

ACHISINA (2017) Performance-based seismic design - An alternative procedure for the analysis and seismic design of buildings. Chilean Association of Seismology and Seismic Engineering (In Spanish), Santiago, Chile

ACI (1983) ACI 318-83: Building code requirements for reinforced concrete. American Concrete Institute, Farmington Hill, USA

ACI (1989) ACI 318-89: Building code requirements for reinforced concrete. American Concrete Institute, Farmington Hill, USA

ACI (1995) ACI 318-95: Building code requirements for reinforced concrete. American Concrete Institute, Farmington Hill, USA

ACI (2005a) ACI 318-05: Building code requirements for reinforced concrete. American Concrete Institute, Farmington Hill, USA

ACI (2005b) Building Code Requirements for Structural Concrete (ACI 318-05) and Commentary (ACI 318R-05). 430

ACI (2014) ACI 318-14: Building code requirements for reinforced concrete. American Concrete Institute, Farmington Hill, USA

Alarcon C (2013) Influence of Axial Load in Seismic Behavior of Reinforced Concrete Wallas with Nonseismic Detailing. Pontificia Universidad Católica de Chile

Alarcon C, Hube MA, Junemann R, de la Llera JC (2015) Characteristics and displacement capacity of reinforced concrete walls in damaged buildings during 2010 Chile earthquake. Bull Earthq Eng 13:1119–1139. doi: 10.1007/s10518-015-9727-0

Araya-Letelier G, Parra PF, Lopez-Garcia D, et al (2019) Collapse risk assessment of a

Chilean dual wall-frame reinforced concrete office building. Eng Struct 183:770–779. doi: 10.1016/j.engstruct.2019.01.006

ASCE (2014) ASCE/SEI 41-13: Seismic evaluation and retrofit of existing buildings. American Society of Civil Engineers, Reston, USA

ASCE (2017) Minimum design loads and associated criteria for buildings and other structures: ASCE/SEI 7-16. American Society of Civil Engineers, Reston, USA

ATC (2010) PEER/ATC-72-1: Modeling and Acceptance Criteria for Seismic Design and Analysis of Tall Buildings. Applied Technology Council, Redwood City, USA

ATC (1996) ATC-40: Seismic evaluation and retrofit of concrete buildings. Applied Technology Council, Redwood City, USA

Baltzopoulos G, Baraschino R, Iervolino I, Vamvatsikos D (2017) SPO2FRAG: software for seismic fragility assessment based on static pushover. Bull Earthq Eng 15:4399–4425. doi: 10.1007/s10518-017-0145-3

Beiraghi H, Kheyroddin A, Kafi MA (2015) Nonlinear fiber element analysis of a reinforced concrete shear wall subjected to earthquake records. Iran J Sci Technol Trans Civ Eng 39:409–422

Bonelli P, Priestley MJN, Klingner R (2011) Impacto en el Diseño Sísmico de los Recientes Terremotos de Chile, Nueva Zelanda y Japón. Instituto del Cemento y del Hormigón de Chile, Santiago, Chile (In Spanish)

Bonelli P, Restrepo JI, Boroschek R, Carvallo JF (2012) The 2010 great Chile Earthquake - changes to design codes. In: International Symposium on Engineering Lessons Learned from the 2011 Great East Japan Earthquake. Tokio, Japan, pp 1778–1787

Boroschek R, Soto P, Leon R, Comte D (2010) Informe Preliminar, Red Nacional de Accelerografos, Terremoto Centro Sur Chile, 27 de Febrero de 2010, Informe

Preliminar No. 4. Santiago, Chile

Candia G, Macedo J, Magna-Verdugo C (2018) An integrated platform for seismic hazard evaluation. In: Eleventh U.S. National Conference on Earthquake Engineering. Earthquake Engineering Research Institute, Los Angeles, USA

Carpenter LD, Naeim F, Lew M, et al (2011) Performance of tall buildings in Viña del Mar in the 27 February 2010. Struct Des Tall Spec Build 20:17–36. doi: 10.1002/tal.672

Coleman J, Spacone E (2001) Localization Issues in Force-Based Frame Elements. J Struct Eng 127:1257–1265. doi: 10.1061/(ASCE)0733-9445(2001)127:11(1257)

CSI (2011) Extended Tridimentional Analysis of Building Structures ETABS V9.7.3

CSI (2016a) PERFORM-3D™: Nonlinear Analysis and Performance Assessment for 3D Structures, Version 6.0.0. Computers and Structures, Inc., Walnut Creek, USA

CSI (2016b) Components and Elements for PERFORM-3D™ Version 6. Computers and Structures, Inc., Walnut Creek, USA

CSI (2016c) User Guide, PERFORM-3D™

CSI (2016d) PERFORM-3D, Nonlinear Analysis and Performance Assessment of 3D Structures, Version 6.0.0. Computers and Structures, Inc., Walnut Creek, USA

Değer ZT, Yang TY, Wallace JW, Moehle J (2015a) Seismic performance of reinforced concrete core wall buildings with and without moment resisting frames. Struct Des Tall Spec Build 24:477–490. doi: 10.1002/tal.1175

Değer ZT, Yang TY, Wallace JW, Moehle JP (2015b) Seismic performance of reinforced concrete core wall buildings with and without moment resisting frames. Struct Des Tall Spec Build 24:477–490. doi: 10.1002/tal

Deierlein GG, Reinhorn AM, Willford MR (2010) Nonlinear structural analysis for seismic

design. Rep. NIST GCR 10-917-5. NEHRP Consultants Joint Venture, Gaithersburg, USA

Ellingwood BR, Celik OC, Kinali K (2007) Fragility assessment of building structural systems in Mid-America. Earthq Eng Struct Dyn 36:1935–1952. doi: 10.1002/eqe.693

Elnashai AS, Mwafy AM (2002) Overstrength and force reduction factors of multistorey reinforced-concrete buildings. Struct Des Tall Build 11:329–351. doi: 10.1002/tal.204

FEMA (2009) FEMA P695: Quantification of building seismic performance factors. Federal Emergency Manage Agency, Washington, D.C., USA

FIB (2003) Displacement-based seismic design of reinforced-concrete buildings. State-of-the-art Rep. Bulletin 25. Fédération Internationale du Beton, Lausanne, Switzerland

Filippou FC, Bertero VV, Popov EP (1983) Effects of bond deterioration on hysteretic behavior of reinforced concrete joints. Report EERC 83-19. Earthquake Engineering Research Center, University of California Berkeley, Berkeley, California, USA

Gerin M, Adebar P (2004) Accounting for shear in seismic analysis of concrete structures. In: 13th World Conference on Earthquake Engineering. Vancouver, Canada

Gogus A (2010) Structural wall systems-nonlinear modeling and collapse assessment of shear walls and slab-column frames. Ph.D dissertation. Dept. of Civil and Environmental Engineering, University of California, Los Angeles

Hagen GR (2012) Performance-based analysis of a reinforced concrete shear wall building. M.Sc. Thesis. California Polytechnic State University

Hube MA, Vizcaino P, Lopez-Garcia D, de la Llera JC (2012) Study on Partial Collapse of a Five Story Reinforced Concrete Building during the 2010 Chile Earthquake. In: 15th World Conference on Earthquake Engineering Proceedings. Lisbon, Portugal

Hueste MBD, Bai J-W (2007) Seismic retrofit of a reinforced concrete flat-slab structure: Part II — seismic fragility analysis. Eng Struct 29:1178–1188. doi: 10.1016/j.engstruct.2006.07.022

Humar J, Rahgozar M (1996) Concept of Overstrength in Seismic Design (Paper No. 639). In: Eleventh World Conference on Earthquake Engineering. Acapulco, México

INN (1957) NCh429Of.57, Hormigón Armado - II Parte. Instituto Nacional de Normalización, Chile

INN (1961) NCh430Of.61: Hormigón Armado - Parte 1. Instituto Nacional de Normalización, Chile

INN (1993) NCh433.Of93: Diseño sísmico de edificios. Instituto Nacional de Normalización, Santiago, Chile

INN (1996a) NCh433.Of96: Diseño sísmico de edificios. Instituto Nacional de Normalización, Santiago, Chile

INN (2008a) NCh430.Of2008: Hormigón armado - Requisitos de diseño y cálculo

INN (1996b) Seismic design of buildings NCh433.Of96. Instituto Nacional de Normalización, Santiago, Chile (in Spanish)

INN (2008b) NCh430.Of2008: Reinforced concrete - design and calculation requirements. Instituto Nacional de Normalización (In Spanish), Santiago, Chile

Instituto de la Construccion (2015) Estadisticas del Registro Nacional de Revisores de Proyecto de Calculo Estructural, 4° trimestre 2014. Santiago, Chile (In Spanish)

Jain S, Navin R (1995) Seismic Overstrength in Reinforced Concrete Frames. J Struct Eng 121:580–585. doi: 10.1061/(ASCE)0733-9445(1995)121:3(580)

Junemann R, de la Llera JC, Hube MA, et al (2015) A statistical analysis of reinforced

concrete wall buildings damaged during the 2010, Chile earthquake. Eng Struct 82:168–185. doi: 10.1016/j.engstruct.2014.10.014

Junemann R, de la Llera JC, Hube MA, et al (2016) Study of the damage of reinforced concrete shear walls during the 2010 Chile earthquake. Earthq Eng Struct Dyn 45:1621–1641. doi: 10.1002/eqe.2750

Karthik MM, Mander JB (2011) Stress-block parameters for unconfined and confined concrete based on a unified stress-strain model. J Struct Eng 137:270–273. doi: 10.1061/(ASCE)ST.1943-541X.0000294

Kayen RE, Carkin BD, Corbet S, et al (2014) Seismic velocity site characterization of thirty-one Chilean seismometer stations by spectral analysis of surface wave dispersion. Technical Report PEER 2014/05. Earthquake Engineering Research Center, University of California Berkeley, Berkeley, USA

Kinali K, Ellingwood BR (2007) Seismic fragility assessment of steel frames for consequence-based engineering: A case study for Memphis, TN. Eng Struct 29:1115–1127. doi: 10.1016/j.engstruct.2006.08.017

Kolozvari K, Piatos G, Beyer K (2017) Practical nonlinear modeling of U-shaped reinforced concrete walls under bi-directional loading. In: 16th World Conference on Earthquake Engineering. Santiago, Chile

Kolozvari K, Tran TA, Orakcal K, Wallace JW (2015) Modeling of cyclic shear-flexure interaction in reinforced concrete structural walls. II: experimental validation. J Struct Eng 141:04014136. doi: 10.1061/(ASCE)ST.1943-541X.0001083

Kolozvari K, Wallace JW (2016) Practical nonlinear modeling of reinforced concrete wtructural walls. J Struct Eng 142:G4016001. doi: 10.1061/(ASCE)ST.1943-541X.0001492

Kowalsky MJ, Priestley MJN (2000) Improved analytical model for shear strength of

circular reinforced concrete columns in seismic regions. ACI Struct J 97:. doi: 10.14359/4633

Krenk S (2001) Mechanics and analysis of beams, columns and cables: a modern introduction to the classic theories, 2nd editio. Springer Science & Business Media

Krolicki J, Maffei J, Calvi GM (2011) Shear Strength of Reinforced Concrete Walls Subjected to Cyclic Loading. J Earthq Eng 15:30–71. doi: 10.1080/13632469.2011.562049

Lagos R, Kupfer M, Lindenberg J, et al (2012) Seismic performance of high-rise concrete buildings in Chile. Int J High-Rise Build 1:181–194

LATBSDC (2015) An alternative procedure for seismic analysis and design of tall buildings located in the Los Angeles region. Los Angeles Tall Buildings Structural Design Council, Los Angeles, USA

Li Y, Ellingwood BR (2007) Reliability of woodframe residential construction subjected to earthquakes. Struct Saf 29:294–307. doi: 10.1016/j.strusafe.2006.07.012

Lowes LN, Lehman DE, Baker C (2016) Recommendations for modeling the nonlinear response of slender reinforced concrete walls using PERFORM-3D. In: 2016 SEAOC Convention. Maui, USA

Lu Y, Panagiotou M, Koutromanos I (2014) Three-dimensional beam-truss model for reinforced-concrete walls and slabs subjected to cyclic static or dynamic loading. Report PEER 2014/18. Pacific Earthquake Engineering Research Center (PEER), Berkeley, USA

MacGregor JG, Hage SE (1977) Stability analysis and design of concrete frames. J Struct Div 103:1953–1970

Mackie KR, Stojadinovic B (2004) Improving probabilistic seismic demand models through

refined intensity measures. In: 13th World Conference on Earthquake Engineering. Vancouver, Canada

Mander JB, Priestley MJN, Park R (1988) Theoretical stress-strain model for confined concrete. J Struct Eng 114:1804–1826

Massone LM, Bonelli P, Lagos R, et al (2012) Seismic Design and Construction Practices for RC Structural Wall Buildings. Earthq Spectra 28:S245–S256. doi: 10.1193/1.4000046

McKenna F, Fenves G, Scott M (2000) Open System for Earthquake Engineering Simulation (OpenSees)

Melek M, Darama H, Gogus A, Kang T (2012) Effects of modeling of RC flat slabs on nonlinear response of high rise building systems. In: 15th World Conference on Earthquake Engineering. Lisbon, Portugal

MINVU (2011a) Decreto Supremo Nº 60. D. Of. la Repub. Chile, 13 diciembre 2011 40.133:1–8

MINVU (2011b) Decreto Supremo N° 61. D. Of. la Repub. Chile, 13 diciembre 2011 40.133:8–12

Miranda E, Taghavi S (2005) Approximate floor acceleration demands in multistory buildings. I: Formulation. J Struct Eng 131:203–211

Mitchell D, Paultre P (1994) Ductility and overstrength in seismic design of reinforced concrete structures. Can J Civ Eng

Moehle J, Bozorgnia Y, Jayaram N, et al (2011) Case studies of the seismic performance of tall buildings designed by alternative means. Report PEER 2011/05. Pacific Earthquake Engineering Research Center (PEER), Berkeley, USA

Moehle JP (2014) Seismic design of reinforced concrete buildings. McGraw Hill

Naeim F, Lew M, Carpenter LD, et al (2011) Performance of tall buildings in Santiago, Chile during the 27 February 2010 offshore Maule, Chile earthquake. Struct Des Tall Spec Build 20:1–16. doi: 10.1002/tal.675

Nazri FM, Yern CK, Kassem MM, Farsangi EN (2019) Assessment of Structure-Specific Fragility Curves for Soft Storey Buildings Implementing IDA and SPO Approaches. Int J Eng 31:2016–2021. doi: 10.5829/ije.2018.31.12c.04

Newmark NM (1959) A method of computation for structural dynamics. J Eng Mech Div 85:67–94

NIST (2012) Comparison of U.S and Chilean building code requirements and seismic design practice 1985-2010. Report NIST GCR 12-917-18. National Institute of Standards and Technology (NIST), Gaithersburg, USA

NIST (2010) NIST GCR 10-917-8 Evaluation of the FEMA P-695 Methodology for Quantification of Building Seismic Performance Factors (ATC 76). Gaithersburg, USA

Panagiotou M, Restrepo JI, Conte JP (2010) Shake-table test of a full-scale 7-story building slice. Phase I: Rectangular wall. J Struct Eng 137:691–704

Park J, Towashiraporn P, Craig JI, Goodno BJ (2009) Seismic fragility analysis of low-rise unreinforced masonry structures. Eng Struct 31:125–137. doi: 10.1016/j.engstruct.2008.07.021

Park R (1996) Explicit Incorporation of Element and Structure Overstrength in the Design Process (Paper No. 2130). In: Eleventh World Conference on Earthquake Engineering. Acapulco, México

Parra PF, Moehle JP (2014) Lateral buckling in reinforced concrete walls. In: Tenth U.S. National Conference on Earthquake Engineering. Anchorage, Alaska

Paulay T, Priestley MJN (1992) Seismic design of reinforced concrete and masonry buildings. John Wiley & Sons, Inc., New York, USA

Pavel F, Calotescu I, Stanescu D, Badiu A (2018) Life-Cycle and Seismic Fragility Assessment of Code-Conforming Reinforced Concrete and Steel Structures in Bucharest, Romania. Int J Disaster Risk Sci 9:263–274. doi: 10.1007/s13753-018-0169-6

Powell GH (2007) Detailed example of a tall shear wall building using CSI's PERFORM 3D Nonlinear Dynamic Analysis. Computers and Structures, Inc., Berkeley, USA

Priestley MJN, Park R (1987) Strength and ductility of concrete bridge columns under seismic loading. ACI Struct J 84:61–76. doi: 10.14359/2800

Pugh JS, Lowes LN, Lehman DE (2015) Nonlinear line-element modeling of flexural reinforced concrete walls. Eng Struct 104:174–192. doi: 10.1016/j.engstruct.2015.08.037

Restrepo JI, Conte JP, Dunham RS, et al (2017) Detailed Nonlinear FE Pushover Analysis of Alto Rio Building. In: 16th World Conference on Earthquake Engineering. Santiago, Chile

Rivera F, Jünemann R, Candia G, et al (2017) Reconnaissance Observations by CIGIDEN after the 2015 Illapel , Chile earthquake and Tsunami. In: 16th World Conference on Earthquake Engineering. Santiago, Chile

Rojas F, Naeim F, Lew M, et al (2011) Performance of tall buildings in Concepcion during the 27 February 2010 moment magnitude 8.8 offshore Maule, Chile earthquake. Struct Des tall Spec Build 20:37–64. doi: 10.1002/tal.674

Saito T, Kono S, Kusunoki K, et al (2011) Damage investigation of reinforced concrete buildings at the 2010 Chile earthquake. In: 8th International Conference on Urban Earthquake Engineering. Tokyo, Japan, pp 679–681

Schotanus MI, Maffei JR (2008) Computer modeling and effective stiffness of concrete wall buildings. In: Walraven J, Stoelhorst D (eds) Tailor Made Concrete Structures. Taylor & Francis Group, London, UK, pp 939–945

Sherstobitoff J, Cajiao P, Adebar P (2012) Repair of an 18-story shear wall building damaged in the 2010 Chile earthquake. Earthq Spectra 28:S335–S348

Siembieda W, Johnson L, Franco G (2012) Rebuild fast but rebuild better: Chile's initial recovery following the 27 February 2010 earthquake and tsunami. Earthq Spectra 28:S621–S641. doi: 10.1193/1.4000025

Song C, Pujol S, Lepage A (2012) The Collapse of the Alto Río Building during the 27 February 2010 Maule, Chile, Earthquake. Earthq Spectra 28:S301–S334. doi: 10.1193/1.4000036

Telleen K, Maffei J, Heintz J, Dragovich J (2012a) Practical lessons for concrete wall design, based on studies of the 2010 Chile Earthquake. In: 15th World Conference on Earthquake Engineering. Lisbon, Portugal

Telleen K, Maffei J, Willford M, et al (2012b) Lessons for Concrete Wall Design From the 2010 Maule Chile Eartquake. In: International Symposium on Engineering Lessons Learned from the 2011 Great East Japan Earthquake. Tokio, Japan, pp 1766–1777

Thomsen JH, Wallace JW (1995) Displacement based design of reinforced concrete structural walls: an experimental investigation of walls with rectangular and T-shaped cross-sections. Potsdam, USA

Tran TA (2012) Experimental and analytical studies of moderate aspect ratio reinforced concrete structural walls. Ph.D. dissertation. Dept. of Civil and Environmental Engineering, University of California, Los Angeles

Ugalde D, Lopez-Garcia D (2017a) Elastic overstrength of reinforced concrete shear wall buildings in Chile. In: 16th World Conference on Earthquake Engineering. Santiago,

Chile

Ugalde D, Lopez-Garcia D (2017b) Behavior of reinforced concrete shear wall buildings subjected to large earthquakes. In: Procedia Engineering, X International Conference on Structural Dynamics, EURODYN 2017. Roma, Italy, pp 3582–3587

Ugalde D, Lopez-Garcia D (2017c) Sobrerresistencia en edificios de muros de concreto reforzado: la experiencia chilena. In: Congreso Estructuras ACIES. Asociación Costarricense de Ingeniería Estructural y Sísmica, San José, Costa Rica (in Spanish)

Ugalde D, Lopez-Garcia D, Parra PF (2019a) Análisis del desempeño sísmico de un edificio de muros de hormigón sin daño utilizando análisis no lineal. In: Congreso ACHISINA. Asociación Chilena de Sismología e Ingeniería Antisísmica, Valdivia, Chile (In Spanish)

Ugalde D, Lopez-Garcia D, Parra PF (2019b) Análisis del impacto de la rigidez efectiva de miembros de hormigón armado en la fragilidad de edificios de muros. In: Congreso ACHISINA. Asociación Chilena de Sismología e Ingeniería Antisísmica, Valdivia, Chile (In Spanish)

Ugalde D, Parra PF, Lopez-Garcia D (2018) Overstrength of 3D fully modeled RC shear wall buildings. In: Eleventh U.S. National Conference on Earthquake Engineering. Earthquake Engineering Research Institute, Los Angeles, USA

Ugalde D, Parra PF, Lopez-Garcia D (2019c) Assessment of the seismic capacity of tall wall buildings using nonlinear finite element modeling. Bull Earthq Eng. doi: 10.1007/s10518-019-00644-x

USGS (2019) Earthquake Lists, Maps, and Statistics ANSS (2-mar-2019). https://earthquake.usgs.gov/earthquakes/browse/

Vamvatsikos D, Cornell CA (2002) Incremental dynamic analysis. Earthq Eng Struct Dyn 31:491–514. doi: 10.1002/eqe.141

Vamvatsikos D, Cornell CA (2006) Direct estimation of the seismic demand and capacity of oscillators with multi-linear static pushovers through IDA. Earthq Eng Struct Dyn 35:1097–1117. doi: 10.1002/eqe.573

Wallace JW (2011) February 27, 2010 Chile Earthquake: Preliminary Observations on Structural Performance and Implications for US Building Codes and Standards. In: Structures Congress 2011. Las Vegas, Nevada, pp 1672–1685

Wallace JW, Massone LM, Bonelli P, et al (2012) Damage and Implications for Seismic Design of RC Structural Wall Buildings. Earthq Spectra 28:S281–S299. doi: 10.1193/1.4000047

Westenenk B, de la Llera JC, Besa JJ, et al (2012) Response of reinforced concrete buildings in Concepción during the Maule earthquake. Earthq Spectra 28:S257–S280. doi: 10.1193/1.4000037

Westenenk B, de la Llera JC, Junemann R, et al (2013) Analysis and interpretation of the seismic response of RC buildings in Concepción during the February 27, 2010, Chile earthquake. Bull Earthq Eng 11:69–91. doi: 10.1007/s10518-012-9404-5

Wood SL (1991) Performance of reinforced concrete buildings during the 1985 Chile earthquake: implications for the design of structural walls. Earthq Spectra 7:607–638. doi: 10.1193/1.1585645

Yang TY, Hurtado G, Moehle JP (2010) Seismic behavior and modeling of flat-plate gravity framing in tall buildings. In: 9th US National and 10th Canadian Conference on Earthquake Engineering. Toronto, Canada

Yassin MHM (1994) Nonlinear analysis of prestressed concrete sructures under monotonic and cyclic loads. University of California, Berkeley

Zekioglu A, Willford M, Darama H, Melek M (2008) A review of procedures for performance based seismic design of reinforced concrete high-rise building structures.

In: 17th Congress of IABSE. Chicago, USA

Zhang P, Restrepo JI, Conte JP, Ou J (2017) Nonlinear finite element modeling and response analysis of the collapsed Alto Rio building in the 2010 Chile Maule earthquake. Struct Des Tall Spec Build 26:. doi: 10.1002/tal.1364

APPENDIX 1

Construction drawings of the study cases

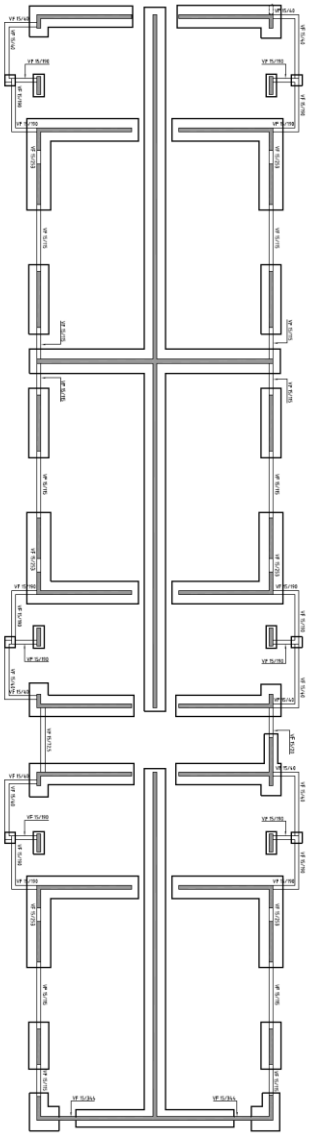

Plan view of the foundations of the 5-story building

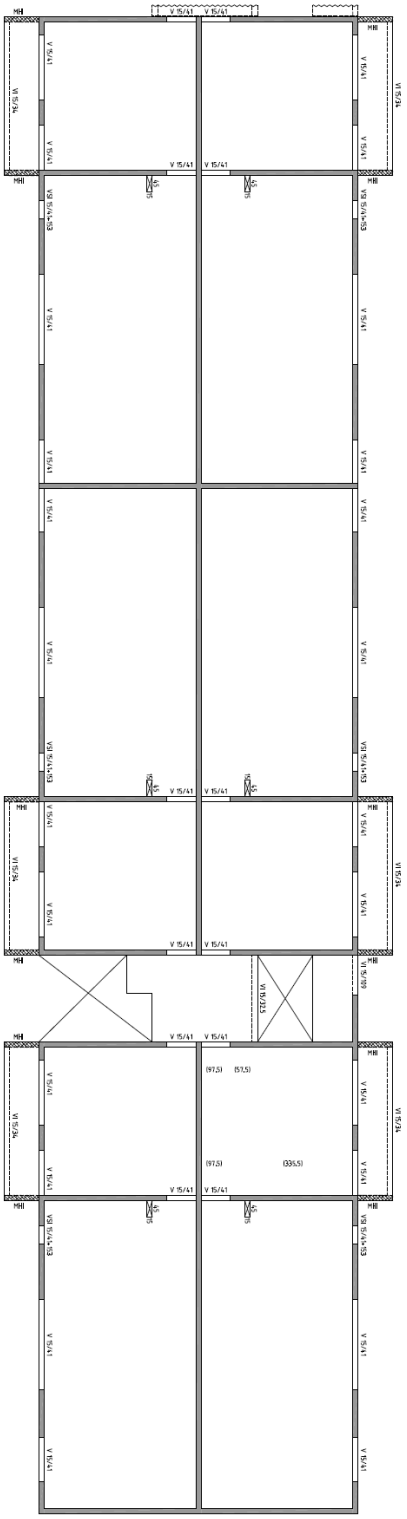

Plan view of the typical story of the 5-story building

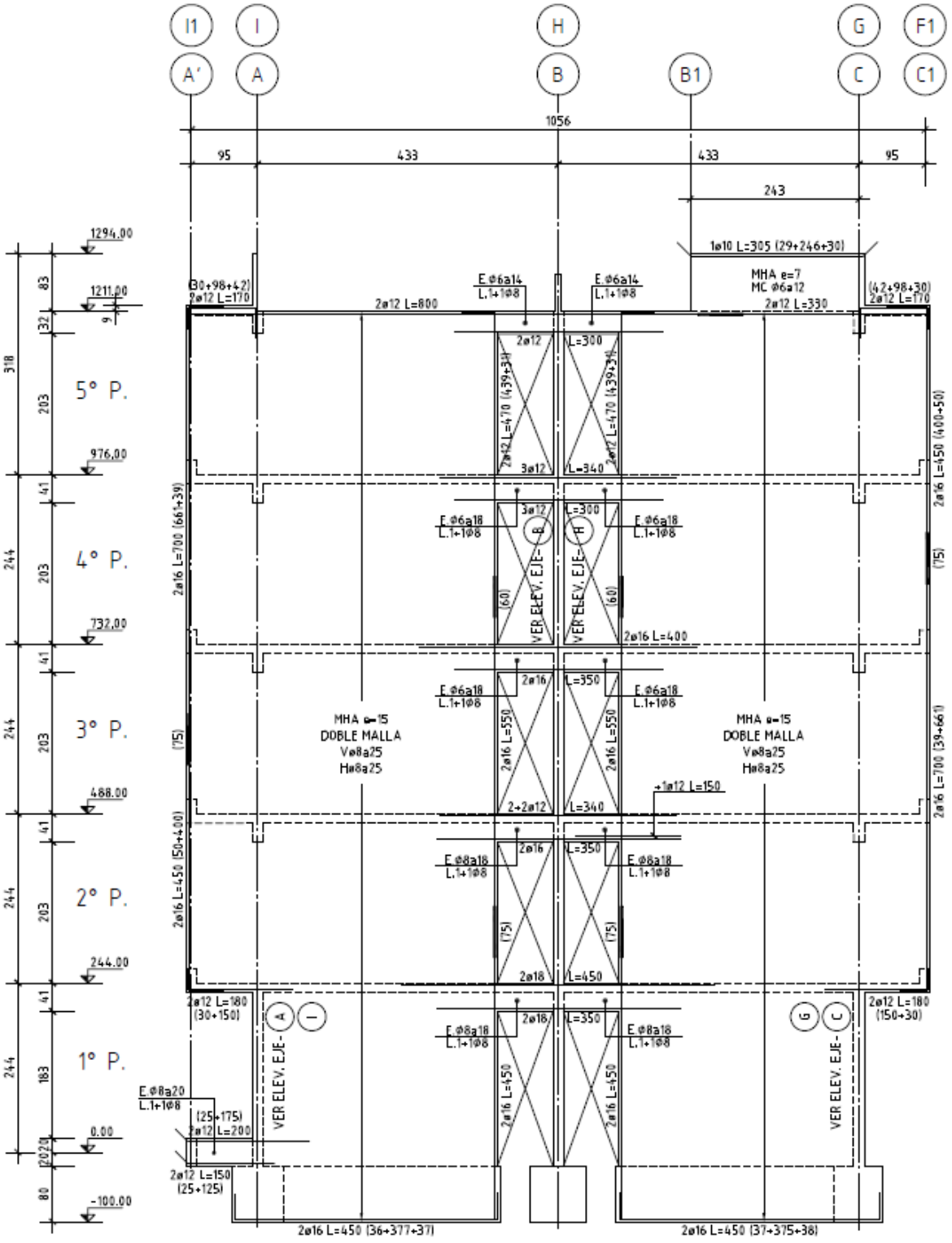

Elevation of a resisting plane of the 5-story building

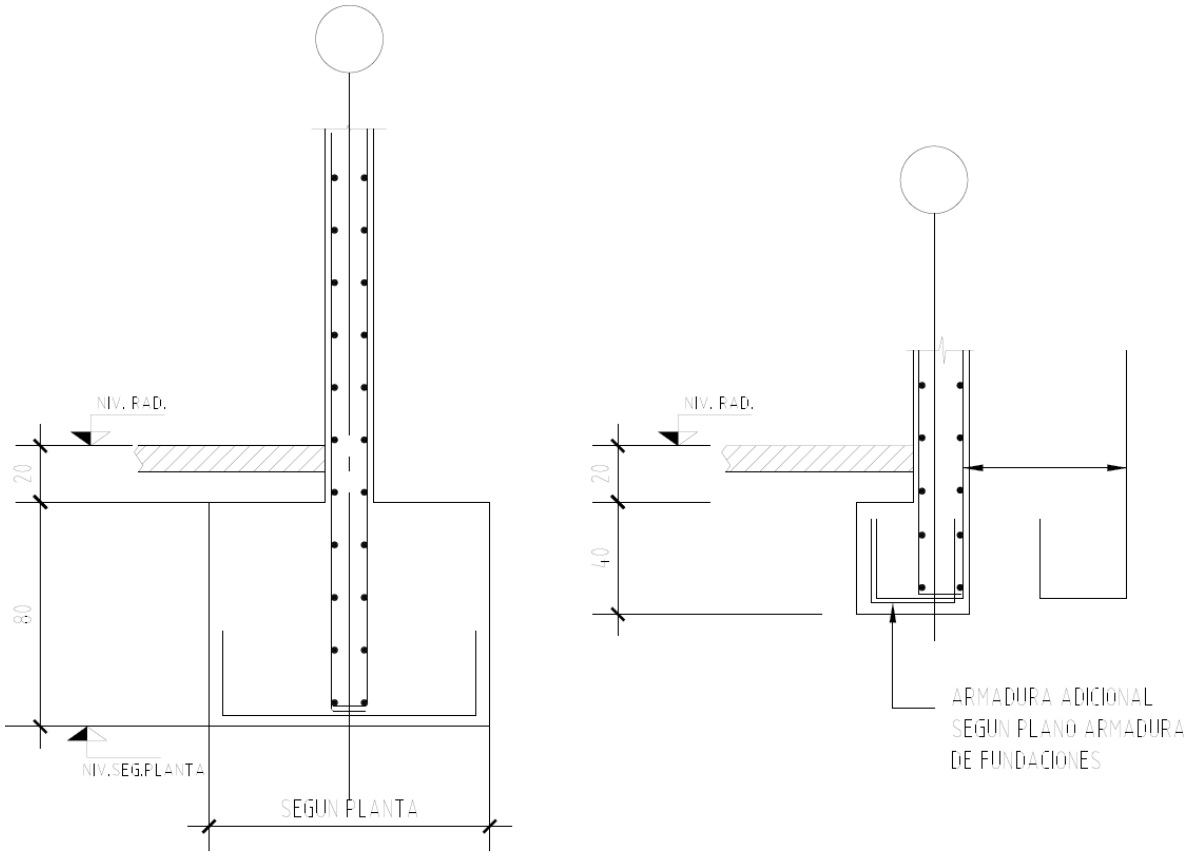

Typical detail for foundation of the 17- and 26-story buildings

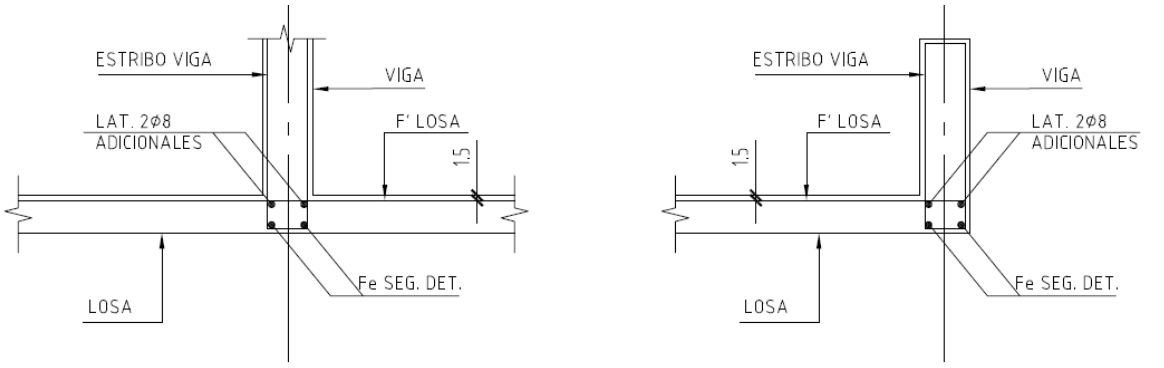

CORTE TIPICO ENCUENTRO VIGA-LOSA

ESC. 1:25

CORTE TIPICO ENCUENTRO LOSA-VIGA

ESC. 1:25

1

2 Typical details for slab-beam connections of the 17- and 26-story buildings

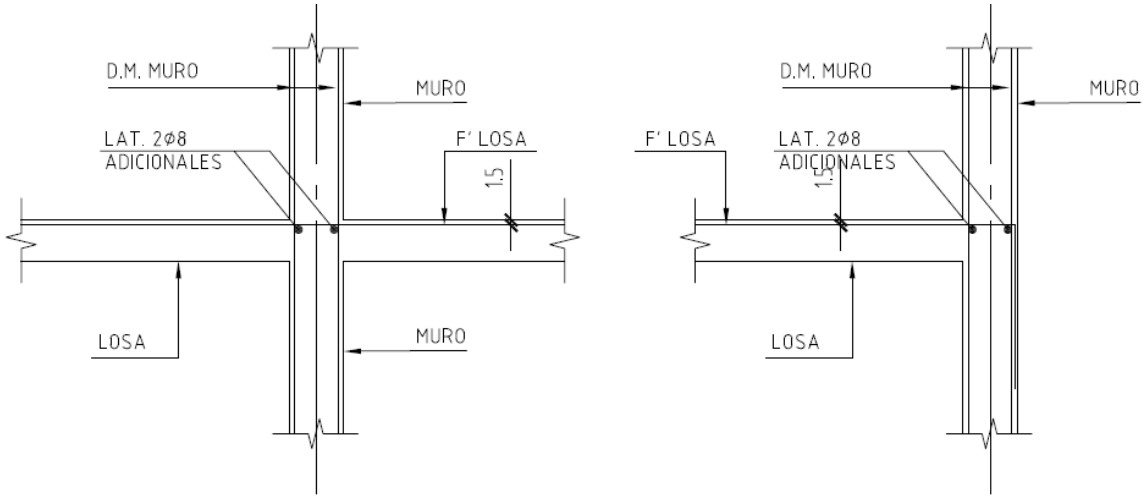

3

CORTE TIPICO ENCUENTRO MURO-LOSA

4

5 Typical details for slab-wall connections of the 17- and 26-story buildings

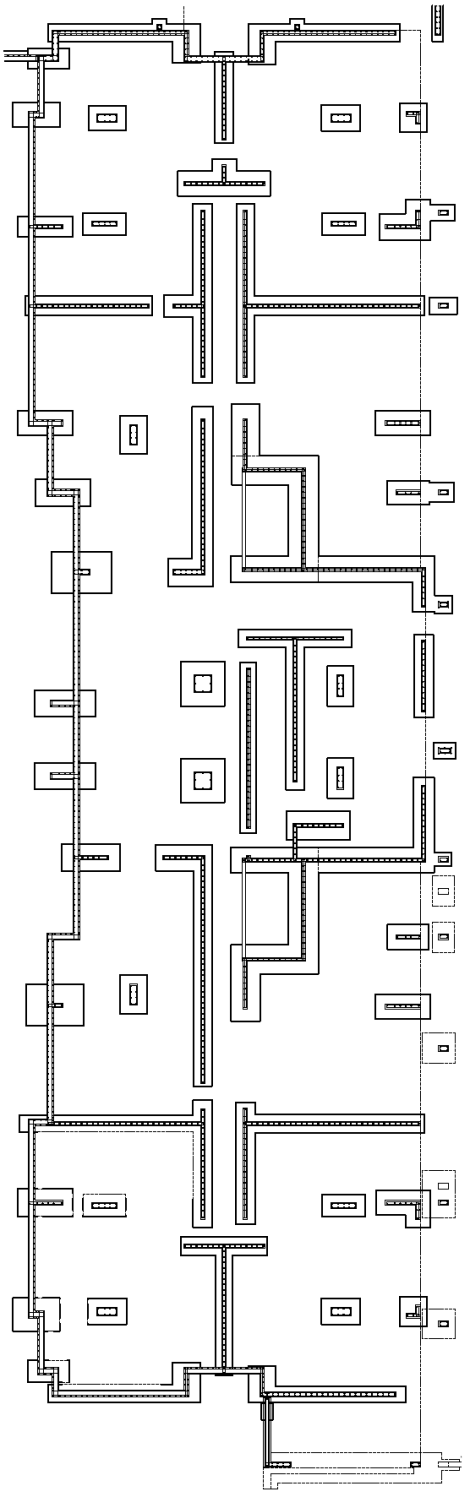

Plan view of the foundations of the 17-story building

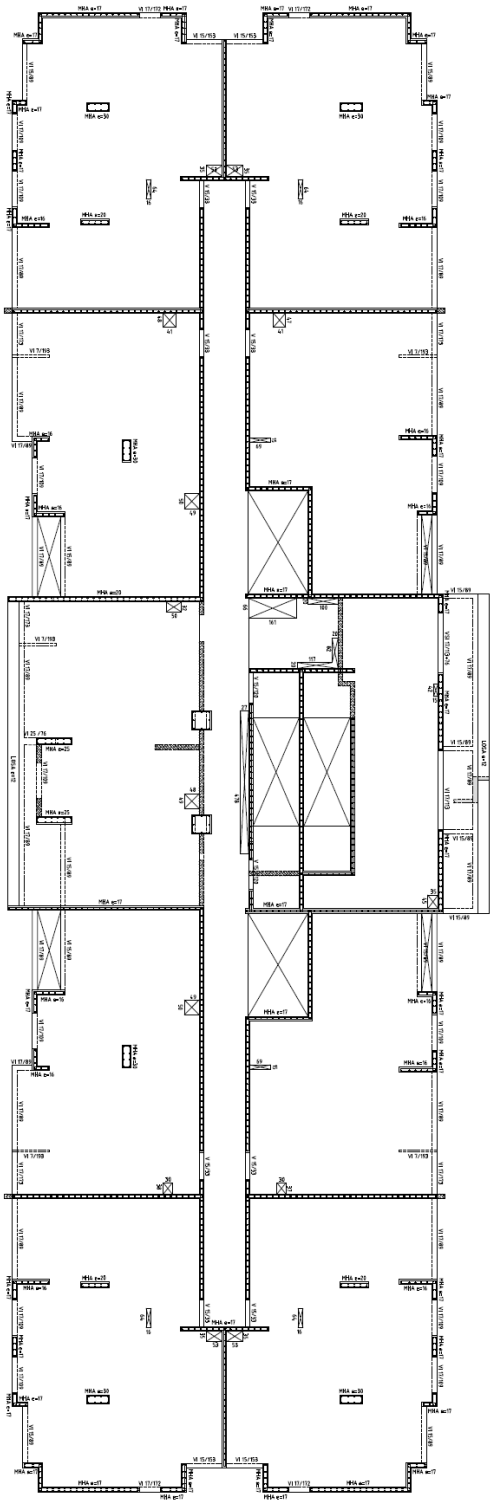

Plan view of the typical story of the 17-story building

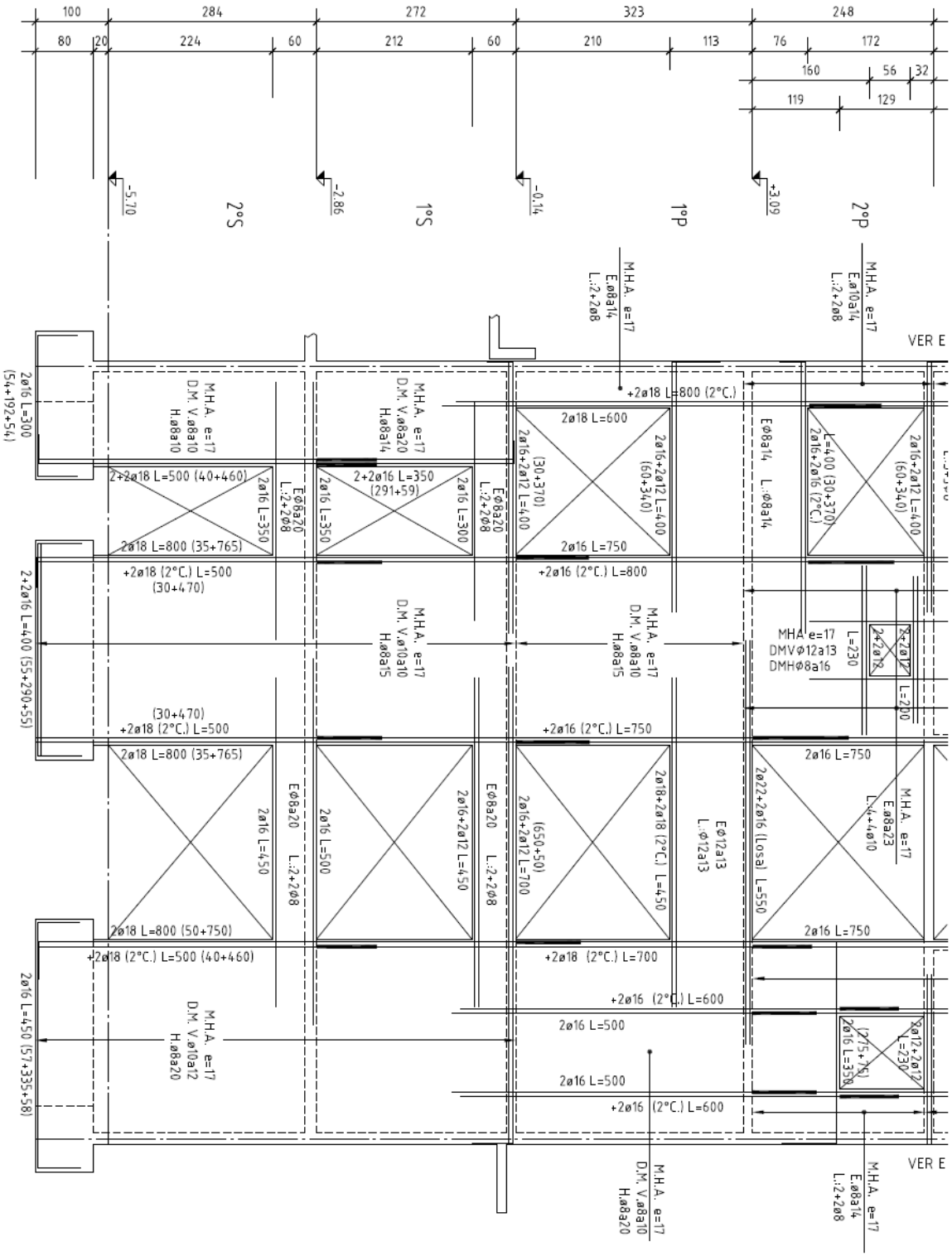

Elevation of a resisting plane of the 17-story building

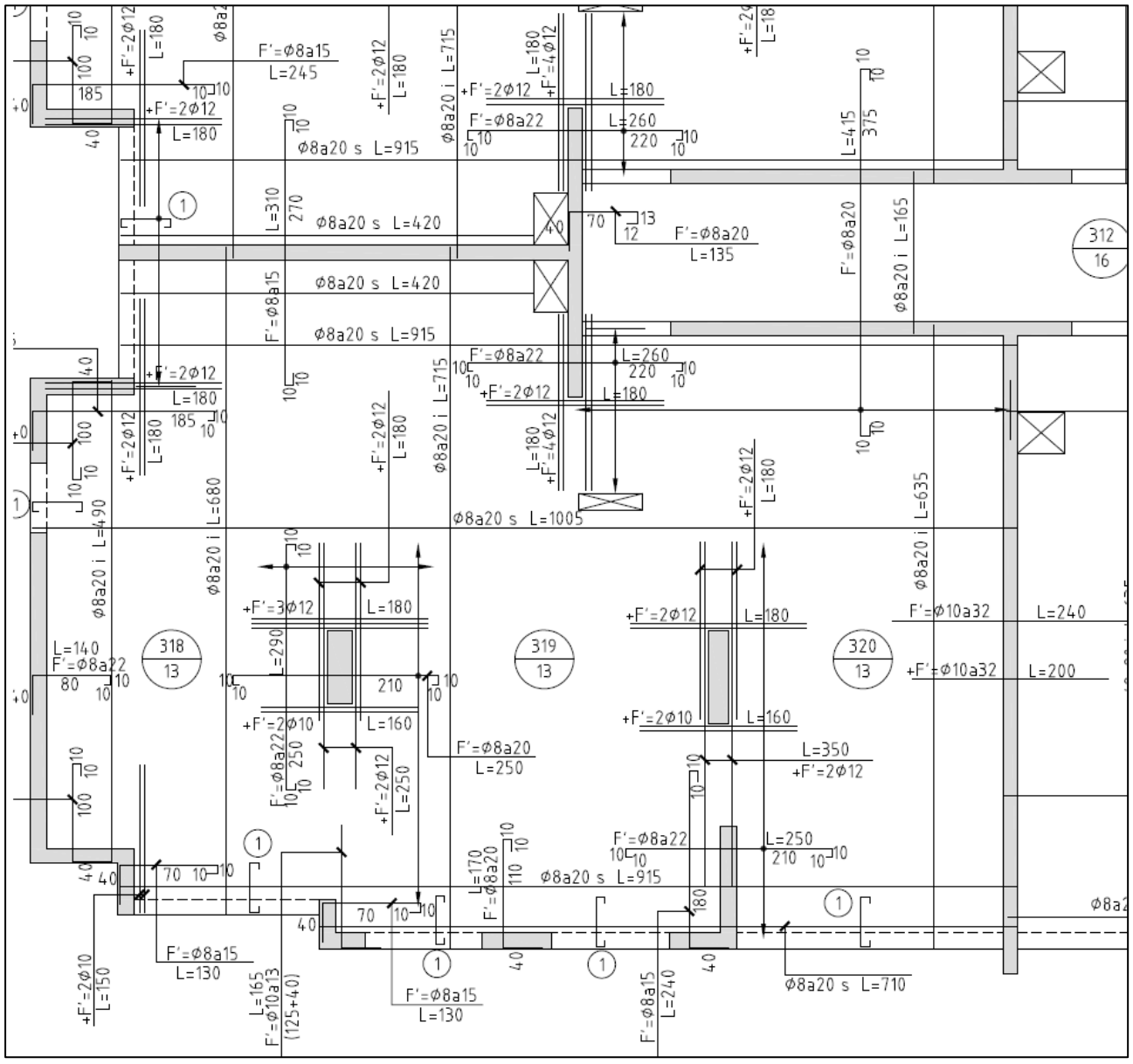

Plan view with of the slab reinforcement of a sector of the 17-story building

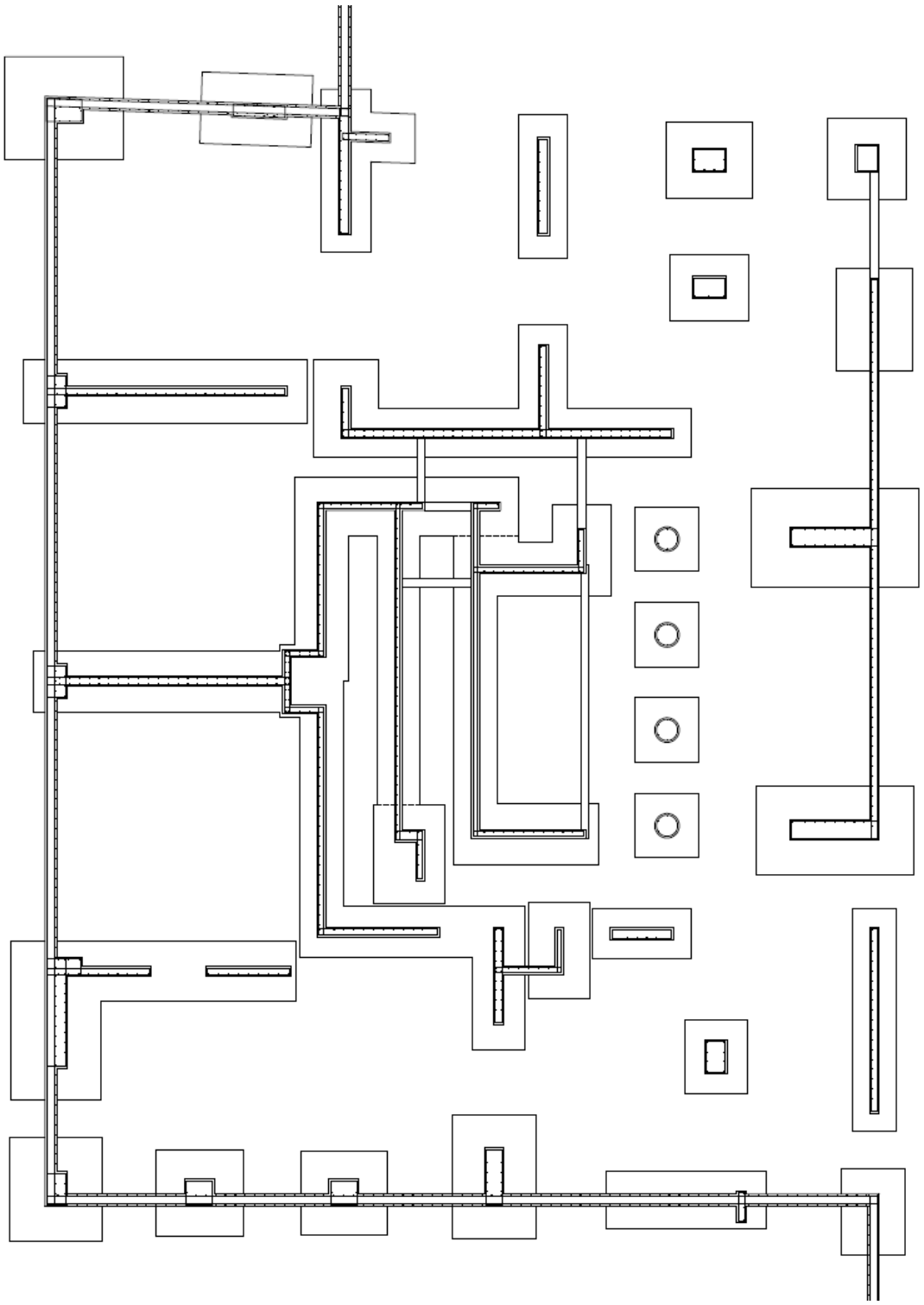

Plan view of the foundations of the 26-story building (podium foundation is not included)

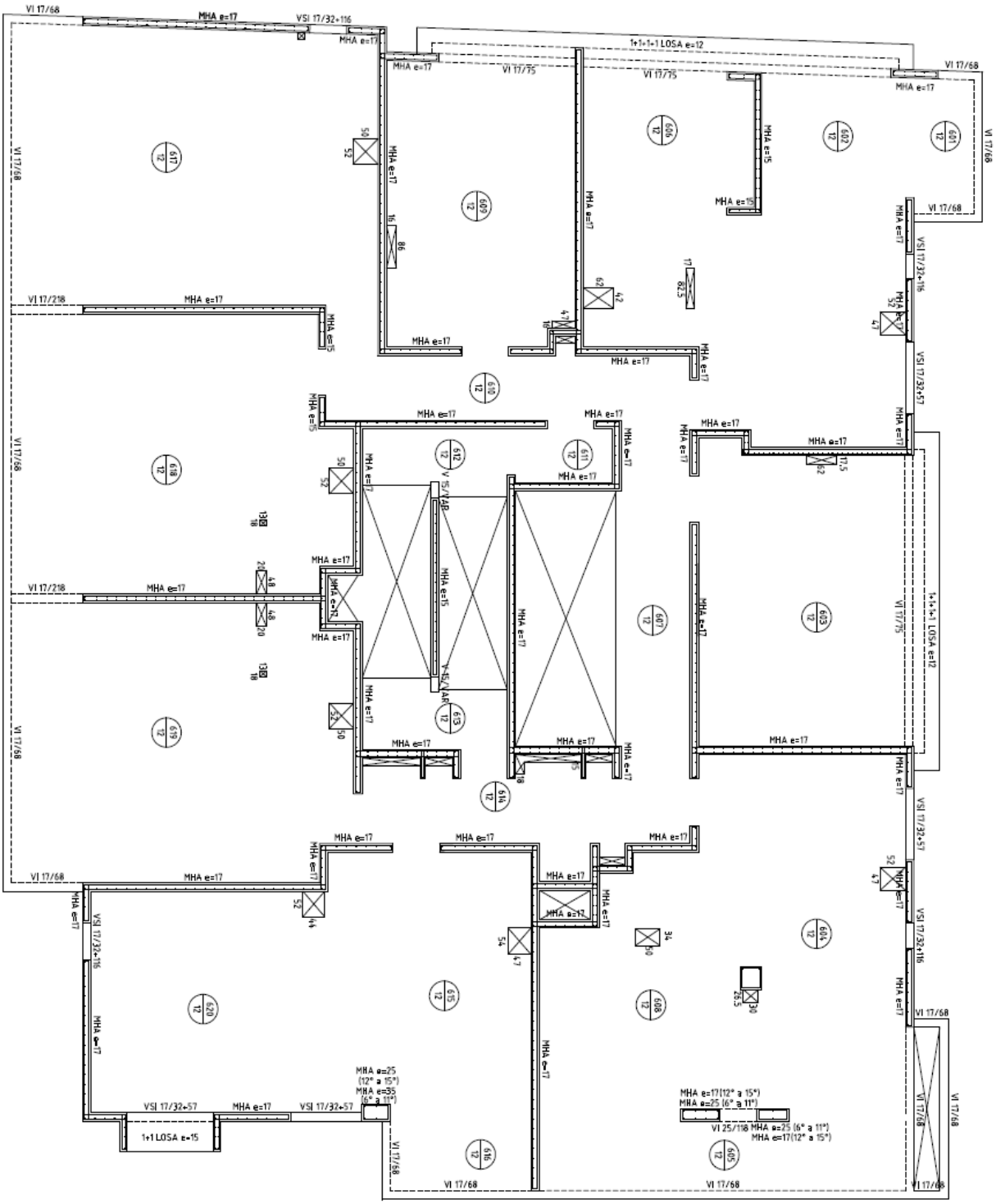

1

2 Plan view of the typical story of the 26-story building

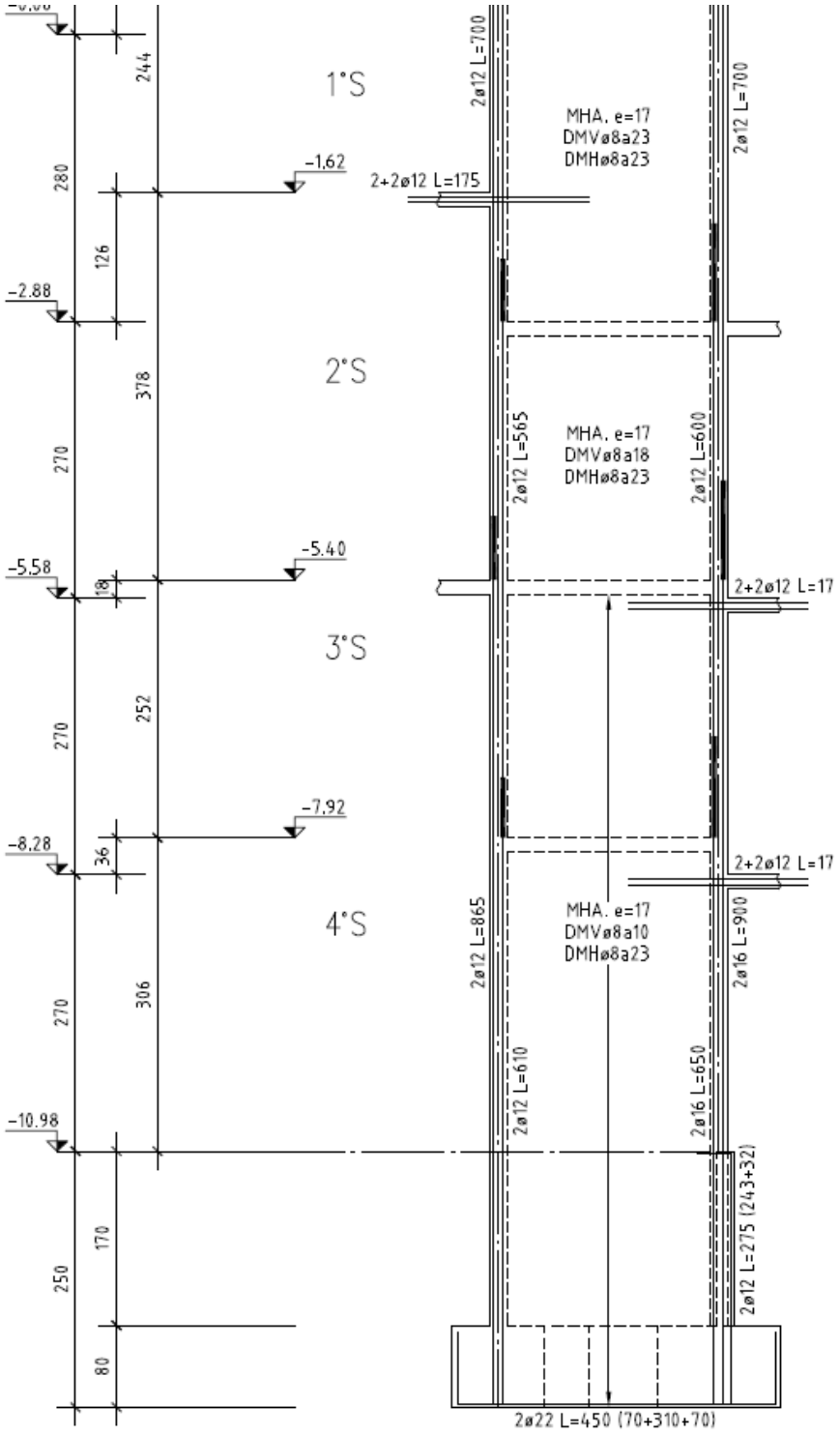

Elevation of a resisting plane of the 26-story building

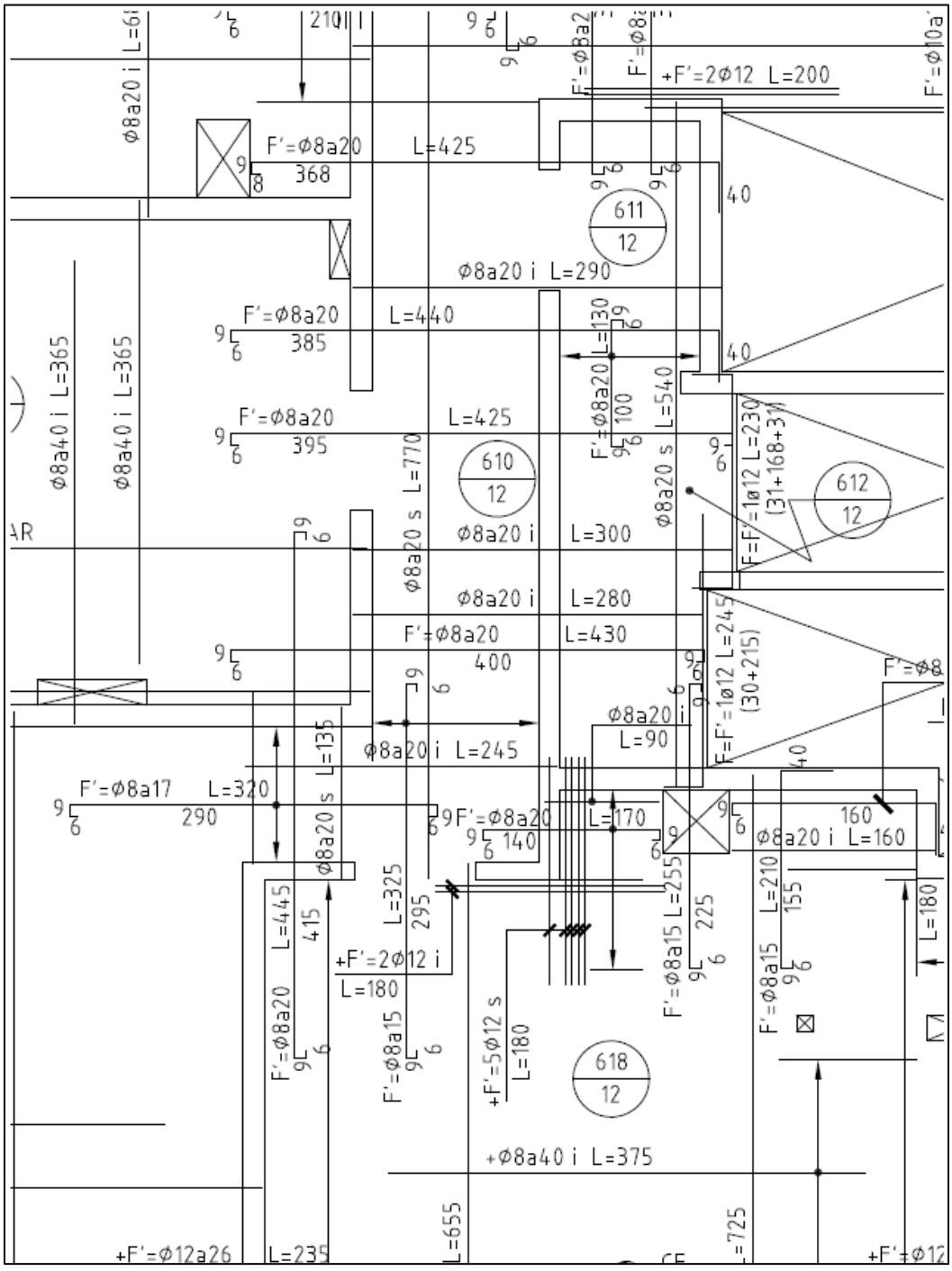

Plan view with of the slab reinforcement of a sector of the 26-story building